LBL-7133

ATOMIC X-RAY PRODUCTION BY RELATIVISTIC HEAVY IONS

John G. Ioannou
(Ph. D. thesis)

December 1977

Prepared for the U. S. Department of Energy
under Contract W-7405-ENG-48

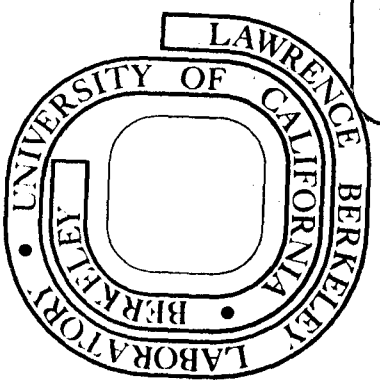

LBL-7133

DISCLAIMER

TABLE OF CONTENTS

ACKNOWLEDGMENTS

I wish to express my sincere indebtedness and deep appreciation to Professor John O. Rasmussen, my research advisor throughout the various phases of this work. Without his guidance, reassurance and support, little of this work would have been possible.

I was fortunate enough to become part of an excellent research team under the leadership of Professor John O. Rasmussen. From the various participants of this collaboration, I would like to thank particularly Dr. R. Anholt who introduced me to the subject and whose contribution to the experimental part of this work was essential. Furthermore I greatly benefited from the presence of Dr. T. Shibata in the team. His expertise in experimental work was rather indispensible in carrying out a variety of measurements involved in this work.

Other deserving thanks are Drs. H. Bowman and D. Raich. Fruitful discussions with Dr. J. Jaklevic and Professor C. A. Tobias have helped significantly in the formulation of certain parts of this work.

I wish also to express my gratitude to a multitude of other people, too numerous to mention by name, who have helped me in one way or another to reach this goal.

This work was supported by the Division of Nuclear Physics of the U.S. Department of Energy.

ATOMIC X-RAY PRODUCTION BY RELATIVISTIC HEAVY IONS

John G. Ioannou

Lawrence Berkeley Laboratory
University of California
Berkeley, California 94720

Ph.D. Thesis

ABSTRACT

The interaction of heavy ion projectiles with the electrons of target atoms gives rise to the production, in the target, of K- , L- or higher shell vacancies which are in turn followed by the emission of characteristic X-rays. The calculation of the theoretical value of the K- and L- shells vacancy production cross section has been carried out for heavy ion projectiles of any energy.

It was found that the total vacancy production cross section for any inner shell could be subdivided into two parts, the longitudinal cross section and the transverse cross section. The longitudinal cross section comes from the instantaneous Coulomb interaction of the projectile-target system while the transverse cross section is due to the virtual photon or radiation field interaction of the same system. The longitudinal part is dominant at lower projectile energies whereas the transverse part contributes appreciably to the total cross section, especially for heavier elements, only at relativistic projectile energies. In this work the transverse component is calculated for the first time in detail and extensive tables of its numerical value as a function of its parameters are also given.

Experimental work for 4.88 GeV protons and 3 GeV carbon ions is described. The K vacancy cross section has been measured for a variety of targets from Ti to U.

The agreement between the theoretical predictions and experimental results for the 4.88 GeV protons is rather satisfactory. For the 3 GeV carbon ions, however, it is observed that the deviation of the theoretical and experimental values of the K vacancy production becomes larger with the heavier target element. Consequently, the simple scaling law of Z_1^2 for the cross section of the heavy ion with atomic number Z_1 to the proton cross section is not true, for the K-shell at least. A dependence on the atomic number Z_2 of the target of the form $(Z_1 - \alpha Z_2)^2$, instead of Z_1^2, is found to give extremely good agreement between theory and experiment. Although the exact physical meaning of such dependence is not yet clearly understood, it is believed to be indicative of some sort of screening effect of the incoming fast projectile by the fast moving in Bohr orbits K-shell electrons of the target.

The enhancement of the K-shell ionization cross section by relativistic heavy ions on heavy targets is also discussed in terms of its practical applications in various branches of science and technology.

I. THEORY OF INNER SHELL IONIZATION BY RELATIVISTIC HEAVY IONS

1.1 Introduction

When a target is bombarded by protons, alphas or heavier ions, electrons are ejected from the atomic shells of the target atoms. If the removal of an electron occurs in an inner shell, e.g. K- or L-shell of the target atom, the electron hole or vacancy produced in that particular shell is filled by one of the outer electrons of the target atom. The energy thus gained by the electron transition from the outer to an inner shell may be emitted as characteristic K or L x-ray radiation of the target atom. Emission of M or N x-rays is also possible in heavier elements if an electron vacancy is created by the incident particle in the M- or N-shell respectively which is in turn filled by an outer electron. In the present work, however, we are going to concentrate mainly on K-shell and partially on L-shell vacancies and not consider other shells. The reason for that is obviously the relative importance of each of these excitations as determined by experiment as well as the difficulty involved in the analytical calculation of the cross section of the process. Returning to our previous discussion, the energy of the excited atom may also, especially for low atomic number elements, convert to kinetic energy of secondary emitted electrons. Here the reference to secondary electrons is made with respect to the electrons emitted from the target atoms by the incident particle or primary electrons. These secondary electrons are then the so called Auger electrons. The cross section for the creation or production of an electron hole or an electron vacancy in an inner shell of a given

element is called the vacancy cross-section of that particular shell and is always larger than the x-ray production cross section of that same shell of the element under consideration. The two cross-sections are related as follows:

$$\sigma_s^{\text{x-ray}}(Z) = \omega_s(Z) \quad \sigma_s^{\text{vac}}(Z) \tag{1.1}$$

(s = K- , L- , etc. shell)

The proportionality coefficient $\omega_s(Z)$ in Eq. (1.1) is called the fluorescent yield of the particular atom Z and shell s and is always less than 1, varying[1] from essentially zero for low Z elements to almost one for high-Z ones. As mentioned earlier, the difference between the two cross sections σ_s^{vac} and $\sigma_s^{\text{x-ray}}$ can be accounted for by the production cross-section of the Auger electrons which is the dominant one for lighter elements and becomes negligible for the heavier atoms. Theoretically one can calculate both $\omega_s(Z)$ and $\sigma_s^{\text{vac}}(Z)$ and hence deduce the value of $\sigma_s^{\text{x-ray}}(Z)$, while experimentally $\omega_s(Z)$ and $\sigma_x^{\text{x-ray}}(Z)$ can be measured and thus $\sigma_s^{\text{vac}}(Z)$ can be deduced. In what follows, we are going to calculate an analytical expression for the $\sigma_s^{\text{vac}}(Z)$ for s, the K- or L-shell of the Z atom, by heavy ions with no restriction or upper limit in the energy of the incident particles. It is assumed here that $\omega_s(Z)$ is nearly independent of the nature of the process forming the vacancy, although there will be some dependence on the state of ionization of other orbitals.

1.2 Theories available for the calculation of σ_s^{vac}.

The inner shell s electron vacancy cross section σ_s^{vac} of an element Z_1 due to a heavy ion Z_2 may be calculated with any of three

existing theories, namely the binary encounter approximation (BEA),[2][3][6] the plane wave Born approximation (PWBA)[5][6] and the semiclassical approximation (SCA).[7][8] In the BEA theory, the ejection of an inner-shell electron to the continuum is considered to occur through the Rutherford scattering of the ejected electron by the incident particle with an energy transfer to the electron in excess of the inner shell binding energy. Since the maximum energy transferred in a Rutherford scattering collision from a projectile of mass M and velocity v_M to an electron of mass m and velocity v_m is[5]

$$E_{max} = \frac{2Mm}{(M+m)^2} (Mv_M - mv_m)(v_M + v_m) \tag{1.2}$$

for a relativistic heavy ion projectile Z_1 and a high atomic number Z_2 target, E_{max} is just lower than, say, the K-shell ionization energy.[9] Thus, unless quantum mechanical modifications are introduced, the theory which is a purely classical one is only good for the description of low velocity incident particle-atomic target electron collisions.

In the PWBA theory the transition probability between specified initial and final states is calculated. The initial and final wave functions are approximated by products of characteristic functions of the Hamiltonian of the target atom which depend only on electron coordinates and eigenfunctions of the wave equation for the motion of the projectile. No internal electron coordinates are considered, and the incident particle wavefunction is assumed to be a plane wave.

Finally, in the SCA theory the excitation probability of an electron from an initial to a final state is calculated via a time integration along the path of the projectile with a given impact parameter and energy as well. The perturbing potential is that of the incident particle's electromagnetic field. Thus one has a more detailed information of the excitation process since the impact parameter of collision enters the calculation.

All the calculations of the electron vacancy cross-section up to the present have been carried out in all of the three theories by assuming heavy ion projectile energies of up to a few tens of MeV per nucleon. In other words, only the electrostatic Coulomb interaction between incident particle and atomic electron has been considered. For higher or relativistic energy projectiles this interaction is clearly inadequate since the total electromagnetic field of the incident particle enters the picture of heavy ion electron interaction. Thus we need both the Coulomb field plus the virtual photon or radiation field of the projectile. One apparent reason for this limited development was the fact that up until recently (1972) no experimental facilities existed which could produce heavy ions of relativistic energies, hence the lack of incentive added to the inherent theoretical difficulty of the problem. What follows is then a first attempt to calculate the inner shell electron vacancy cross section and specifically the K- and L-shell vacancies with emphasis placed on the K-shell one. From the three above mentioned theories only the PWBA and SCA are qualified for relativistic energy projectiles calculations, the BEA being completely disqualified, in its classical

form at least. Furthermore, for lower energies the PWBA has been used and explored far more than the SCA, so that one naturally would choose the PWBA as a starting theory to extend it to higher energies. As we will see shortly, the choice of the PWBA theory for our calculations in this work is, in fact, well justified for relativistic energy projectiles.

1.3 The PWBA at relativistic projectile energies

As mentioned already, use of the plane wave Born approximation for inelastic collisions implies that one may neglect the distortion of the wave function of the incident particle, assumed to be a plane wave, by the atomic electron which is removed from its inner shell ground state orbit and is ejected into the continuum state. The condition for the validity of this approximation is that the inequality

$$\frac{Z_1 e^2}{\hbar v} = \frac{Z_1 \alpha}{\beta} \ll 1 \tag{1.3}$$

is satisfied.[5],[10] In Eq. (1.3) $Z_1 e$ denotes the charge of the projectile with velocity v, $\beta = v/c$, and α is the fine structure constant. Thus, the faster the projectile and the lower its charge the more justifiable the plane-wave Born approximation is. Qualitatively Eq. (1.3) if satisfied indicates that the resultant from the scattering of projectile-electron secondary wave amplitude (i.e. the distortion of the primary wave) is very small compared to the primary wave amplitude and thus negligible. Consequently relativistic projectile energies (large v's) may very well be treated in the PWBA theory. It could be argued, however, that for very high projectile velocities the de Broglie wavelength of the projectile may become very small compared

with the dimensions of the scattering field (~ few fm). Thus, instead of a plane wave representation of the incident particle one may consider its classical trajectory so that quantum mechanical treatment of the problem (Born approximation) is not necessary. However, the latter is not a sufficient condition either.[10] Since the initial conditions in a scattering problem are a well-defined incident velocity and a random impact parameter, in a classical treatment of this problem one has to proceed by considering the scattering procedure in more detail. That is, a well-defined incident particle trajectory with a definite impact parameter followed by calculation of the well-defined deflection of the projectile due to the collision are needed. Now this procedure is admissible as long as the extra details considered could be observed without radically disturbing the collision with respect to the quantity calculated, namely the deflection due to the scattering. If the collision forces are too weak, then this procedure is not valid. Therefore, a classical treatment is inadmissible and one has to proceed in a manner which does not break up the random incidence. This can be done in a quantum-mechanical treatment of the problem in which the incident particle with a random parameter can be represented by a plane wave. Equation (1.3) tells us then how valid the undistorted plane wave Born approximation is, assuming that the incident particle is represented by a plane wave.

Examining further the validity of the PWBA, we consider the effect of the incident particle on the electron orbits of the target atom. If the charge of the incident particle is not much greater in absolute value than the electron charge and at the same time small compared with the charge of the atomic nucleons, the electron orbits

will not be polarized significantly by the approaching projectile. Hence, we may use for the electron the atomic wave function of the unperturbed atom. It is obvious that the use of unperturbed atomic wave functions will be more justifiable for higher atomic number target elements and inner shells from which the electrons are ejected. Thus the present method should be at best justified for K-shell electrons from heavy atoms and should be better for protons than, say, carbon projectiles.

An additional condition for the velocity of PWBA is:[5],[11]

$$Z_1 Z_2^2 \frac{\alpha^2}{n} \frac{mc^2}{E} \ll 1 \qquad (1.4)$$

where in Eq. (1.4) $\alpha = 1/137$, the fine structure constant, Z_1 projectile, Z_2 target, n is the principal quantum number of ejected electron of rest energy mc^2, and E is the kinetic energy of the incident particle. The condition of Eq. (1.4) implies essentially that scattering of the projectile from the target nucleons can be neglected if the radius of the orbit of the ejected electron in the atom is large compared with the distance of the closest approach, say b, of the particle to the nucleons (a heavy particle can be fairly accurately assigned a classical orbit). In conclusion, if Eq. (1.4) is satisfied, nuclear scattering is then negligible and one may use plane-wave instead of Coulomb-wave functions describing the motion of the projectile in the electromagnetic field of the nucleons. Specifically for the case of K-shell ionization (η=1), it has been shown[11] that if Eq. (1.3) and Eq. (1.4) are both satisfied, nuclear scattering can be neglected and plane waves

can be used for the projectile since the relevant phase shifts are reasonably independent of the angular momentum and energy of the incident particle. Again the validity of Eq. (1.4) is enhanced by relativistic projectiles although the approximation is better for low atomic number projectiles and even more so for low atomic number target atoms.

1.4 Calculation of σ_s^{vac} in the PWBA theory.

In the spirit of the first-order perturbation theory, the cross section for the process, i.e. removal of an electron from an inner shell of the target by a projectile, is taken to be proportional to the absolute value of the square of the matrix element of the electromagnetic interaction between the incident particle and the atomic electron. If v, $\bar{p}$ and v', $\bar{p}'$ are the velocities and momenta of the incident particle before and after the collision with an atomic electron and $\bar{q}$ is the momentum transfer from one to the other as depicted schematically in Fig. 1 so that

$$\hbar\bar{q} = \bar{p} - \bar{p}' \tag{1.5}$$

then the differential cross section in the Born approximation is given by[5]

$$d\sigma_{n'n}(q) = 8\pi Z_1^2 \left(\frac{e^2}{\hbar v}\right)^2 \frac{dq}{q^3} \left| < \psi_{n'} | H | \psi_n > \right|^2 \tag{1.6}$$

where in Eq. (1.6) ψ_n ($\psi_{n'}$) are the initial (final) wave functions of the

electron and H is the electromagnetic interaction Hamiltonian between the incident heavy ion of atomic number Z_1 and the atomic electron.

The electromagnetic interaction between the charge and spin, if any, of the incident particle and those of atomic electrons may be subdivided into two terms. One of these terms consists of the unretarded Coulomb interaction and the other of the interaction through emission and reabsorption of virtual photons. This subdivision is called the "Coulomb gauge" representation or "transverse gauge" representation for reasons which will become apparent shortly. Formally, if the vector component $\bar{A}$ of the four vector potential A_μ of the electromagnetic field satisfies the condition[12]

$$\nabla\cdot\bar{A} = 0 \tag{1.7}$$

then the scalar component ϕ of A_μ satisfies the equation

$$\nabla^2\phi = -4\pi\rho \quad , \quad \phi(\bar{r},t) = \int \frac{\rho(\bar{r}',t')}{|\bar{r}-\bar{r}'|}\, d^3\bar{r}' \tag{1.8}$$

The scalar potential ϕ is then the instantaneous Coulomb potential due to the charge density $\rho(\bar{r},t)$ and hence the name "Coulomb gauge" of the representation of Eqs. (1.7) and (1.8). Furthermore $\bar{A}$ and ϕ satisfy the inhomogeneous wave equation[12]

$$\nabla^2\bar{A} - \frac{1}{c^2}\frac{\partial^2\bar{A}}{\partial t^2} = -\frac{4\pi}{c}\bar{J} + \frac{1}{c}\bar{\nabla}\left(\frac{\partial\phi}{\partial t}\right) \tag{1.9}$$

If the current $\bar{J}$ is written as the sum of a longitudinal and a transverse part

$$\bar{J} = \bar{J}_\ell + \bar{J}_t \tag{1.10}$$

where

$$\nabla \times \bar{J}_\ell = 0 \quad , \quad \nabla \cdot \bar{J}_t = 0 \tag{1.11}$$

then one has

$$\bar{J}_\ell = -\frac{1}{4\pi} \bar{\nabla} \int \frac{\nabla' \cdot \bar{J}}{|\bar{r} - \bar{r}'|} d^3 \bar{r}'$$

$$\bar{J}_t = \frac{1}{4\pi} \bar{\nabla} \times \nabla \times \int \frac{\bar{J}}{|\bar{r} - \bar{r}'|} d^3 r' \tag{1.12}$$

Then from Eqs. (9) and (12) one obtains

$$\nabla \frac{\partial \phi}{\partial t} = 4\pi \bar{J}_\ell \tag{1.13}$$

and

$$\nabla^2 \bar{A} - \frac{1}{c} \frac{\partial^2 \bar{A}}{\partial t^2} = - \frac{4\pi}{c} \bar{J}_t \tag{1.14}$$

or that the static Coulomb potential ϕ can be expressed in terms of the longitudinal current $\bar{J}_\ell$ while the vector potential $\bar{A}$ can be expressed in terms of the transverse current $\bar{J}_t$ and therefore, the second name of this representation "transverse gauge". In other words, in the case of mutually interacting particles (so that $J_\mu \neq 0$) $\bar{A}$ is decomposed into

$$\bar{A} = \bar{A}_\ell + \bar{A}_t \tag{1.15}$$

$\bar{A}_\ell$, $\bar{A}_t$ being such that

$$\nabla \cdot \bar{A}_t = 0 \qquad\qquad \nabla \times \bar{A}_\ell = 0 \tag{1.16}$$

which can always be done[13] and where $\bar{A}_\ell$ and $\bar{A}_t$ are called the longitudinal and transverse component of $\bar{A}$. Then $\bar{A}_\ell$ and ϕ together give rise to the instantaneous static Coulomb interaction between the charged particles, whereas $\bar{A}_t$ accounts for the electromagnetic radiation or virtual photon interaction of moving charged particles (E. Fermi, 1930).[14]

We now examine the two interactions, longitudinal and transverse, separately. The Coulomb or longitudinal interaction between the incident particle of charge $Z_1 e$ at the position $\bar{r}$ and an atomic electron at $\bar{r}_j$ can be represented as a Fourier integral[15]

$$\frac{Z_1 e^2}{|\bar{r} - \bar{r}_j|} = \frac{Z_1 e^2}{2\pi^2} \int d^3 \bar{k} \; \frac{\exp\left[i\bar{k} \cdot (\bar{r} - \bar{r}_j)\right]}{k^2} \tag{1.17}$$

The usefulness of representational Eq. (1.17), as it will be seen shortly, is based on the fact that each Fourier component with wave vector $\bar{k}$ serves to transfer the momentum $\hbar\bar{k}$ from the incident particle to the electron. On the other hand the transverse interaction implies that the same momentum $\hbar\bar{k}$ can be transmitted by emission and re-absorption of a virtual photon of momentum $\pm\hbar k$. Thus, the convenience of the Coulomb interaction as a Fourier integral by Eq. (1.15) becomes apparent. Now the longitudinal component can be treated on the same footing as the transverse one. Moreover the emission of a photon of momentum $\hbar\bar{k}$ by the incident particle at $\bar{r}$ is proportional to the matrix element of the interaction Hamiltonian[14],[15]

$$Z_1 ec\ \bar{\alpha}_j \cdot \bar{\varepsilon}_\lambda \exp(-i\,\bar{k}\,.\,\bar{r}) + \frac{Z_1 e\hbar}{Mc}\,\bar{\sigma} \cdot \nabla\times\left(\bar{\varepsilon}_\lambda \exp(-i\bar{k}\,.\,\bar{r})\right) \tag{1.18}$$

The absorption of the same photon by the j-th electron of the target atom is proportional to the matrix element of the corresponding Hamiltonian operator

$$Z_1 ec\ \bar{\alpha}_j \cdot \bar{\varepsilon}_\lambda \exp(-i\bar{k} \cdot \bar{r}_j) + \frac{Z_1 e\hbar}{mc}\,\bar{\sigma}_j \cdot \nabla\times\left(\bar{\varepsilon}_\lambda \exp(i\bar{k}\,.\,\bar{r}_j)\right) \tag{1.19}$$

In Eqs. (1.18) and (1.19) $\bar{\varepsilon}_\lambda$ is the unit polarization vector of the photon with $\lambda = 1,2$ for the two orthogonal directions. Furthermore $Z_1 ec\,\bar{\alpha}$ and $Z_1 ec\,\bar{\alpha}_j$ are the relativistic current operators of the incident particle and j-th electron, respectively, where $\bar{\alpha}$ and $\bar{\alpha}_j$ are

vector operators whose three components are given in terms of the Dirac γ matrices, i.e. $\bar{\alpha}_j = -i\,\gamma^4\,\bar{\gamma}_j$ for the electron, and essentially in terms of the momentum $\bar{p}$ for the incident heavy ion. Finally $\bar{\sigma}$ and $\bar{\sigma}_j$ are the spin operators of the incident heavy particle of mass M and the j-th electron of mass m, respectively. Since the heavy ion can have spin 0 or 1/2 the second part of Eq. (1.16) can be zero or non-zero whereas the second part of Eq. (1.12) is always non zero since the electron has spin equal to one-half. We proceed now to calculate the matrix element $\langle\psi_n, |H|\psi_n\rangle$ where H consists of the longitudinal interaction described by Eq. (1.17) and the transverse interaction described by Eqs. (1.18) and (1.19). We note that in the case of the transverse interaction the transmission of a photon with momentum $\pm\,\bar{k}$ proceeds through an intermediate state whose energy differs from that of the initial and final states by $\hbar ck \pm w_s$, w_s being the energy of the final stationary state of the atom whose initial energy E_o was 0. Thus, if the final state is that of the continuum, then w_s is nothing else but the binding energy of the ejected j-th electron in its ground state of s-shell plus its kinetic energy if any. Combining the longitudinal and transverse contributions, we obtain for the matrix element of the incident heavy ion-atomic electron interaction

$$\langle\psi_n, |H|\psi_n\rangle = \frac{Z_1 e^2}{2\pi}\int d^3\bar{k}\left\{\left[\frac{\langle\bar{p}'|e^{-i\,\bar{k}\cdot\bar{r}}|\bar{p}\rangle\langle n'|\sum_j e^{i\,\bar{k}\cdot\bar{r}_j}|n\rangle}{k^2}\right]+\right.$$

$$+ \sum_{\lambda=1,2} \left[< \bar{p}' \mid \bar{\alpha} \cdot \bar{\varepsilon}_\lambda \; e^{-i\bar{k}\cdot\bar{r}} \mid \bar{p} > < n' \mid \Sigma_j \bar{\alpha}_j \cdot \bar{\varepsilon}_\lambda \; e^{i\bar{k}\cdot\bar{r}_j} \mid n > \; + \right.$$

$$\left. + \; < \bar{p}' \mid \frac{\hbar}{M_c^2} \bar{\sigma} \cdot \nabla \times \left(\bar{\varepsilon}_\lambda \; e^{-i\bar{k}\cdot\bar{r}} \right) \mid p > < n' \mid \Sigma_j \frac{\hbar}{mc^2} \bar{\sigma}_j \cdot \nabla \times \left(\bar{\varepsilon}_\lambda \; e^{i\bar{k}\cdot\bar{r}} \right) \mid n > \right] \times$$

$$\times \frac{1}{k^2 - \frac{w_s^2}{\hbar c}} \Bigg\} \tag{1.20}$$

From conservation of momentum one has

$$< p' \mid e^{-i\bar{k}\cdot\bar{r}} \mid \bar{p} > = (2\pi)^3 \; \delta\left(\bar{k} + \frac{\bar{p}' - \bar{p}}{\hbar} \right) \tag{1.21}$$

$$< \bar{p}' \mid \bar{\alpha} \cdot \bar{\varepsilon}_\lambda \; e^{-i\bar{k}\cdot\bar{r}_j} \mid \bar{p} > = (2\pi)^3 \; \bar{\beta} \cdot \bar{\varepsilon}_\lambda \; \delta\left(\bar{k} + \frac{\bar{p}' - \bar{p}}{\hbar} \right) \tag{1.22}$$

where $\bar{\beta} = \bar{v}/c$. In addition.

$$\sum_{\lambda=1,2} \bar{\beta} \cdot \bar{\varepsilon}_\lambda \; \bar{\alpha}_\lambda \cdot \bar{\varepsilon}_\lambda = \bar{\beta}_t \cdot \bar{\alpha}_j$$

with

$$\bar{\beta}_t = \bar{\beta} - (\bar{\beta} \cdot \hat{q}) \; \hat{q} \tag{1.24}$$

where $\bar{\beta}_t$ is the component of $\bar{\beta}$ perpendicular to $\hat{q}$ as depicted in Fig. 1. We may also ignore in Eq. (1.20) the spin term in the sum over λ, since many nuclei which have been experimentally accelerated have spin zero, e.g. ^4He, ^{12}C, ^{20}Ne, ^{40}Ar, etc. Furthermore nuclear magnetic moments are so small that the nuclear spin contribution should be negligible. The only exception is p.

If we substitute now Eqs. (1.21), (1.22), and (1.23), into Eq. (1.19), then substitute that into Eq. (6), and finally sum the differential cross section of Eq. (6) over all the substates of an initially filled atomic shell (labeled s) and integrate over all directions of the ejected electron, the differential cross section for an energy transfer between w and w + dw can be written in the form[5],[15]

$$d^2\sigma_{ws} = 8\pi Z_1^2\left(\frac{e^2}{\hbar v}\right)^2 2q\, dq\left[\frac{|F_s(q)|^2}{q^4} + \frac{|\bar{\beta}_t\cdot\bar{G}_s(q)|^2}{\left[q^2-\left(\frac{w_s}{\hbar c}\right)^2\right]^2}\right] dw \qquad (1.25)$$

where in Eq. (1.25) the form factors $F_s(q)$ and $\bar{G}_s(q)$ of the longitudinal and transverse interactions respectively are given by the following expressions:

$$F_s(q) = \sum_j \langle n'|e^{i\bar{q}\cdot\bar{r}_j}|n\rangle \qquad (1.26)$$

$$\bar{G}_s(q) = \sum_j \langle n'|\bar{\alpha}_j\, e^{i\bar{q}\cdot\bar{r}_j}|n\rangle \qquad (1.27)$$

the summation in Eqs. (1.26) and (1.27) is carried over all the electrons j of a filled atomic shell s. Also, the factor 2 in Eq. (1.25) takes into account explicitly the double occupation of each inner electron orbit.

It should be mentioned at this point that up to now all calculations of inner shell ionization by heavy ions have ignored the transverse

term in Eq. (1.25). The reason is that for low incident projectile energies the transverse term being proportional to β_t or essentially the β of the projectile is insignificant. The objective of the present work is to calculate this component of the total cross section of the electron vacancy production of the inner shells of atoms, which of course implicitly assumes that the projectile ions must have relativistic energies.

If we integrate the differential cross-section of Eq. (1.23) over the momentum q and energy w, we obtain the total cross-section σ_s of electron vacancy production of the shell s in the obvious form

$$\sigma_s = \sigma_s^{\ell} + \sigma_s^{t} \tag{1.28}$$

where in Eq. (1.28) σ_s^{ℓ} and σ_s^{t} stand for the longitudinal and transverse components of the total cross-section. We call these two components the longitudinal and transverse electron vacancy cross-section, respectively. Such terminology is self-explanatory in the light of our previous development, i.e. the decomposition of the electromagnetic interaction between incident ion and electron into longitudinal and transverse components. Thus, the instantaneous Coulomb interaction which exerts a force along the direction of $\bar{q}$, the momentum transfer from the incident heavy ion to the atomic electron, is responsible for the σ_s^{ℓ} component of the total cross section. On the other hand, the virtual photon or radiation field interaction between incident heavy-ion and atomic-electron exerts a force perpendicular in direction to that of the Coulombic interaction, since photon fields are perpendicular to $\bar{q}$. The virtual photon field is responsible for the σ_s^{t} component of the total cross-section.

Next we examine the limits of integration of the differential cross-section of Eq. (1.25) over q and w, by which integration we obtain the total cross-section of Eq. (1.28).

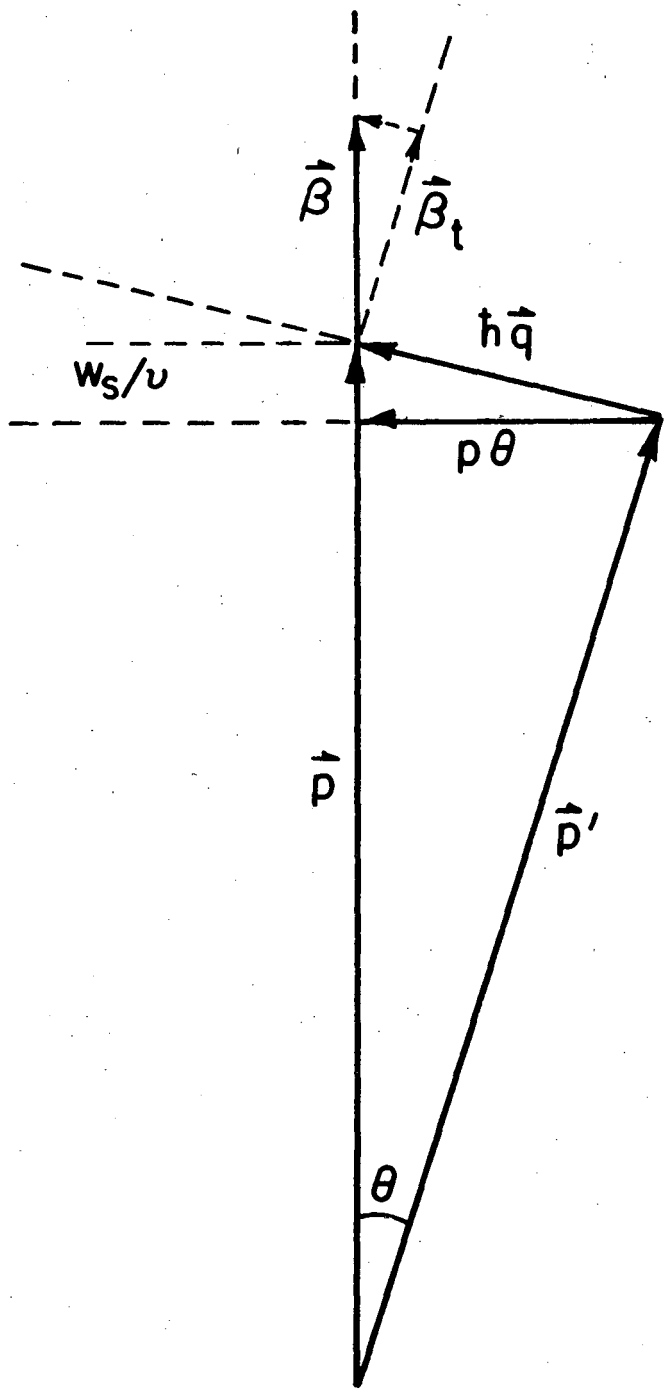

XBL 7711-6395

Fig. 1. Momentum transfer diagram in a heavy-ion inelastic collision.

To find these limits conservation of momentum and energy has to be employed. It is assumed that the energy loss of the projectile to the electron is small compared with the energy of the projectile itself. This assumption has already been used in the derivation of Eq. (1.6) in the Born approximation. Thus, if the energy loss of the projectile of mass M and energy E to the electron of mass m is w, one has:

i. For the minimum momentum transferred to the electron q_{min}:

$$\hbar^2 q_{min}^2 = 2M \left(\sqrt{E} - \sqrt{E-w}\right)^2 \simeq \frac{1}{2} M \frac{w^2}{E} \left(1 + \frac{w}{2E}\right) \tag{1.29}$$

or since $w << E$

$$q_{min}^2 = \frac{1}{2} M \frac{w^2}{\hbar^2 E} = \frac{w^2}{\hbar^2 v^2} \tag{1.30}$$

with v projectile velocity.

ii. For the maximum momentum transferred to the electron q_{max}:

$$\hbar^2 q_{max}^2 = 2M \left(\sqrt{E} + \sqrt{E-w}\right) \simeq 8\ ME \tag{1.31}$$

Without appreciable error we may in most cases set

$$q_{max} = \infty \tag{1.32}$$

It should be noted also that in the derivation of Eqs. (1.29) and (1.31) non-relativistic formalism has been used. However, these results hold true in a relativistic formalism as well. (see Appendix B)

iii. For the minimum energy transferred to the s-shell electron:

$$w_{min} = E_s \tag{1.33}$$

The energy of Eq.(1.33) is the lowest energy required for the promotion of an s-shell electron to the continuum. It has been shown[16] that the excitation to the discrete states of the atom can be taken into account by simply extending the integration over w down to the value of energy transferred when an s-shell electron is lifted to the first unoccupied level. This, however, is a small correction which can be neglected. Thus for all practical purposes E_s in Eq. (1.31) is the binding energy of the s-shell electron.

iv. For the maximum energy transferred to the electron:

$$w_{max} = E \simeq \infty \tag{1.34}$$

Equation (1.34) is true for all practical purposes.

Finally, if w is the energy transferred from the incident particle to the electron which is assumed to have been ejected into the continuum from the s-shell, then one has

$$w_s = T + E_s = \frac{\hbar^2 k^2}{2m} + E_s \tag{1.35}$$

where in Eq. (1.35) T is the kinetic energy of the ejected electron, and k its wave number.

1.5 The longitudinal cross section σ_s^{ℓ}

We shall now discuss briefly the first component of Eq. (1.26) σ_s^{ℓ} which has been studied extensively, even exclusively, for reasons already mentioned. The longitudinal cross section σ_s^{ℓ}

may be written, upon integration over q and w of the corresponding part of Eq. (1.25), in the form[5]

$$\sigma_s^{\ell} = 8\pi\, Z_1^2\, a_o^2\, Z_{2s}^{-4}\, \frac{f_s}{n_s^{\ell}} \tag{1.36}$$

where in Eq. (1.36):

Z_1 is the projectile atomic number

a_o is the hydrogen Bohr radius $\dfrac{\hbar^2}{m_e e^2} = 0.529 \times 10^{-8}$ cm

Z_{2s} is the screened atomic number of the s-shell of the target given by[17]

$Z_{2K} = Z_2 - 0.3$ for the K-shell

$Z_{2L} = Z_2 - 4.5$ for the L-shell (all three sub shells L_1, L_2, L_3).

Furthermore, in Eq. (1.36):

$$\eta_s^{\ell} = \frac{1}{2}\,\frac{m_e c^2}{Z_{2_s}^2 R_\infty}\,\beta^2 \quad , \quad R_\infty = 13.61 \text{ eV} \tag{1.37}$$

(Infinite mass Rydberg Constant)

If we assume the idealized or "Slater rule" binding energy $U_s = R_\infty Z_{2s}^2$ then η_s^{ℓ} is the ratio $\left(\frac{v}{v_s}\right)^2$ of the velocities of the incident particle and s-shell electron for low Z_2. For high Z_2 Eq. (1.35) is not equal to $\left(\frac{v}{v_s}\right)^2$ anymore but requires some relativistic correction as we will see in the examination of the transverse component of the cross section σ_s. Finally, f_s in Eq. (1.34) is essentially the double integral of the form factor of Eq. (1.23) over q and w and is a function of η_s^{ℓ}

and another quantity θ_s which is the ratio of the experimental or real binding energy E_s to the idealized or "Slater rule" binding energy so that:

$$\theta_s = \frac{E_s \; s^2}{Z_{2s}^2 \; R_\infty} \tag{1.38}$$

with s = 1 for the K-shell, s = 2 for the L-shell, etc. For strongly bound K-shell electrons of high Z_2 elements one has to take into account the relativistic effect of those electrons. Then Eq. (1.36) is modified[18] as follows:

$$\theta_K = \frac{E_K}{Z_{2K}^2 \; R_\infty} - \left[\frac{Z_{2K}}{274}\right]^2 \tag{1.39}$$

Although it is not possible to express $f_s(\eta_s^\ell \, , \, \theta_s)$ in a closed form, the following integral representation[5][19] is an alternative expression:

$$f_s \; (\eta_\sigma^\ell, \theta_s) = \int_{\theta_s}^{\infty} I \; (\eta_s^\ell, w) \; dw \tag{1.40}$$

with w in Eq. (1.40) given by

$$w \; Z_{2s}^2 \; R_\infty = T + E_s \tag{1.41}$$

which is different from Eq. (1.35) in that here w is a dimensionless quantity. In Eq. (1.38) $I(\eta_s^\ell, w)$ is given by another integral representation:

$$I(\eta_s^{\ell}, w) = \frac{Z_{2s}^2}{a_o^2} \int_{\frac{w \cdot Z_{2_s}}{\sqrt{4\eta_s^{\ell}}\, a_o}}^{\infty} |F_s(q)|^2 \frac{2q\, dq}{q^4} \tag{1.42}$$

The function $f_s(\eta_s^{\ell}, \theta_s)$ has been evaluated numerically.[5],[9]

Its numerical value as a function of the quantities η_s^{ℓ} and θ_s for s = 1 and s = 2 (K- and L-shells) has also been tabulated[19] so that one readily obtains the value of σ_s^{ℓ} by using Eq. (1.34) for a projectile of given velocity and for a given target atom with a specific shell excitation.

The ratio f_s/η_s^{ℓ} and thus the longitudinal cross section σ_s^{ℓ} of Eq. (1.36) for given projectile (Z_1) and target (Z_2) atoms has a maximum when the incident projectile velocity is near that of the Bohr orbital velocity of the s-shell electron which is ejected. Figure 2 depicts qualitatively the variation of f_s/η_s^{ℓ} or for that matter σ_s^{ℓ} with respect to the energy of the incident projectile. For all elements but the heavier ones the projectile velocity for which σ_s^{ℓ} has a maximum or $\eta_s^{\ell} = 1$ is clearly in the non-relativistic domain. As the projectile velocity increases so that $\eta_s^{\ell} > 1$ the cross-section σ_s^{ℓ} decreases until for certain $\eta_s^{\ell} >> 1$ the cross section reaches a plateau. Any further increase of η_s^{ℓ} or the velocity of the incident particle leaves the longitudinal cross-section σ_s^{ℓ} virtually unchanged (Fig. 2). On the other hand, for a given projectile energy per nucleon the cross section σ_s^{ℓ} of Eq. (1.34) is proportional to the square of the atomic number of the projectile. These two properties of σ_s^{ℓ} may

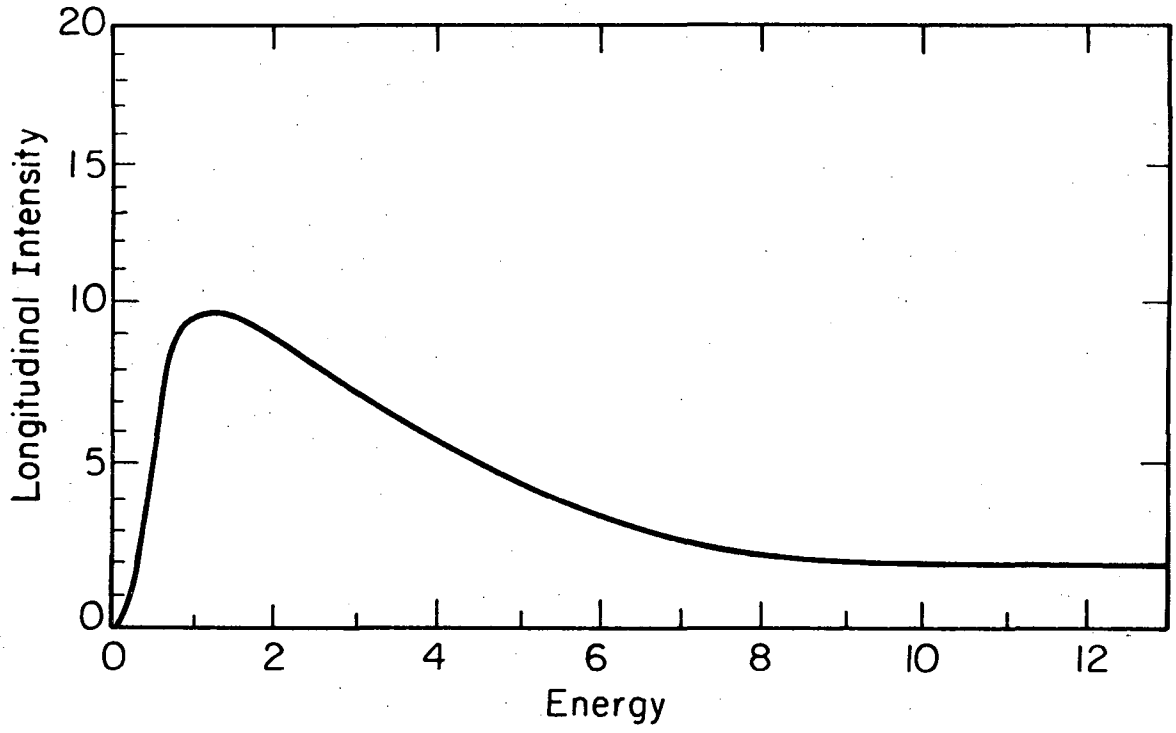

Fig. 2. Longitudinal intensity of inner shell ionization as a function of incident particle energy. The abscissa is in units of η_s. The units of intensity are arbitrary.

be summarized as follows:

The longitudinal cross section σ_s^{ℓ}

1. Has a maximum for E(projectile energy) $\simeq A_1 \frac{M}{m} E_s$

A_1 mass number of projectile, E_s electron binding energy

2. Scales as $\left(\frac{Z_1}{Z_1'}\right)^2$ for $\frac{E}{A_1} = \frac{E'}{A_1'}$, (1.43)

1.6 The transverse component σ_s^{t}

Our task now is to calculate the transverse component σ_s^{ℓ} of the total cross section of Eq. (1.26). To do so we depart from the differential expression for this cross-section given as the second term in Eq. (1.23). Our previous assumption of small energy transfer from the projectile to the electron, small being defined with respect to the energy of the incident particle (projectile), may be expressed by

$$\frac{q}{p} << 1 \tag{1.44}$$

If Eq. (1.44) holds true, then the exponential in the expression for $\bar{G}_s(q)$ can be expanded in powers of q to the lowest nonvanishing order, namely q°. This is obvious from Eq. (1.27) or in words the fact that the transverse interaction transmits one unit of odd parity with respect to reflection on the plane through $\bar{q}$ perpendicular to the $(\bar{p},\bar{p}')$ plane. The aforementioned expansion assumes that $\hbar/q$ is much larger from the linear dimension of the atomic system under consideration. That this is true, is easy to show. Consider the extreme case of w = 100 keV which can occur for K-shell ionization of elements with $E_K \sim 100$ keV or $Z \sim 90$. In that case $\hbar q = 0.33$ MeV/c and $\hbar/q \sim 600$ fm $\sim 10^{-2} r_H$. But

the K-shell electron orbits of $Z \sim 90$ elements have a radius $\sim 10^{-4} r_H$ or 100 times less. The matrix element $\bar{G}_s(q)$ reduces under the above approximation then to velocity matrix elements.[15] Thus one has:

$$|\bar{\beta}_t \cdot \bar{G}_s(q)|^2 \simeq \beta_t^2 \ |\bar{G}_s(q)|^2 \tag{1.45}$$

Furthermore, in our approximation if one equates $\bar{\alpha}_s$ with $\bar{v}_{j/c}$ Eq. (1.45) becomes[15]

$$|\bar{\beta}_t \cdot \bar{G}_s(q)|^2 \simeq \beta_t^2 \ \frac{w_s^2}{(\hbar c)^2} \ |(\Sigma_j \ y_j)_{n'n}|^2 \tag{1.46}$$

where in Eq. (1.44) Y_j are electron coordinates in the direction of $\bar{\beta}_t$. Thus one has to calculate the quantity $|(\Sigma_j Y_j)_{n'n}|^2$ which is proportional to the optical electric dipole oscillator strength for excitation from the ground level n to the level n'. Here we assume again, as has been done in the calculation of the longitudinal cross-section σ_s^{ℓ}, that the final state n' is a continuum state or in other words that the ejected electron is emitted to a continuum state. Given also that in this case the field which exerts a force on the electrons, thereby ejecting them to the continuum, is that of virtual photons, the quantity $\bar{G}_s(q)$ can be recognized as the matrix element for the photoelectric absorption of high energy photons. In other words, $|(\Sigma_j Y_j)_{n'n}|^2$ is proportional to the number of electrons emitted from an atom by high energy photons. This observation is clearly significant, since detailed calculations of the photo-electric absorption of high energy photons (x-rays) have

already been performed.[20] In the spirit of the evaluation of $F_s(q)$ for the longitudinal cross-section, non relativistic hydrogenic K-shell, L-shell electron and continuum wave functions are used for the calculation of the matrix element $|(\sum_j Y_j)_{n'n}|^2$. It should be pointed out that the electron representation by nonrelativistic wave functions is not justified for the case of the K-shell electrons of heavy atoms not only in the transverse but in the longitudinal cross-section calculation as well. Few attempts have been made to employ Dirac wave-functions in the case of the longitudinal cross-section.[22] However, the problem becomes extremely involved to be carried out analytically, and no substantial success toward a numerically calculable form of the cross-section has been achieved. For the K-shell then the matrix elements in $|(\sum_j Y_j)_K|^2$ are calculated between the nonrelativistic hydrogenic one-electron 1s wave function[22],[23] and the continuum wave function differing from the ground state by an energy w_K,[22],[23] w_K being defined by Eq. (1.35). Since the calculation is rather involved, it is not repeated here. Instead the final answer is given as follows:

$$\left|\sum_j y_{j\ K}\right|^2 = 5\times 10^{-3} \frac{(Z_2 a)^6 \exp\left[\frac{2Z_2 a}{k} \arctan\left[\frac{2Z_2 a k}{k^2 - Z_2^2 a^2 - q^2}\right]\right]}{\left[(q^2+(Z_2 a)^2+k^2)^2 - 2q^2k^2\right]^2 \left[1-\exp\left(-\frac{2\pi Z_2 a}{k}\right)\right]\left[k^2+(Z_2 a)^2\right]} \tag{1.47}$$

where in Eq. (1.47) a is the inverse of the hydrogen Bohr radius a_o, $a = \frac{1}{a_o} = \frac{m_c e^2}{\hbar^2}$.

For the L-shell each matrix element in $\left|\left(\sum_j Y_j\right)_L\right|^2$ is calculated as the square root of the sum of the squares of the matrix elements obtained between each of the four distinct nonrelativistic hydrogenic electron wave functions of the L-shell and the continuum wave function differing from the ground L-shell state by an energy w_L.[20],[24] The assumption was made that there is a common average energy transfer w_L appropriate to the several subshells of the L-shell given by Eq. (1.35). Again we omit the involved calculation of $\left|\left(\sum_j Y_j\right)_L\right|^2$ and give the final result:

$$\left|\left(\sum_j y_j\right)_L\right|^2 = 4\times 10^{-2}\ \frac{(Z_2a)^6 \exp\left[-\frac{4Z_2a}{k}\arctan\frac{k}{\left[k^2+\left(\frac{Z_2a}{2}\right)^2\right]^{1/2}}\right]}{1-\exp\left(-\frac{\pi Z_2a}{k}\right)}$$

$$\times\ \frac{\left[k^2+(Z_2a)\right]^2-\frac{(Z_2a)^4}{16}}{\left[k^2+\left(\frac{Z_2a}{2}\right)^2\right]^7} \qquad (1.48)$$

In Eq. (1.48) a is again the inverse of the hydrogen Bohr radius a_o defined earlier. Note that Z_2, in both Eq. (1.47) and Eq. (1.48), is the target atomic number. In addition in both these expressions k is the wave number of the ejected electron defined by Eq. (1.35). Notice that we have used in Eq. (1.33) a nonrelativistic expression for the kinetic energy of the ejected electron. This implies that T is rather small, nonrelativistic, despite the fact that the projectile

energy may be highly relativistic. Theoretically and also experimentally it is well established that no matter what the energy of the incident projectile is, the average kinetic energy transferred to the electron is small (less than one keV).[25] Thus, our classical expression for the kinetic energy of the emitted electron is completely justified.

We are now ready to calculate the K- and L-shell transverse cross-sections using Eq. (1.44) along with Eq. (1.45) and Eq. (1.46) in Eq. (1.23). However before we start this calculation, one small step is in order, namely the expression of β_t^2 in Eq. (1.44) in terms of known quantities. To do so we have, using Eq. (1.24)

$$\beta_t^2 = \left(\bar{\beta} - (\bar{\beta} \cdot \hat{q})\hat{q}\right)^2 = \beta^2 - (\bar{\beta} \cdot \hat{q})^2 \tag{1.49}$$

Since the component of $\bar{q}$ parallel to $\bar{p}$ and hence $\bar{\beta}$ ($\bar{p} \,//\, \bar{\beta}$) is fixed by energy conservation at

$$\hbar\, \bar{q}\cdot\bar{p} = \frac{p^2 - p'^2}{2p} + \frac{\hbar q^2}{2p} \simeq p - p' \simeq \frac{dp}{dw} w = \frac{w}{v} \tag{1.50}$$

so that

$$\bar{\beta} \cdot \hat{q} = \beta(\bar{\beta} \cdot \bar{q}) = \beta(\hat{p} \cdot \hat{q}) = \frac{\beta}{q} (\hat{p} \cdot \bar{q}) =$$

$$= \frac{\beta}{q} \frac{w}{\hbar v} = \beta \frac{q_{min}}{q} \quad , \tag{1.51}$$

where in deriving Eq. (1.51) use of Eq. (1.30) has been made.

Substitution of Eq. (1.51) into (1.49) yields then

$$\beta_t^2 = \beta^2 \left(1 - \frac{q_{min}^2}{q^2}\right) \tag{1.52}$$

Combining Eqs. (1.25),(1.46) and (1.52) we obtain for the transverse cross-section σ_s^t the general formula:

$$\sigma_s^t = 8\pi Z_1^2 \left(\frac{e^2}{\hbar v}\right)^2 \int_{w_{min}=E_s}^{w_{max}=\infty} dw_s \int_{q_{min}=\frac{w}{\hbar v}}^{q_{max}=\infty} dq \; \frac{2q\beta^2}{\left[q^2-\left(\frac{w_s}{\hbar c}\right)^2\right]^2} \left(1-\frac{q_{min}^2}{q^2}\right)\left(\frac{w_s}{\hbar c}\right)^2 \left|\left(\sum_j y_j\right)_s\right|^2 \tag{1.53}$$

where in Eq. (1.53) use of Eqs. (1.30) through (1.34) has been made in order to establish the limits of integration w and q. We can now evaluate Eq. (1.53) for s being the K-shell and the L-shell separately using the results of Eqs. (1.47) and (1.48) respectively.

1.7. The K-shell transverse cross-section σ_K^t

For the K-shell vacancy transverse cross-section σ_K^t, we substitute Eq. (1.47) into Eq. (1.53) and obtain

$$\sigma_K^t = 8\pi Z_1^2 \left(\frac{e^2}{\hbar v}\right)^2 \int_{E_K}^{\infty} dw_K \int_{\frac{w_K}{\hbar v}}^{\infty} dq \; \frac{2q\beta^2\left(1-\frac{q_{min}^2}{q^2}\right)\left(\frac{w_K}{\hbar c}\right)^2}{\left[q^2-\left(\frac{w_K}{\hbar c}\right)^2\right]^2} \times$$

$$\times 5 \times 10^{-3} \quad \frac{(Z_2 a)^6}{\left[k^2 + (Z_2 a)^2\right]}$$

$$\times \frac{\exp\left[\frac{2Z_2 a}{k} \arctan\left[\frac{2Z_2 a k}{(k^2 - (Z_2 a)^2 - q^2)}\right]\right]}{\left[(q^2 + (Z_2 a)^2 + k^2)^2 - 2q^2 k^2\right]^2 \left[1 - \exp\left(-\frac{2\pi Z_2 a}{k}\right)\right]} \qquad (1.54)$$

We now proceed to calculate the double integral of Eq. (1.54). To do so we effect the substitutions

$$x = \frac{q_{min}^2}{q^2} \qquad y = \frac{k^2}{(Z_2 a)^2} \qquad (1.55)$$

In other words we change variables in Eq. (1.55) from (q,w) to (x,y) via the transformation of Eq. (1.5) Under this transformation Eq. (1.54) can be written in the form[25]

$$\sigma_K^t = 8\pi Z_1^2 \beta^2 \left(\frac{e^2}{\hbar c}\right)^2 5 \times 10^{-3} a_o^2 g_K(\eta_K^t, \beta^2) \qquad (1.56)$$

where in Eq. (1.54) $a_o = \frac{1}{a}$ = hydrogen Bohr radius and the quantity $g_K(n_K^t, \beta^2)$ is a function defined by the integral expression:

$$g_K(\eta_K^t, \beta^2) =$$

$$= \int_{y=1}^{\infty} dy \int_{x=o}^{1} dx \; \frac{(1-x)}{(1-\beta^2 x)^2 (1+y)} \; \frac{\exp\left[\frac{2}{\sqrt{y}} \arctan\left(\frac{2\sqrt{y}}{y-1-Q}\right)\right]}{\left[1 - \exp\left(-\frac{2\pi}{\sqrt{y}}\right)\right]\left[(Q+1+y)^2 - 2yQ\right]^2} \qquad (1.57)$$

In Eq. (1.55) we have called for simplicity $Q = \frac{(1+y)^2}{4x\,\eta_K^t}$ and η_K^t is defined by

$$\eta_K^t = \frac{\beta^2}{2(\gamma_K - 1)} = \frac{mc^2}{2E_K}\,\beta^2 = \frac{mc^2}{2Z_2^2 R_\infty}\,\beta^2 \qquad (1.58)$$

γ_K being the relativistic gamma factor of the ejected K-shell electron with binding energy E_K. The equivalence of the first two expressions for η_K^t in Eq. (1.56) arises from the fact that the kinetic energy of the bound electron in the K-shell is equal to its binding energy in that shell. From Eq. (1.56), we observe also that for low kinetic energies of the bound electron, i.e. low Z_2 elements, η_K^t reduces to the classical expression $\eta_K^t = \frac{\beta^2}{\beta_K^2} = \left(\frac{v}{v_K}\right)^2$ with v_K the velocity of the electron in its K-shell orbit. For this low Z_2 ($Z_2 \leq 40$) limit η_K^t becomes equal to η_K^ℓ of Eq. (1.37) in the longitudinal component of the cross-section. The third expression for η_K^t in Eq. (1.36) is valid if we assume that the binding energy E of the K-shell electrons is given by the hydrogen atom type of formula $Z_2^2\, R_\infty$ where Z_2 is the real atomic number of the target element. No Slater rule[11] type of correction has been introduced in the calculation of the transverse

component, in contrast to the calculation of the longitudinal component. Furthermore the equivalence of the third expression in Eq. (1.56) to the other two of the same equation implies that $\theta_K = 1$, θ_K having been defined by Eq. (1.37). Although this assumption is true only for the heaviest of the elements, it is nonetheless necessary for the further evaluation of the function g_K. In other words what this approximation does is that it reduces the variables of g_K in Eq. (1.57) from three to two so that

$$g_K(n_K^t, \theta_K, \beta^2) \longrightarrow g_K(n_K, \beta^2) \tag{1.59}$$

Since the integrals in Eq. (1.57) cannot be carried out analytically, one has to tabulate the values of the function g_K. Obviously, from this point of view two variables are by far more desirable than three, when one has to construct tables of values of a quantity as a function of its independent variables. As mentioned already, θ_K approaches one as Z_2 becomes large (> 70) so that the higher the Z_2 of the target the better the approximation. The result of our approximation in the numerical value of Eq. (1.55) is that it makes it smaller since the lower limit of y in it is equal to 1 instead of a little smaller. Finally, we may use in Eq. (1.56) either the real value of the binding energy or the value $Z_2^2 R_\infty$ which is normally bigger than the former. In the latter case one gets a smaller η_K^t and thus a smaller cross-section, given that g_K is an increasing function of η_K^t. That g_K^t is an increasing function of η_K^t can be seen in Fig. 3, where the general behavior of g_K as a function of η_K^t for β constant,

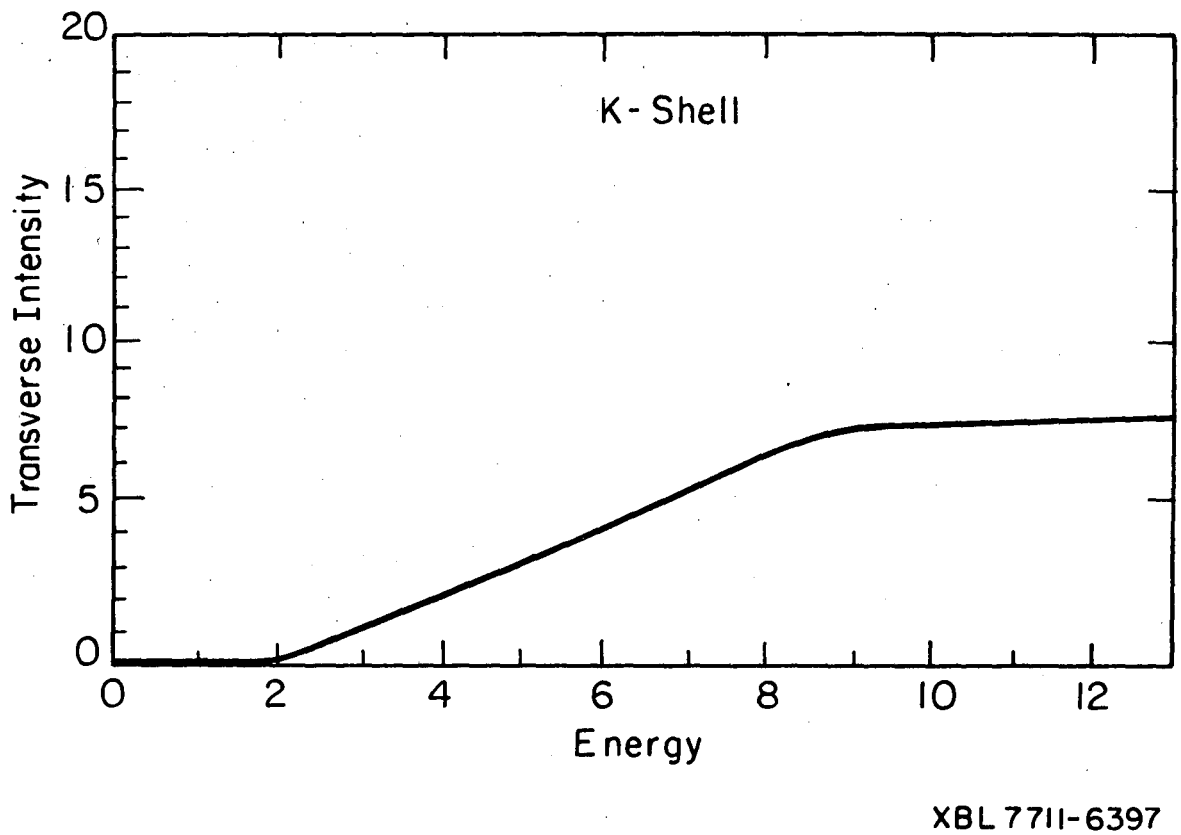

Fig. 3. Transverse intensity of the K-shell ionization as a function of incident particle energy. The abscissa is in units of η_K. The units of intensity are arbitrary.

approximately equal to one, is depicted schematically.

At any rate, substituting into Eq. (1.56) all the numerical values of the constants one gets the equation

$$\sigma_K^t = 1.889 \times 10^2 \, Z_1^2 \, \beta^2 \, g_K(n_K^t, \beta^2) \quad \text{(barns)} \tag{1.60}$$

The values of g_K as a function of η_K^t and β^2 have been tabulated and are given in a format similar to the one for the longitudinal function $f_s^{(19)}$ in Appendix A. Also, for the sake of illustration Figs. 4,5, and 6 depict schematically the variations of all three cross-sections σ_K, σ_K^ℓ, and σ_K^t as functions of the energy of the incident projectiles, assumed to be protons ($Z_1 = 1$) for three target atoms Ca ($Z_2 = 20$), Mo ($Z_2 = 42$), and Pb ($Z_2 = 82$), respectively.

A final remark about the variation of σ_K^t with respect to the velocity of incident particle is in order. From Eqs. (1.57) and (1.55) we note that for $\beta \to o$ or $\beta << 1$

$$\sigma_K^t \propto \beta^2 \tag{1.61}$$

which verifies that σ_K^t is negligible for low velocity projectiles. This can also be seen schematically in Figs. 4, 5 and 6. Furthermore for very high incident velocities g_K reaches a plateau and essentially remains constant so that the cross-section σ_K^t stops increasing beyond certain point, as can be seen again in the same figures. The dependence of σ_K^t on the atomic number Z_1 of the incident particle is, in our approximation, the same as for σ_K^ℓ, namely, proportional to Z_1^2.

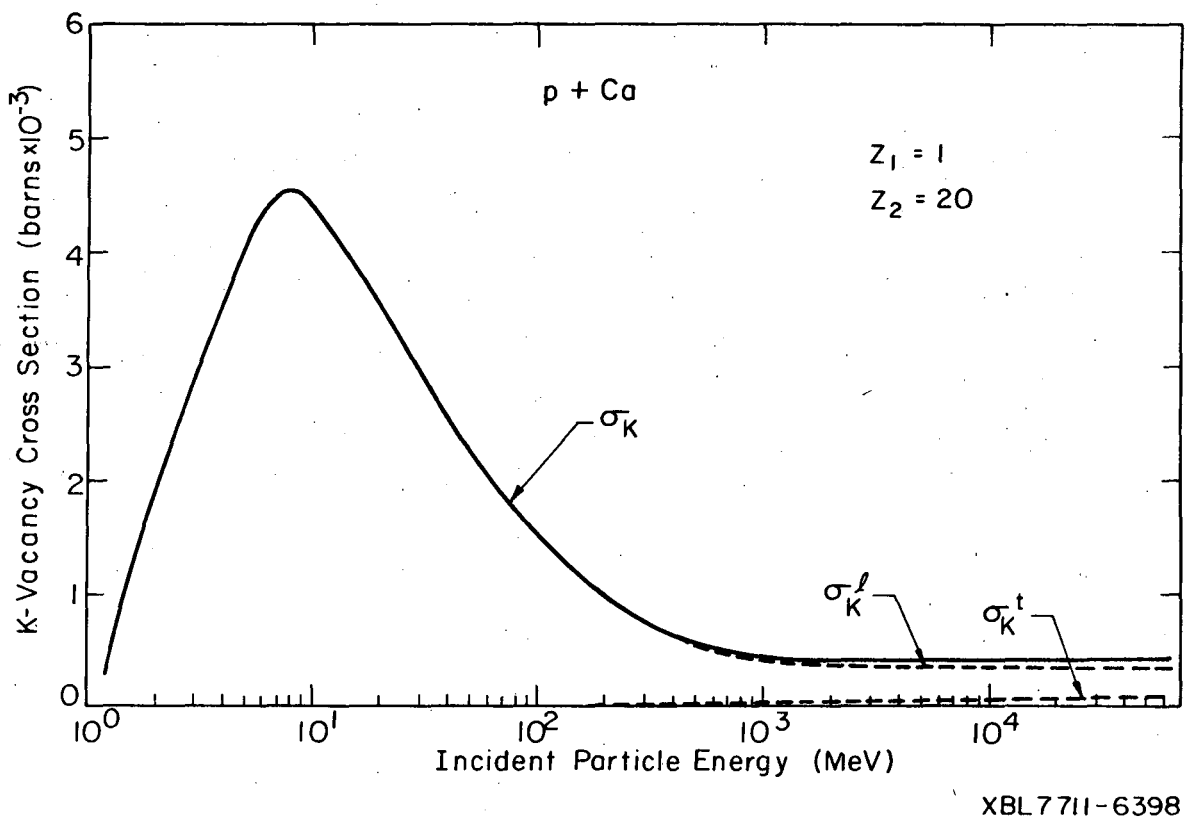

Fig. 4. K vacancy production cross section for protons on Ca. The total cross section σ_K is the sum of the longitudinal $\sigma_K{}^\ell$ and transverse $\sigma_K{}^t$ cross sections.

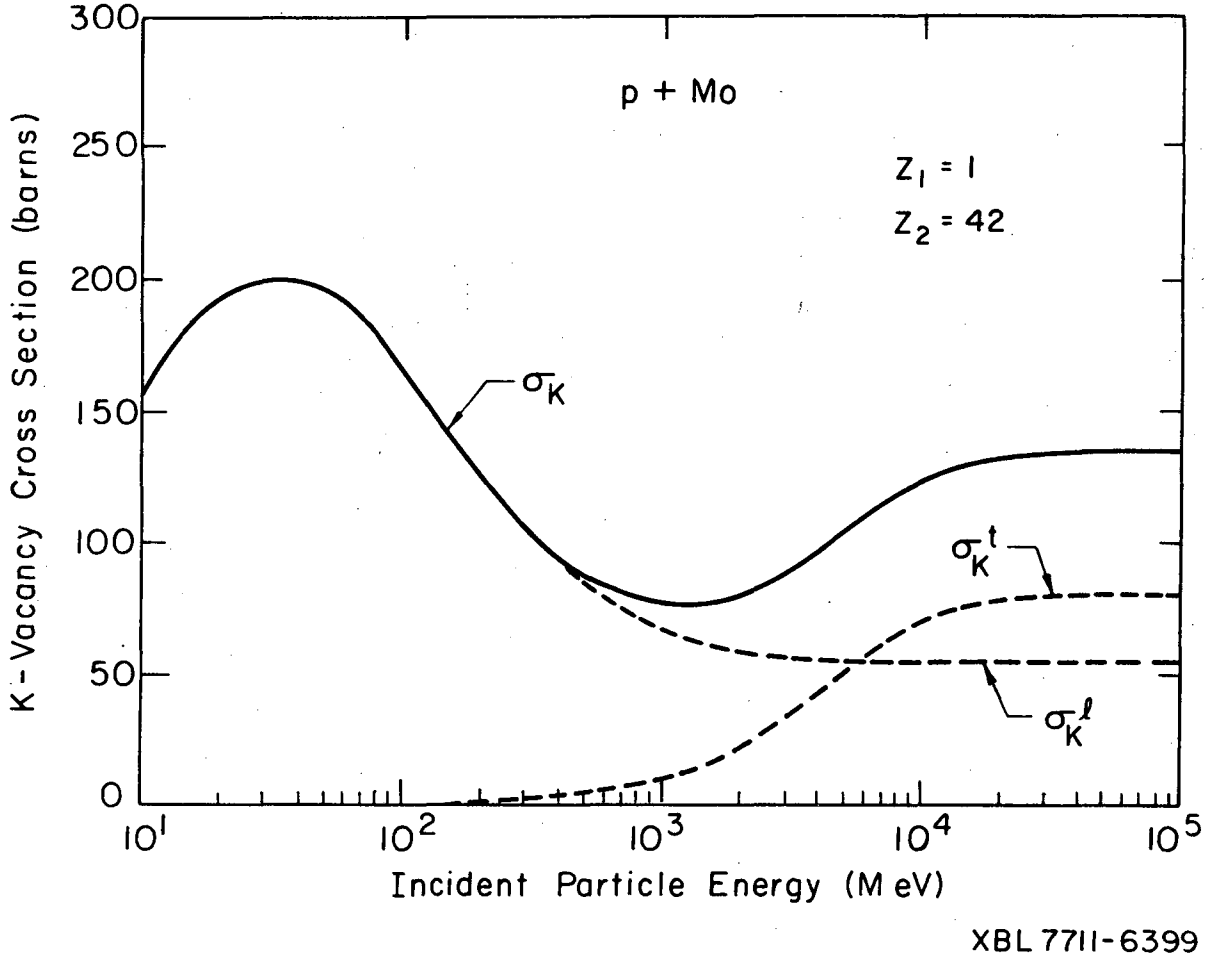

Fig. 5. K vacancy production cross section for protons on Mo. The total cross section σ_K is the sum of the longitudinal σ_K^{ℓ} and transverse σ_K^{t} cross sections.

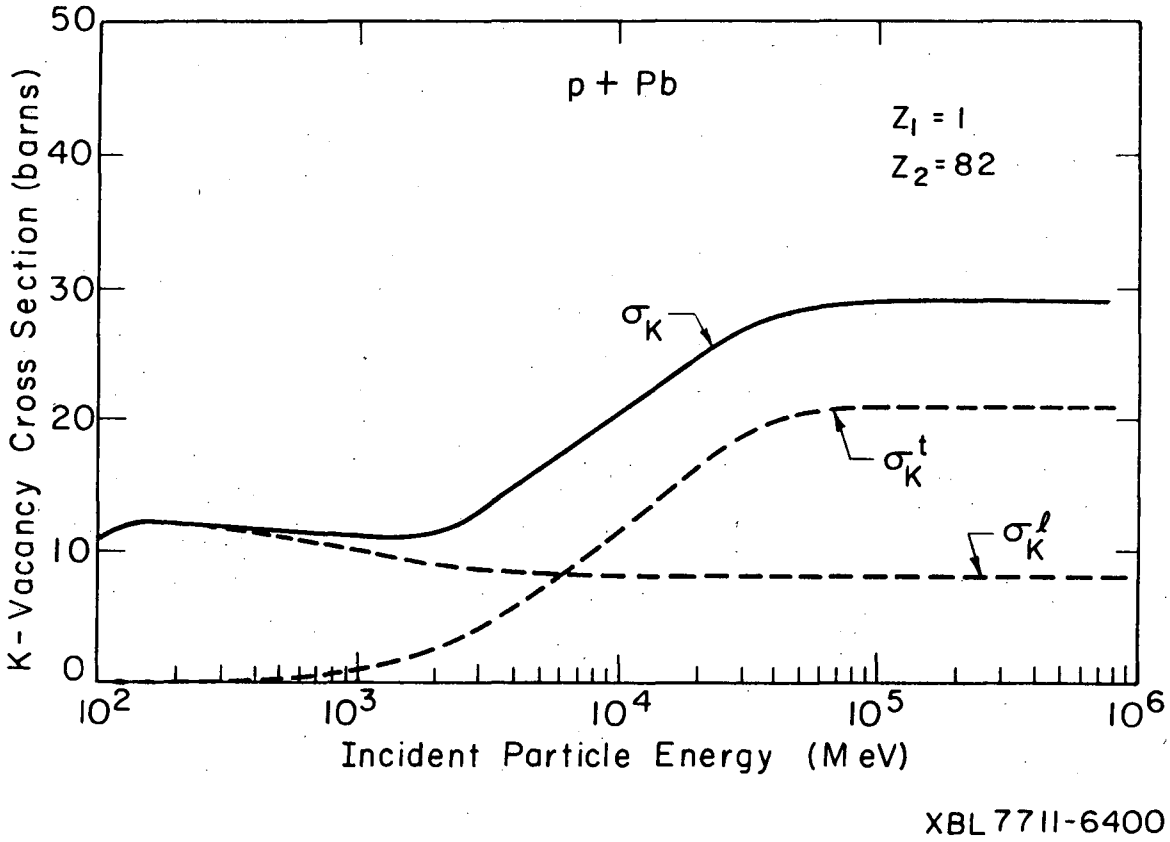

Fig. 6. K vacancy production cross section for protons on Pb. The total cross section σ_K is the sum of the longitudinal σ_K and transverse $\sigma_K{}^t$ cross sections.

1.8 The L-shell transverse cross-section σ_L^t

Again by substitution of Eq. (1.48) into (1.53) we obtain

$$\sigma_L^t = 8\pi Z_1^2 \left(\frac{e^2}{\hbar v}\right) \int_{E_L}^{\infty} dw_L \int_{\frac{w_L}{\hbar v}}^{\infty} dq \; \frac{2q\beta^2\left(1-\frac{q^2_{min}}{q^2}\right)\left(\frac{w_L}{\hbar c}\right)^2}{\left[q^2-\left(\frac{w_L}{\hbar c}\right)^2\right]^2}$$

$$\times \frac{4\times 10^{-2}\times (Z_2 a)^6 \exp\left[-\frac{4Z_2 a}{k}\arctan\left[\frac{k}{\left[k^2+\left(\frac{Z_2 a}{2}\right)^2\right]^{1/2}}\right]\right]\left[k^2+(Z_2 a)^2-\left(\frac{Z_2 a}{2}\right)^4\right]}{\left[1-\exp\left(-\frac{\pi Z_2 a}{k}\right)\right]\left[k^2+\frac{(Z_2 a)^2}{4}\right]^7} \qquad (1.62)$$

where Eq. (1.62) gives the total cross-section for excitation in all three subshells L_1, L_2, L_3 of the L-shell. E_L is then the average of the binding energy over all the subshells of the L-shell.[19]

Making once more use of the transformation of Eq. (1.55) in Eq. (1.62), we obtain for σ_L^t

In Eq. (1.63) we have for $g_L(\theta_L, \beta^2)$ the integral expression

$$\sigma_L^t = 8\pi Z_1^2 \left(\frac{e^2}{\hbar v}\right)^2 \beta^2 \times 4\times 10^{-2} \times a_o^2 \; g_L(\theta_L, \beta^2) \qquad (1.63)$$

$$g_L(\theta_L,\beta^2) =$$

$$= \int_0^1 \frac{(1-x)}{(1-\beta^2x^2)^2}\,dx \int_{\theta_{2/4}}^{\infty} \frac{\exp\left[-\frac{4}{\sqrt{y}}\arctan\frac{\sqrt{y}}{(y+1/4)^{1/2}}\right]\left[(y+1)^2-\frac{1}{16}\right]}{(y+\frac{1}{4})^7\left[1-\exp(-\frac{\pi}{\sqrt{y}})\right]}\,dy \tag{1.64}$$

We observe that Eq. (1.64) does not depend on η_L^t and thus can be separated into the x and y parts. Also θ_L is the screening factor for the L-shell as defined in Eq. (1.36). The x integral in Eq. (1.61) is double so that one obtains for it

$$\int_o^1 \frac{(1-x)}{(1-\beta^2x)^2}\,dx = \frac{\ell n\gamma^2-\beta^2}{\beta^4} \tag{1.65}$$

The y integral cannot be done analytically, and in any case is a function of θ_L. If in the spirit of the θ_K^t calculation we assume again that $\theta_L = 1$ or that the binding energy of the L-shell electrons is on the average given by $Z_2^2 R_\infty/4$, we have

$$\int_1^{\infty} \frac{\exp\left[-\frac{4}{\sqrt{y}}\arctan\frac{\sqrt{y}}{(y+1/4)^{1/2}}\right]\left[(y+1)^2-\frac{1}{16}\right]}{(y+1/4)^7\left[1-\exp\left(-\frac{\pi}{\sqrt{y}}\right)\right]}\,dy \simeq 1.69\times10^{-2} \tag{1.66}$$

where in Eq. (1.65) the integral has been calculated numerically. Combining Eqs. (1.64) and (1.65) with Eq. (1.62), we obtain after substitution of the various constants by their numerical values

$$\sigma_L^t = 0.254 \times 10^2 \, Z_1^2 \, \frac{\ell n\gamma^2 - \beta^2}{\beta^2} \quad \text{(barns)} \tag{1.67}$$

for the average L-shell vacancy transverse cross-section.

We examine briefly the properties of σ_L^t as given by Eq. (1.64). The variation of σ_L^t with respect to the atomic numbers of projectile Z_1 and target Z_2 is the same as for all others cross-sections σ_K^ℓ, σ_L^ℓ, σ_K^t. For very small β, we can easily establish that $\frac{\ell n\gamma^2}{\beta^2} \to 1$ as $\beta \to 0$ so that $\sigma_L^t \propto \beta^2$. Thus again σ_L^t is essentially negligible for small projectile velocities as is σ_K^t. However for higher projectile velocities there is a difference between σ_K^t and σ_L^t. This difference is that while σ_K^t, as we already saw, increases rapidly with projectile velocity to reach a plateau after certain velocity and remain constant thereafter, σ_L^t increases as $\ell n\gamma$ with projectile energy so that eventually for very relativistic energies σ_L^t overtakes σ_K^t, becoming infinite. This rather unphysical result is due to the fact that the original Born approximation breaks down for energies higher than the GeV range.[15] However, there is no problem for projectile energies of the order of several tens of GeV per nucleon which in any case are yet to be attained experimentally for all heavy-ions with the exception of protons.

II. MEASUREMENT OF K-VACANCY PRODUCTION BY RELATIVISTIC HEAVY IONS

2.1 Introduction

Investigations of inner-shell vacancy production by heavy ions have been carried out for almost 50 years. However, it is only during the last 15 years or so that experimental and theoretical results have provided a cohesive picture of the phenomena under consideration. This is due on the one hand to the application of experimental techniques new to this area and on the other hand to the refinement of various relevant theoretical calculations .

In the last decade particularly, much effort has been devoted to measuring the inner-shell vacancy cross sections by protons and alpha particles. Both K- and L- x-ray measurements have been made, although the more complicated structure of the L-shell with three subshells L_1, L_2, and L_3 makes x-ray measurements related to L x-rays a much more difficult task than K x-ray measurements.[45]

In most measurements up to now the energy per nucleon of the projectiles (protons and alphas) has been ranging from 15 keV to 30 MeV. There exists also a measurement with 160 MeV protons.[27] The targets involved have ranged from helium to uranium.

From the previous theoretical development in this work it has been concluded that the inner-shell vacancy cross section by heavy ions starts to rise as the projectile energy becomes relativistic. Although there is no clear-cut lower limit between non relativistic and relativistic projectile energy, we set it rather arbitrarily at 150 MeV per nucleon of the incoming projectile. Thus, in order to examine the

validity as well as agreement with reality of the previously developed inner-shell vacancy production theory we must use projectiles of energy in the vicinity of a few hundred MeV per nucleon at least, and possibly move into the GeV per nucleon domain. As mentioned earlier, up until recently (1972) no accelerator existed that could accelerate heavy ions into the Gev per nucleon energy range. It was therefore the creation of the Bevalac facility of the Lawrence Berkeley Laboratory which partially motivated the present work. On the other hand similar measurements using as projectiles relativistic electron beams have been performed[28] and a theory which can account for the measured K-shell vacancy production has been developed.[29] In the case of relativistic electron beam excitation it was found that the K-shell vacancy production cross-section could be described as a sum of two terms. One term is due to the Moller scattering or interaction[30] for close collisions and is present at any projectile electron energy, relativistic or non relativistic. The other term is due to the virtual photon field of the relativistically moving projectile electrons and obviously is significant only at relativistic electron energies.[47] It becomes now apparent that there is an analogy between the electron and heavy-ion ionization, so that experiments with relativistic heavy-ions were rather imperative at this point. It is worth noting that no significant deviation of the experimental K-shell vacancy production cross-section from the thoretical one by the 160 MeV protons, attributable to the high energy of the proton projectiles, could be observed.[27] Apparently the energy of 160 MeV for proton projectiles is around the threshold of the contribution of the transverse component of the

cross section to its total value.

Thus the measurement of the K-shell vacancy cross section was undertaken at two energies and with two different projectiles. No L-shell vacancies were measured due to the inherent difficulty of such a measurement compared with the K-shell vacancy.

2.2 Measurement of the K-shell vacancy cross section

The characteristic radiation of x-rays emitted when a K-shell electron vacancy is filled by an outer shell was measured. Depending on the origin of the electron filling the K-shell vacancy which was produced by the incident heavy-ion, two groups of K x-rays are obtained, namely Kα and Kβ. The Kα x-rays are emitted when the K-shell vacancy is filled by an electron originating from the L-shell. The Kβ x-rays are emitted when the K-shell vacancy is filled by an electron coming from either the M-shell or N-shell of the atom provided that the atom is heavy enough to have electrons occupying any of the M- or N-shell. Furthermore the Kα line is split into the $K\alpha_1$ and $K\alpha_2$ depending on whether the L-shell electron filling the vacancy originates in the L_3 or L_2 subshell, respectively. Similarly the Kβ line is split into $K\beta_1$, $K\beta_2$, and $K\beta_3$, $K\beta_4$, and $K\beta_5$ emitted when the transition electron comes from the M_3, N_3, M_2, N_2, and M_4 subshells, respectively.[31] Other transitions, for instance from L_1 to K, are forbidden by the relevant selection rules.[48] Energetically the $K\alpha_1$ line lies higher than the $K\alpha_2$ line, while normally the $K\beta_1$, $K\beta_3$, and $K\beta_5$ are combined into a line called $K\beta_1'$, and $K\beta_2$ and $K\beta_4$ into the $K\beta_2'$, which is more energetic than the $K\beta_1'$. The combination of the five Kβ lines into

two is due to the fact that the lines in each of the $K\beta_1'$ and $K\beta_2'$ groups are so close in energy that they are essentially unresolved. Finally all the Kβ lines are higher in energy than the Kα lines, as can be deduced from the corresponding electron transitions. In our measurements we obtained the Kα and Kβ lines resolved for all target elements. However, only for target elements with atomic number greater than 60 could we partially resolve the $K\alpha_1$ and $K\alpha_2$ lines of the Kα line as well as the $K\beta_1'$ and $K\beta_2'$ lines of the Kβ line. By "partially resolve" here we mean partially overlapping peaks of the corresponding lines, $K\alpha_1$ and $K\alpha_2$, $K\beta_1$ and $K\beta_2$, in the x-ray spectrum. Obviously the degree of resolution of the Kα and Kβ x-rays does not bear any significance on the measured cross sections, since we are interested in the total K-shell vacancy cross-section, which is the sum of all partial (Kα, Kβ) cross sections.

To a good approximation the emitted x-ray radiation is isotropically distributed. This point has been investigated and found valid for L x-rays from gold[5] and K x-rays from various targets excited by high energy electron beams.[28] Hence, a target element (Z_2,A_2) will give rise to a number of K x-ray counts n_{K_i} in a detector occupying a solid angle of $\Delta\Omega$ steradians, which is given by

$$n_K = \sigma_K^{vac}\ \omega_K\ N_1 \frac{\rho_2 t_2 No}{A_2}\ \frac{\Delta\Omega}{4\pi}\ \varepsilon_{d_K}\ C_K \qquad (2.1)$$

where in Eq. (2.1) σ_K^{vac} is the K-shell vacancy production cross section, ω_K is the fluorescent yield, N_1 the number of incident heavy ion projectiles (Z_1,A_1), p_2 and t_2 target density and linear thickness respectively, N_o is Avogadro's number 6.022531×10^{23} mol^{-1}, ε_{d_K} is the efficiency of the detector, and C_K is the absorption reduction factor of the emitted K x-rays while traveling through the target, air, external absorbers etc. The last two quantities, ε_{d_K} and C_K, depend on the energy of the detected K x-ray, as will be seen shortly. If the K peak in the spectrum is resolved into Kα and Kβ lines or even further into $K\alpha_1$, $K\alpha_2$, $K\beta_1'$, and $K\beta_2'$ lines, as described earlier, then Eq. (2.1) is applied for each of these lines individually and the cross section σ_K^{vac} can be determined from each of these lines separately. Obviously all lines should yield the same value for σ_K^{vac}. In our case the K line is always resolved into the Kα and Kβ lines, while further resolution of the Kα and Kβ peaks occurs somewhat for heavier elements. However since this latter resolution is not complete because the Kα, and $K\alpha_2$ or the $K\beta_1'$ and $K\beta_2'$ lines partially overlap with each other in every case, we consider always the two peaks Kα and Kβ, so that Eq. (2.1) can be modified to

$$n_{K_i} = \sigma_K^{vac}\ \omega_K\ N_1\ \frac{\rho_2 t_2 N_o}{A_2}\ \frac{\Delta\Omega}{4\pi}\ \varepsilon_{d_{K_i}}\ C_{K_i} \qquad (2.2)$$

with i being either α or β.

Thus, for a given peak n_{K_i} can be determined from its spectrum while the rest of the quantities in Eq. (2.2) except for σ_K^{vac} are either known such as ω_K or can be measured independently such as $N_1, p_2, t_2, \Delta\Omega, \varepsilon_{d_{K_i}}$ or can be calculated, such as C_{K_i}.

The objective of the experiment then is to measure, determine, or calculate all quantities involved in Eq. (2.2). Hence, the value of σ_K^{vac} can be determined for a multitude of targets and a variety of projectiles with their respective energies.

In what follows we examine first the experimental set-up and then the way by which the magnitudes of the various quantities in Eq. (2.2) were measured, so that a value of the K vacancy production cross section could be obtained for a given target and a projectile of certain incident energy. Specifically, two types of projectiles were used. A 4.80 GeV proton (p) beam and a 250 MeV/N or 3 GeV total energy Carbon ion (^{12}C) beam. The targets used in both cases varied from elements with atomic numbers in the vicinity of 20 up to uranium.

2.3 Experimental Set-up

The experimental configuration used for both the 4.8 GeV protons and the 3 GeV carbon ions was the same. It is schematically illustrated in Fig. 7. The incident particle beam (protons or carbons) from the Lawrence Berkeley Laboratory Bevatron/Bevalac facility passed through:

1. An Ag (silver) monitor foil of 0.0254 mm in thickness.
2. A target foil varying from 0.0060 to 0.0508 mm in thickness for various elements.
3. A scintillation paddle.

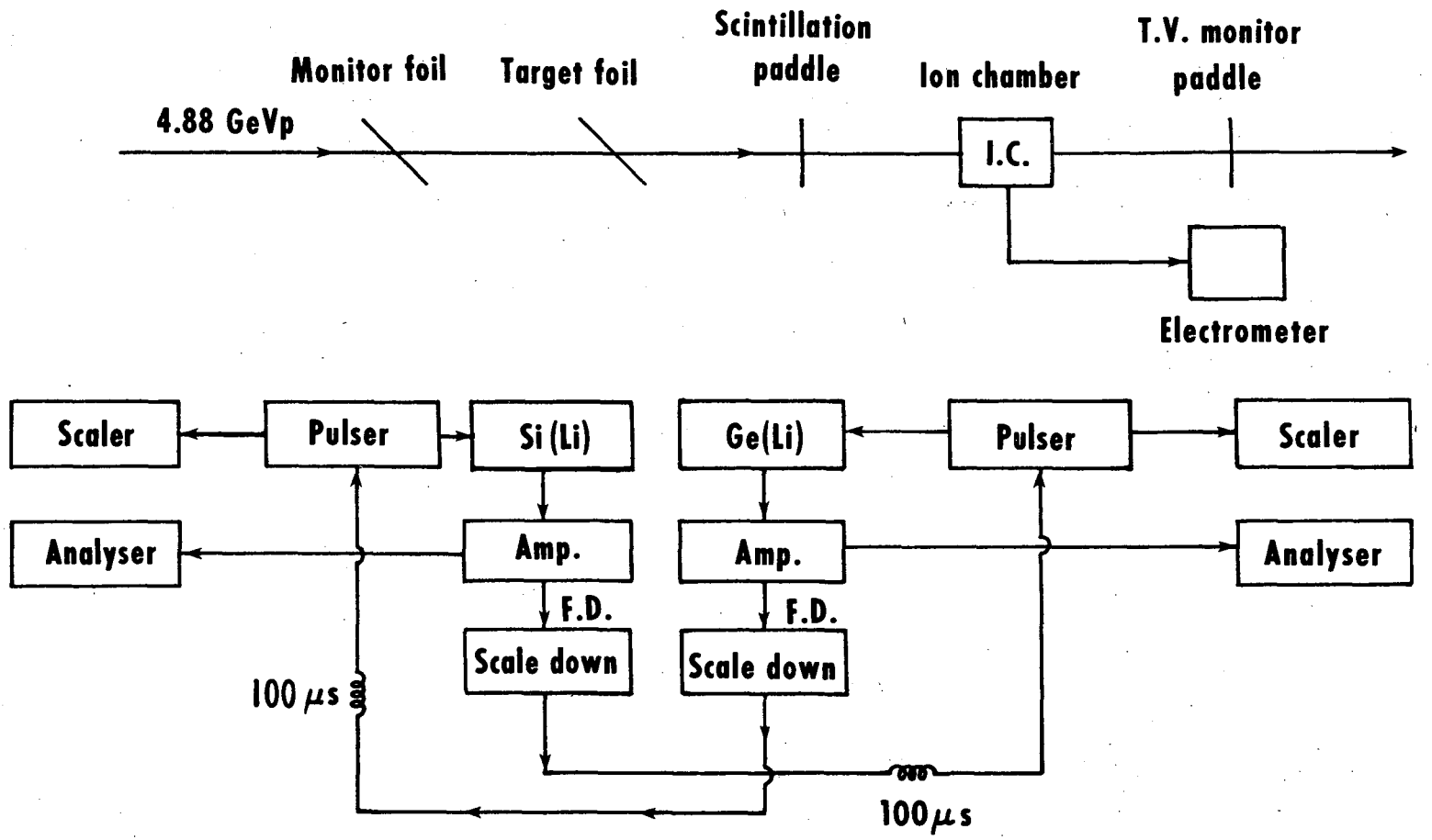

Fig. 7. Schematic diagram of experimental setup.

XBL759-3992

4. An ion chamber

5. A T.V. monitor paddle

The beam loss going through all five elements with a total thickness of at most several tens of mg/cm^2 was negligible.

Two detectors were used for the detection of the produced x-rays. A lithium-drifted silicon Si(Li) detector placed on the side of the target at the same horizontal level with it, viewed the target at right angles to the incoming beam. A second planar lithium-drifted germanium Ge(Li) detector placed under the target vertically and facing upward, viewed the target again at right angles to the beam. The use of semiconductor detectors for the low energy (below 100 keV) electromagnetic radiation detection was rather essential. The nature of conversion of the incident radiation into an electrical pulse by them results in a greatly improved resolution as well as efficiency[32] over other kinds of scintillators at the low energy x-ray spectra we are concerned with.

The target was tilted vertically by 45° and then rotated by 45 degrees; in other words, there was made a first rotation about a horizontal axis by 45 degrees and a second rotation about a vertical axis by 45 degrees with both axes perpendicular to the beam direction through its imaginary center. The purpose of these two rotations was that the normal on the target's surface formed a 45 degree angle with the plane of the face of either one of the two detectors. Such a configuration is a most desirable one from the point of uniformity of the solid angle of emission of the x-rays. Under these rotations then the direction of the beam formed a 30 degree angle with the plane of the target or a

60 degree angle with the normal on it. Knowledge of the angle of rotation of 45 degrees was essential in determining the self-absorption of x-rays in the target, while that of the beam incidence angle of 60 degrees was necessary in the determination of the effective target thickness, as will be seen later.

The Ag monitor foil was placed 10 cm upstream from the target perpendicular to the beam and was viewed by both the Si(Li) and Ge(Li) detectors. The angles of the viewing of each detector at the Ag monitor foil were calculated by measuring the distances from the center of the plane face of each detector to the center of the Ag foil and the incoming beam direction. Those angles were again necessary for determining the effective thickness of the Ag foil as was seen by the x-rays produced in it and detected by either of the two detectors. The significance of the presence of Ag foil was that it could be used to minimize the errors of the measurement of the K vacancy production cross section of the target elements, as will be described in the sequel.

The ion chamber was coupled to an electrometer and integrator to integrate the relative beam intensity from run to run. Thus, one could determine the charge going through the ion chamber. Besides this relative beam intensity calibration, the ion chamber readings were in conjunction with the dead time correction, as will be seen shortly.

The T.V. monitor was intended to constantly observe the beam spot position on the screen from drifting due to accidental change of the magnetic fields of the quadrupole magnets upstream from the target

position. The beam spot position on the screen corresponded to a beam going exactly through the aligned centers of the Ag foil and the target and was determined at the beginning of each run by placing a polaroid film on the target and exposing it to a few beam bursts. Normally two to three film exposures were necessary before the beam could be focused to the center of the target by the operators of the accelerator following the instructions given to them after each film exposure.

The beam itself had a diameter of approximately 2 cm and was coming in bursts of one second duration every five seconds on the average.

The count rate was rather high, of the order of three to four thousand counts per beam burst. It was therefore essential that a means of correcting our data for deadtime had to be devised. In our case the following rather simple procedure called the "crossed" detector trigger system" was adopted. This can be schematically seen in Fig. 7. Each of the two detectors fired a fast discriminator which supplied one pulse every hundred pulses to trigger a pulser on the other detector. Each pulse triggering the pulser of the other detector was delayed for approximately 100 μs prior to doing so. The number of pulses triggered were thus recorded in the spectrum along with the x-rays counted at the same time.

The data taking system consisted primarily of a Hewlett-Packard 4096 channel pulse height analyzer with the spectra recorded on magnetic tape by a Kennedy 1510 magnetic tape drive system.[33] Also

a Northern Scientific 1024 channel pulse height analyzer was occasionally used with data again recorded on magnetic tape.[34]

2.4 K x-ray Counts Measurement

As mentioned earlier, in order to calculate the K vacancy production cross section σ_K^{vac} from Eq. (2.2) or Eq. (2.1) one has to determine the number of counts n_{K_i} under the peak of the line K_i in the obtained spectrum. Typical spectra appear in Figs. (8) through (12). Obviously, for a given peak one can determine the area under the peak after subtracting the appropriate background, which in the case of our spectra is rather apparent, and thus obtain the number of counts corresponding to that peak of the spectrum. The determination of the area under the given peak or line of the x-rays can be done most easily if, for instance, one knows the total number of counts in each channel over which the peak under consideration extends. By subtracting the appropriate background counts from the total counts of each channel one obtains the net number of counts in each channel. Then by adding all the numbers of net counts, for each channel one obtains the total number of counts under the peak or line of the spectrum which is being examined.

If, however, the count rate during the experiment is rather high, one is confronted with the problem of deadtime. In other words, the counts calculated under any given time of the spectrum are not the real ones but smaller by a certain factor, the so called deadtime correction factor. This deadtime correction factor takes into account the fact that the detector while counting an event remains inactive for a short period of time during which if other x-ray photons arrive at the detector, they will not be counted. The higher then the counting

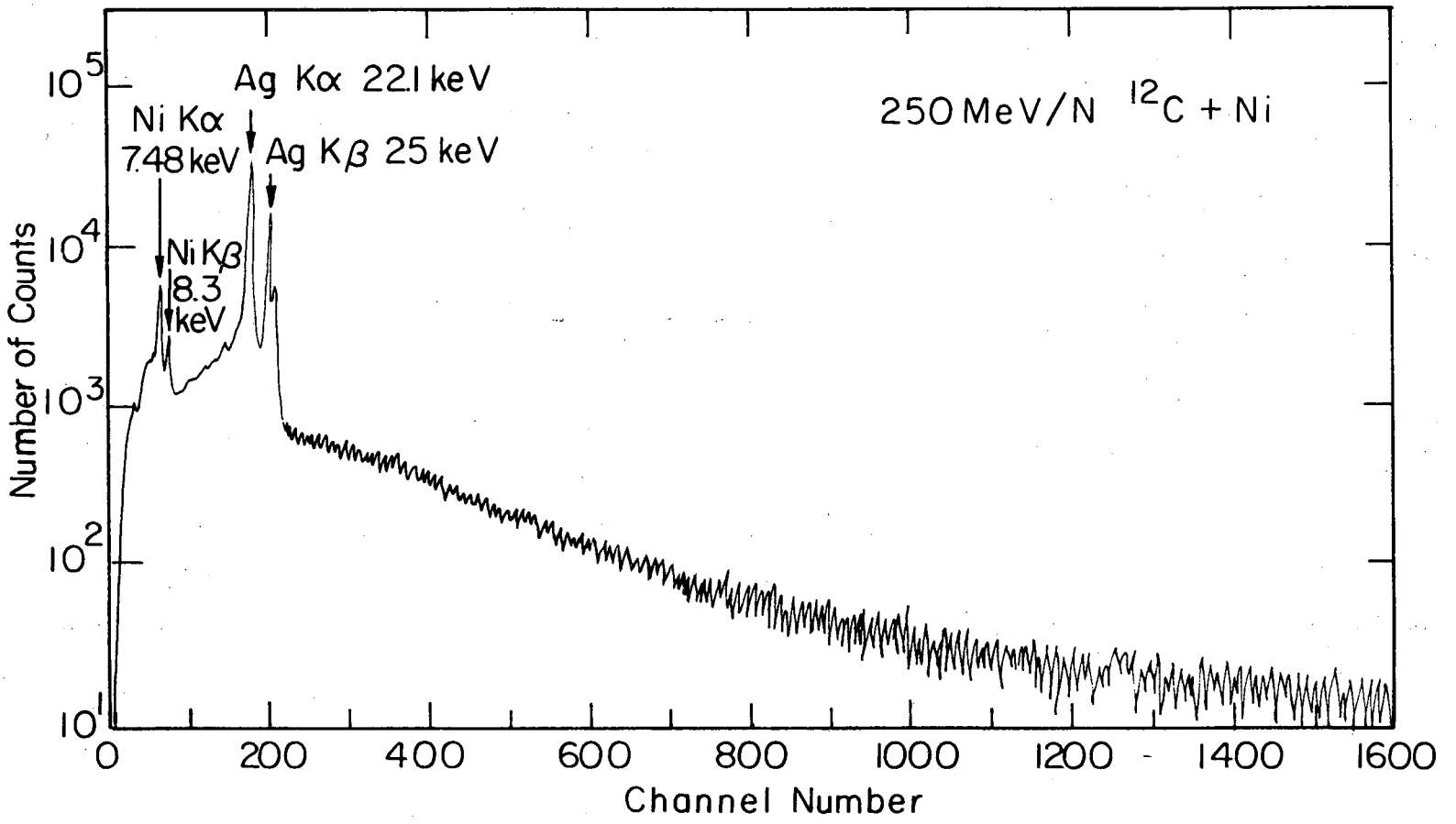

XBL 7711-6407

Fig. 8. X ray spectrum of Ni excited by 250 MeV/N ^{12}C ions.

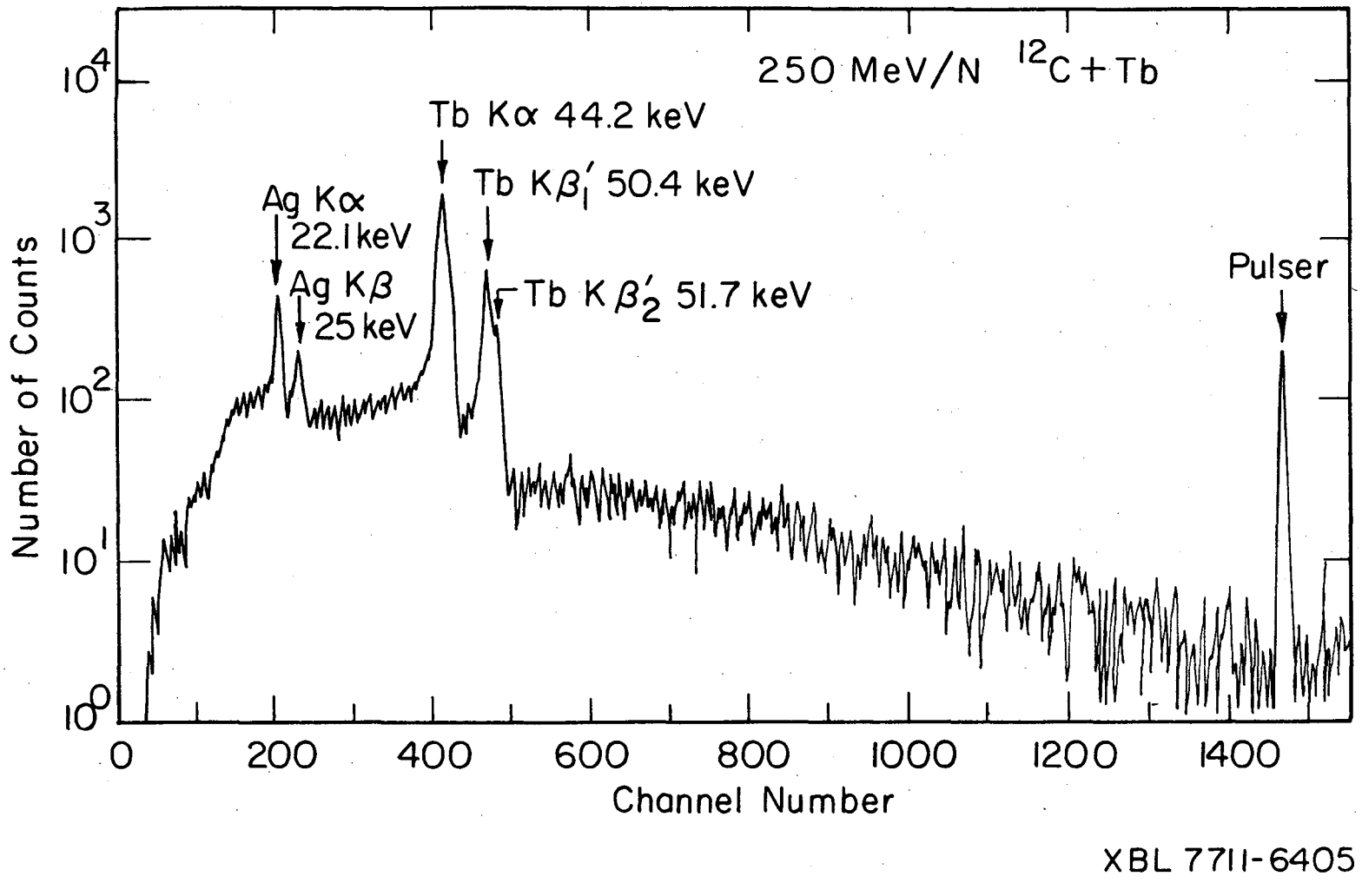

Fig. 9. X ray spectrum of Tb excited by 250 Mev/N ^{12}C ions. The pulser pulse is also shown.

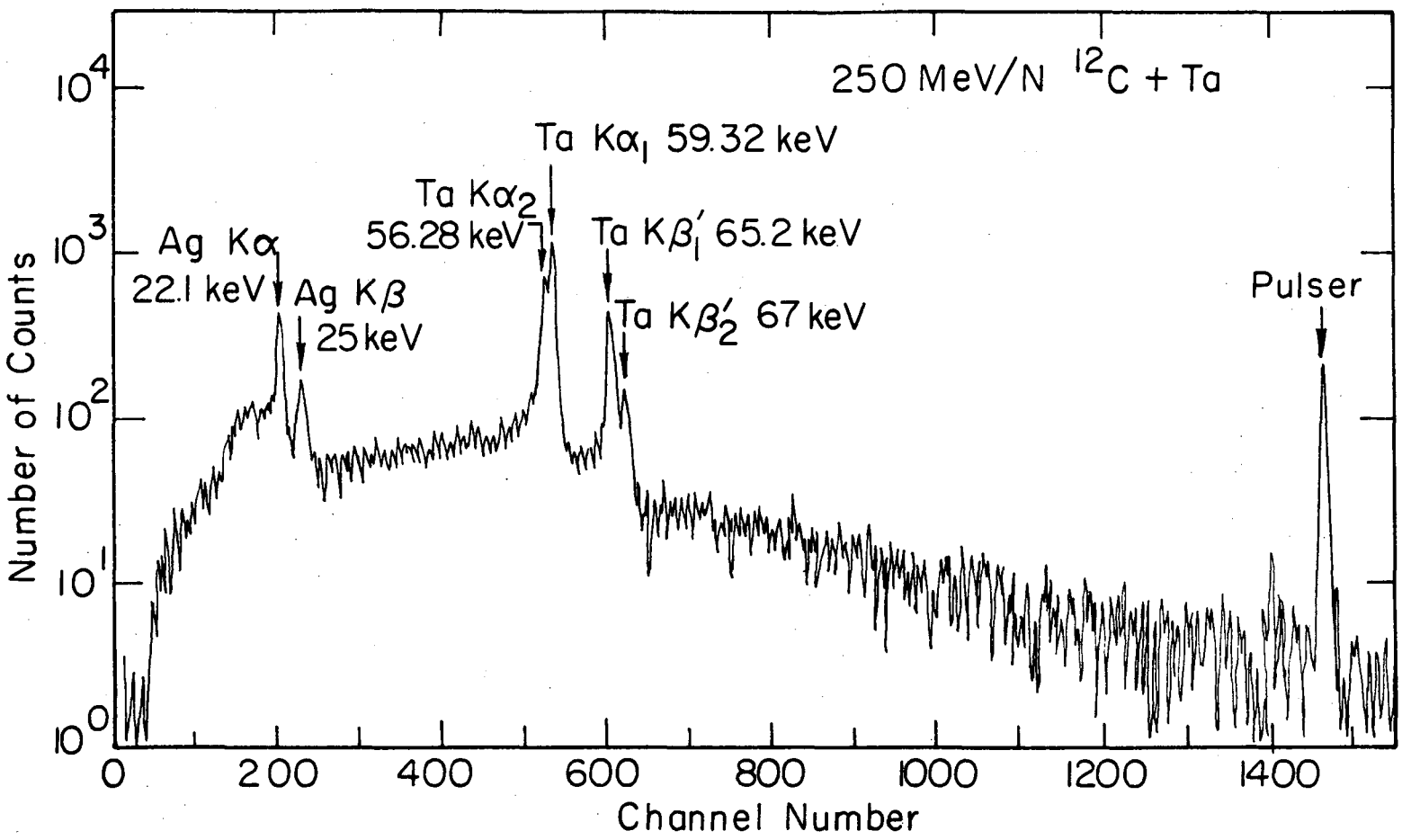

XBL 7711-6406

Fig. 10. X ray spectrum of Ta excited by 250 MeV/N ^{12}C ions. The pulser pulse is also included.

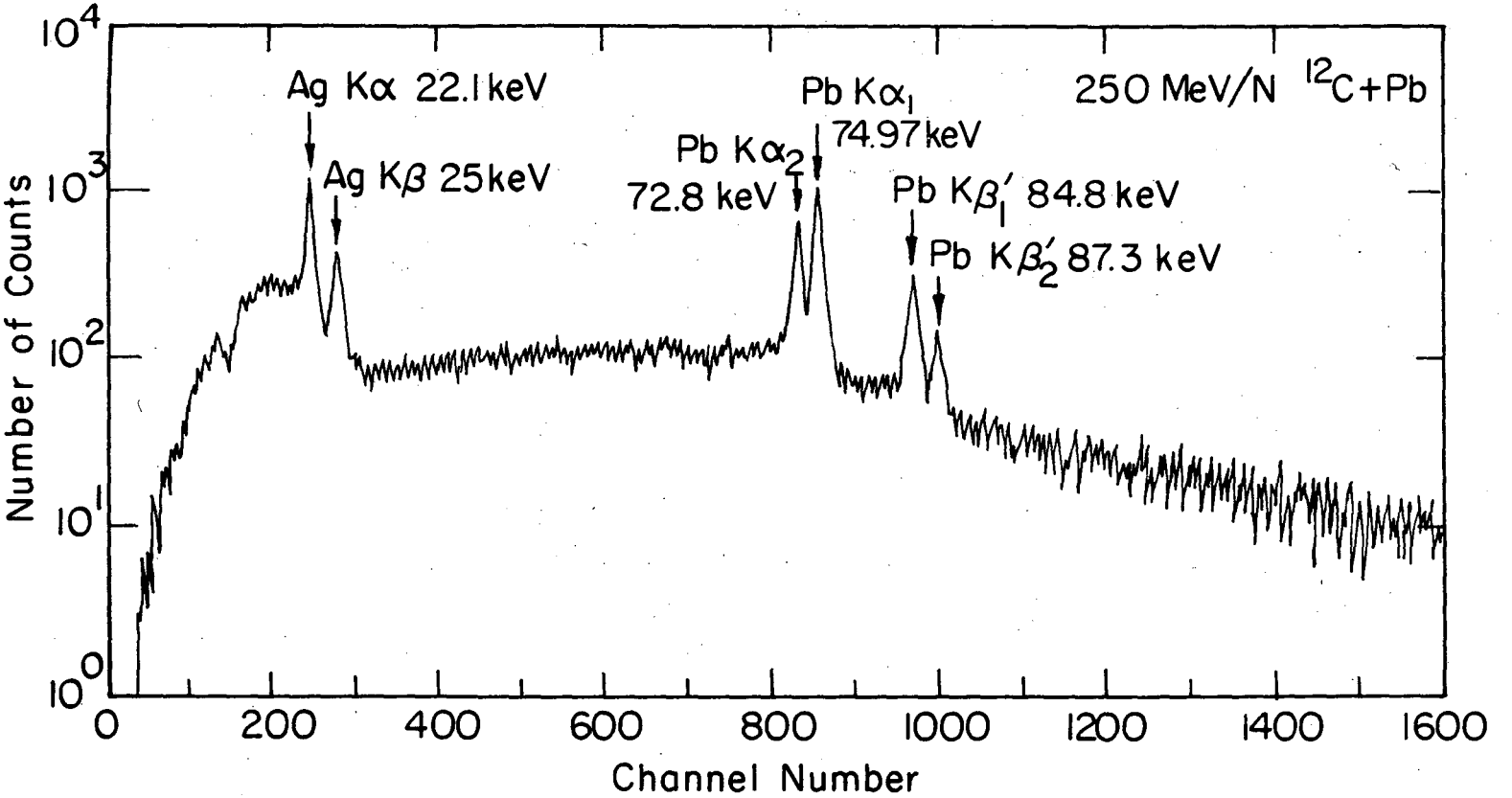

Fig. 11. X ray spectrum of Pb excited by 250 Mev/N ^{12}C ions.

XBL 7711-6408

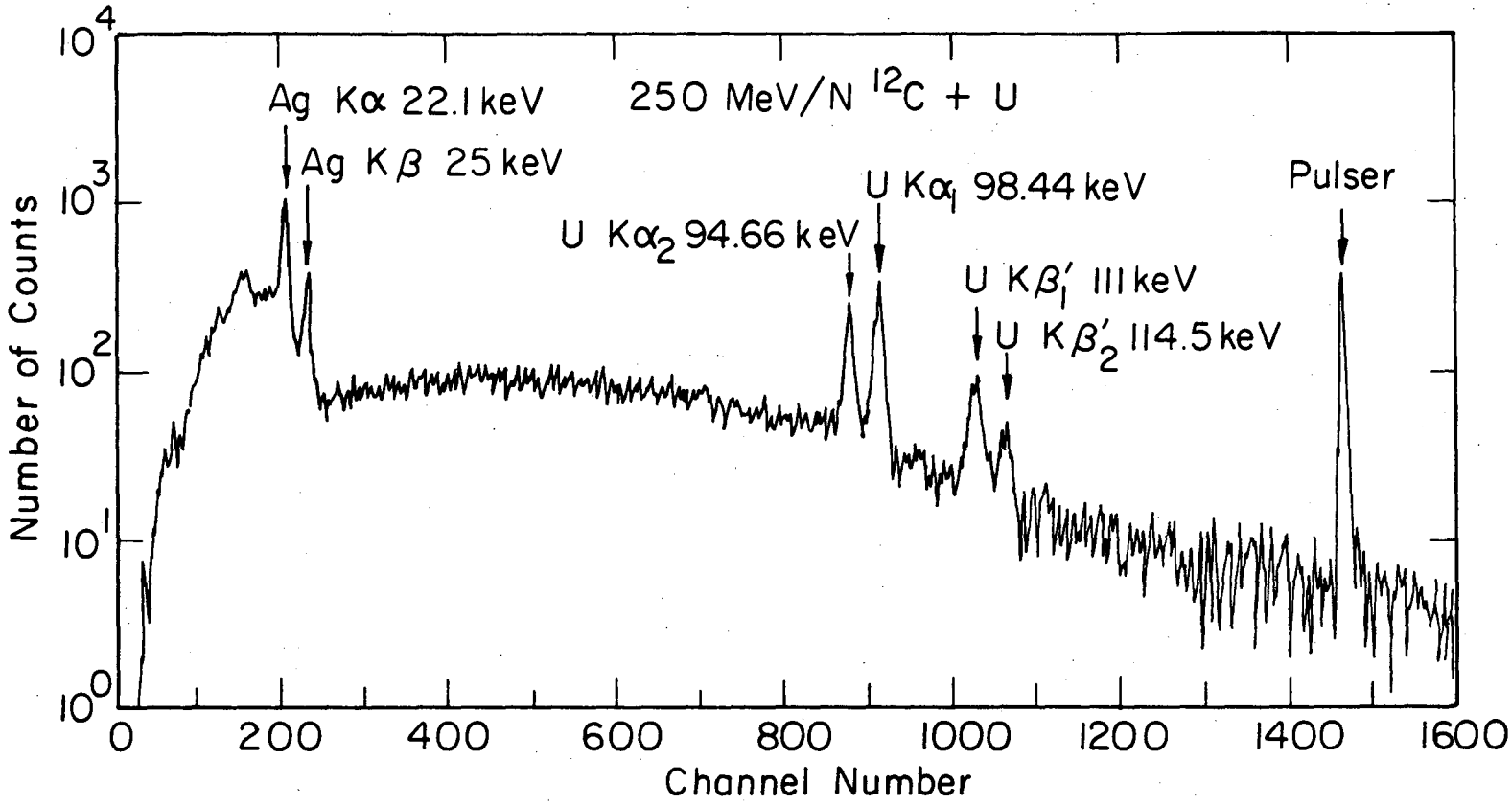

XBL 7711-6404

Fig. 12. X ray spectrum of U excited by 250 MeV/N ^{12}C ions. The pulser pulse is also shown.

rate of a count-measuring system, the more events are rejected during the inactivation of the detector, and thus the higher the deadtime correction factor becomes.

It was for this reason that a crossed detector trigger system was used throughout our x-ray measurements. To measure then the deadtime correction factor one had to compare the number of pulses recorded in the multichannel pulse-height analyzer with the number of test pulses fed into the preamplifier of the detector. The number of pulses triggered n_t was recorded and later from the analysis of the obtained spectron the number of pulses counted n_c was found (for instance in Fig. (12) n_c would be the area under the pulser peak after the background has been subtracted). The deadtime DT is given then by the ratio

$$DT = 1 - \frac{n_c}{n_t} \tag{2.3}$$

with DT always less than one.

Thus if the number of counts or events under any line of the spectrum is found to be n_{K_i}', then the number of counts n_{K_i} which ought to have been measured by the detector under that particular line is

$$n_{K_i} = n_{K_i}' \frac{1}{1 - DT} = n_{K_i}' \frac{n_t}{n_c} \tag{2.4}$$

The quantity 1/(1-DT) in Eq. (2.4) is then what we called earlier the deadtime correction factor. It was found in our preliminary measurements and later on in the actual ones reported here that the deadtime varied between 0.4% and 50%. This result indicated that

the deadtime correction factor could affect the value of the total cross section by as much as a factor of two. It was therefore necessary that cross section values insensitive to the uncertainty of the detector deadtime had to be obtained. To do so we had to use the thin Ag foil upstream from the target, as has been described already. In each run the Kα x-rays of Ag were measured along with the Kα and Kβ lines of the target element. The yields then of each target element (Kα and Kβ) could be calibrated against the yield of the Kα line of silver. In addition, the Kα x-rays of silver were calibrated against the ion chamber reading which was actually the integrated relative intensity of the beam. Thus, for each run we calculated the quantity

$$\chi = \frac{n'_{K\alpha}(Ag)}{R_{ic}} \cdot \frac{n_t}{n_c} \qquad (2.5)$$

where in Eq. (2.5) $n'_{K\alpha}(Ag)$ is the yield of the Kα x-rays of silver as measured under the respective line in the spectrum, R_{ic} is the ion chamber reading, and n_t, n_c are the same quantities appearing in Eq. (2.3). The quantity χ then of Eq. (2.5) had to be a constant under perfect measurement conditions. Perfect measurement here has the connotation of measurement without error. Since under realistic measurement-conditions χ varies from measurement to measurement, the average value of χ has been calculated for all runs. Thus, the real number of counts n_{K_i} for the line K_i, which should have been measured by the detector under ideal circumstances, i.e. no deadtime, is given by

$$n_{K_i}(Z_2) = \frac{n_{K_i}'(Z_2)}{n_{K_i}'(Ag)} \cdot \frac{<\chi>}{R_{ic}} \qquad (2.6)$$

where in Eq. (2.6) $<\chi>$ is the average value of χ of Eq. (2.5), $n_{K_i}'(Z_2)$ are the events observed under the K_i peak of the spectrum for the target element of atomic number Z_2, and R_{ic} is the ion chamber reading corresponding to the respective spectrum measurement. The same procedure could have been followed if, instead of the Kα, the Kβ line of silver had been used. Furthermore, in all the cases where the Kα and Kβ lines of the excited target atom were completely resolved, one had to do the calculation of the cross-section σ_K^{vac} twice, once for each line, and then take the average of the two values as a better numerical value of the K vacancy production cross-section. Finally, the analysis of the data on magnetic tape involved the use of the CDC 7600 system of the Computer Center of the Lawrence Berkeley Laboratory and a PDP-7 minicomputer system of the Nuclear Science Division of the Lawrence Berkeley Laboratory too. The first step of the data analysis involved the rewriting of the data originally taken on magnetic tape by the Hewlett-Packard and Northern Scientific analyzers to another magnetic tape in a format that was readable by the PDP-7 system. This step was accomplished by developing two programs called WRIS and BCDIS. The first of these was for the transition from the Hewlett-Packard to the PDP-7 format and the second for that from the Northern-Scientific to PDP-7 format. The transition task was executed with the use of the CDC 7600 system of the Computer

Center of LBL. The second step involved the real data analysis by using the PDP-7 system of the Nuclear Science Division of LBL. The analysis included the finding of the number of events n_{K_i}' under each line K_i of any spectrum after appropriate subtraction of the background which was determined by a polynomial fit through a number of points in it suitably chosen.[35]

2.5 Absolute Beam Calibration

As mentioned earlier, a relative beam intensity calibration was possible by taking the readings of the ion chamber for each run. Thus, one could deduce how many charged particles (beam) went through the target for a given run relative to another run. In this way one could find the cross-section of the vacancy production for a target element relative to another target element. The reading of the ion chamber, for any run, is proportional to the quantity N, of Eq. (2.2). However, one must know the value of N_1 for a given run in order to calculate the absolute value of the cross section σ_n^{vac} of the target element irradiated in that run.

An absolute beam intensity calibration was then done by irradiating graphite targets placed at the ordinary target position for a period of about 10 min each time at various times (approximately every six hours) during the experiment. As a result of the irradiation of graphite, ^{11}C was produced according to the reaction

$$A + {}^{12}C \longrightarrow X + {}^{11}C \qquad (2.7)$$

where in Eq. (2.7) A stands for the incident beam element. Also no beam fragmentation is assumed in Eq. (2.7) but this is irrelevant to the ^{11}C production, since only the primary beam particles are presumably energetic enough to remove a neutron from the ^{12}C of the graphite target. The importance of the reaction of Eq. (2.7) lies in the fact that ^{11}C is a β^+ emitter with a half-life of 20.4 min.[38] The emitted positrons almost instantaneously encounter electrons in the graphite target and a (e^+,e^-) annihilation radiation occurs.

The annihilation radiation from each (e^+,e^-) pair may consist of one or two quanta. One quantum emission is possible when the positron annihilates an electron bound to a nucleus capable of absorbing the recoil momentum. In that case the quantum is always monoenergetic. However, if the capability of absorption of the recoil momentum due to the kinetic energy of the positron by a third partner is lacking, then a two-quanta annihilation occurs too. The latter process happens to be the predominant mode of decay of the positron, electron pair. The two photons are simultaneously emitted at an angle to one another. If the positron slows down and then interacts annihilatively with an electron, two γ quanta are emitted essentially of energy 0.511 MeV each at an angle of 180 degrees to one another.[37] This last configuration is the most probable one among the various possible two γ quanta emission configuration and is the one which is of the utmost interest to us in our measurements.

The graphite target, after having been irradiated approximately for ten minutes by a heavy ion beam, was placed immediately in a nearby located positron counter which measured the coincidence rate of the

emission of the two 0.511 MeV photons at 180 degree to one another. A 400 channel pulse-height analyzer was connected to the counter and in each channel the number of coincidences over a period of 30 seconds was measured, moving successively from one channel to the next. The decay curve of ^{11}C was thus obtained and from that, knowing the exact time of stopping the irradiation of the graphite target and the time when the measurement of positron decay of ^{11}C started, one by extrapolation backwards in time could determine the decay rate of the irradiated target at the time the irradiation was terminated. Knowing that and the cross section of production of ^{11}C from the incident beam at a given energy, one can then determine the number of beam particles which struck the graphite target during its irradiation. Thus for a graphite target of N_o ^{12}C atoms/cm^2, the number of ^{11}C nuclei present $N(t_o)$ after an irradiation time t_o by a beam of intensity of I projectiles per sec is given by

$$N(t_o) = \frac{N_o \sigma I}{\lambda} (1 - e^{-\lambda t_o}) \qquad (2.8)$$

where λ is the decay constant of ^{11}C and σ is the ^{11}C production cross section dependent on the type and energy of incident projectiles.

Using Eq. (2.8), one can deduce I if σ is known. Furthermore, if during the graphite irradiation time the ion chamber reading R_{ic} is recorded, one can now calibrate the ion chamber by calculating the quantity P_{ic} , number of particles going through the ion chamber per ion chamber reading, given by

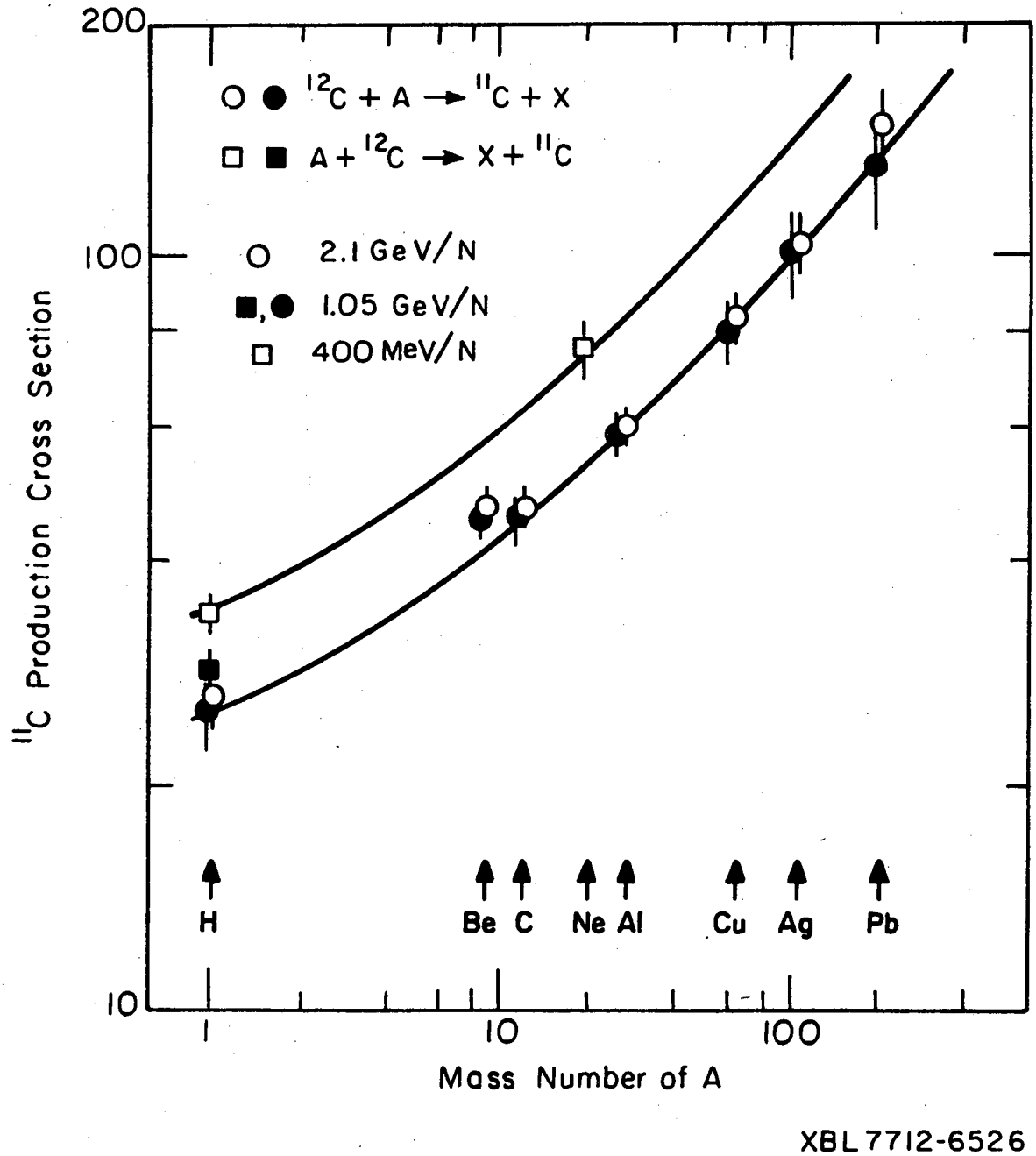

Fig. 13. ^{11}C production cross section from ^{12}C versus mass number A of exciting nucleus.

$$P_{ic} = \frac{I \cdot t_o}{R_{ic}} \tag{2.9}$$

Of course, in practice one has to average the number P_{ic} over several runs, so that a better value can be reached. It should be also pointed out that in Eq. (2.9) it is assumed that the beam intensity I remains constant over a period of time, so that the total number of particles in the beam over time t_o is $I\ t_o$. Application then of the ^{11}C production and decay measurement technique allows us to establish an absolute calibration of the beam intensity or essentially the absolute value of the quantity N_1 in Eq. (2.2).

Before we leave the subject of the absolute beam intensity calibration, two things ought to be mentioned. First, the calibration of the positron counter was done by using a standard ^{22}Na source which decays by β^+ emission with a half-life of 2.6 years. By placing the ^{22}Na source of the same position with respect to the two Na(I) crystals of the positron counter and with the same settings as while the ^{11}C is measured one could determine the positron detector efficiency, geometry, and deadtime corrections. Second, the problem of using the appropriate value for the ^{11}C production cross section in Eq. (2.8) is rather complex. The value of the cross section had to be estimated from the existing data for protons[38),(40)] and for carbon ions.[39] On the basis of these existing data Fig. 13 was drawn and used for the determination of the ^{11}C production cross

section at our energy. Thus, we used for the 4.88 Gev protons the value of 28 mb for the $^{12}C(p,pn)\ ^{11}C$ reaction cross section, while for the 3 Gev carbon ions the value of 70 mb for the $^{12}C(^{12}C,\chi)\ ^{11}C$ reaction cross section. It was also established as a general rule that the relation

$$\sigma_y = A^{1/3}\ \sigma p \qquad (2.10)$$

was approximately true, relating the ^{11}C production cross section σ_y of a projectile A_y with mass number A to the proton cross section σ_p for the same reaction and with the same kinetic energy per nucleon for the heavy ions as for protons.

2.6 Target Thickness Corrections

Two kinds of corrections are associated with the thickness of the target. First, the correction related to the change of the real thickness of the target due to its rotation, as described already. Since the target has been rotated about a vertical axis by 45° and a horizontal axis by 45° also its real thickness t_2' is related to its effective thickness t_2 by

$$t_2 = \frac{t_2'}{(\cos 45°) \times (\cos 45°)} \tag{2.11}$$

The value for t_2 of Eq. (2.11) is the appropriate one to be used in Eq. (2.2) for the calculation of the σ_K^{vac} cross section with t_2' the real thickness of the target in, cm. The implication of the expression "effective thickness" is rather obvious in that it refers to the actual beam path through the target. From Eq. (2.10) it can be seen that the effective thickness is bigger by a factor of two compared with the real thickness t_2'. Thus the correction due to the effective target thickness is 50% or rather -50% since it decreases the value of the cross section by a factor of two.

The second correction associated with the target thickness, although it turns out to be not as large as the first one, is of much more profound origin than the first. There is an implicit assumption in Eq. (2.2) concerning the target thickness t_2. Thus Eq. (2.2) where the yield of K_i x-rays is simply proportional to the thickness t_2 of the irradiated target is applicable only when the target has essentially zero thickness. As the target thickness increases other processes besides the primary one, consisting of the interaction of the incoming beam particles with the target atomic electrons, may contribute to the enhancement of the K_i x-ray yield of a particular target element. Hence the value of the K_i vacancy cross section σ_K^{vac}

would appear to be larger than what it really is. Out of a variety of other processes contributing to the K x-ray production, two are considered to be the most important, accounting for practically all secondary K x-ray production[27] - although here we are exclusively dealing with K x-ray production, the described processes are also applicable to any other inner shell secondary production as well. These two processes are the following:

i. The incident heavy ions produce secondary electrons in the target which are energetic enough to excite K-vacancies in turn.

ii. The incident heavy ions produce energetic secondary electrons which emit bremsstrahlung radiation as they slow down colliding with other nuclei in the target. This bremsstrahlung radiation may then excite photoelectrically K-vacancies.

The targets used in our experimental measurements were of thickness up to 100 mg/cm^2. It is important to realize that in this type of measurement one has to restrict the target thickness to the aforementioned values. One reason is that thicker targets would lead to severe x-ray self-absorption, thus making their detection more difficult in addition to increasing the uncertainties in the measured cross sections. Another reason for using thin targets, related to our present discussion, is that significant beam fragmentation occurs along with high energy transfer from the beam particles to the target nuclei or fragments thereof. Then other processes, in addition to the two mentioned already, may enter the picture of secondary K x-ray production leading thus to further enhancement of the value of the

K-vacancy production cross section. Clearly one wants to avoid complicating matters more than it is necessary.

Assuming thus that we are dealing with a thin target - thin here meaning of the already mentioned thickness order - then process (i) increases the cross section linearly with target thickness while process (ii) increases it quadratically. The latter dependence of the K-vacancy production cross section versus the target thickness is shown schematically for Au and Ni targets in Fig. 14.

The adjustment of our measured cross sections to zero target thickness was made by using semiempirical expressions based on approximate theoretical calculations for the two processes of secondary K x-ray production under consideration here.[41] The calculations were made for the following two extreme cases:

(1a) All secondary electrons pass through the target without loss of energy.

(1b) All secondary electrons are stopped inside the target.

The first limiting case (1a) is that of zero thickness target approximation, whereas the second limiting case (1b) is that of infinite thickness target approximation.

Furthermore, two rather simplifying assumptions, concerning the bremsstrahlung emission, were made. These were the following:

(2a) The bremsstrahlung radiation from the secondary electrons is isotropic.

(2b) The bremsstrahlung radiation from the secondary electrons is forward peaked.

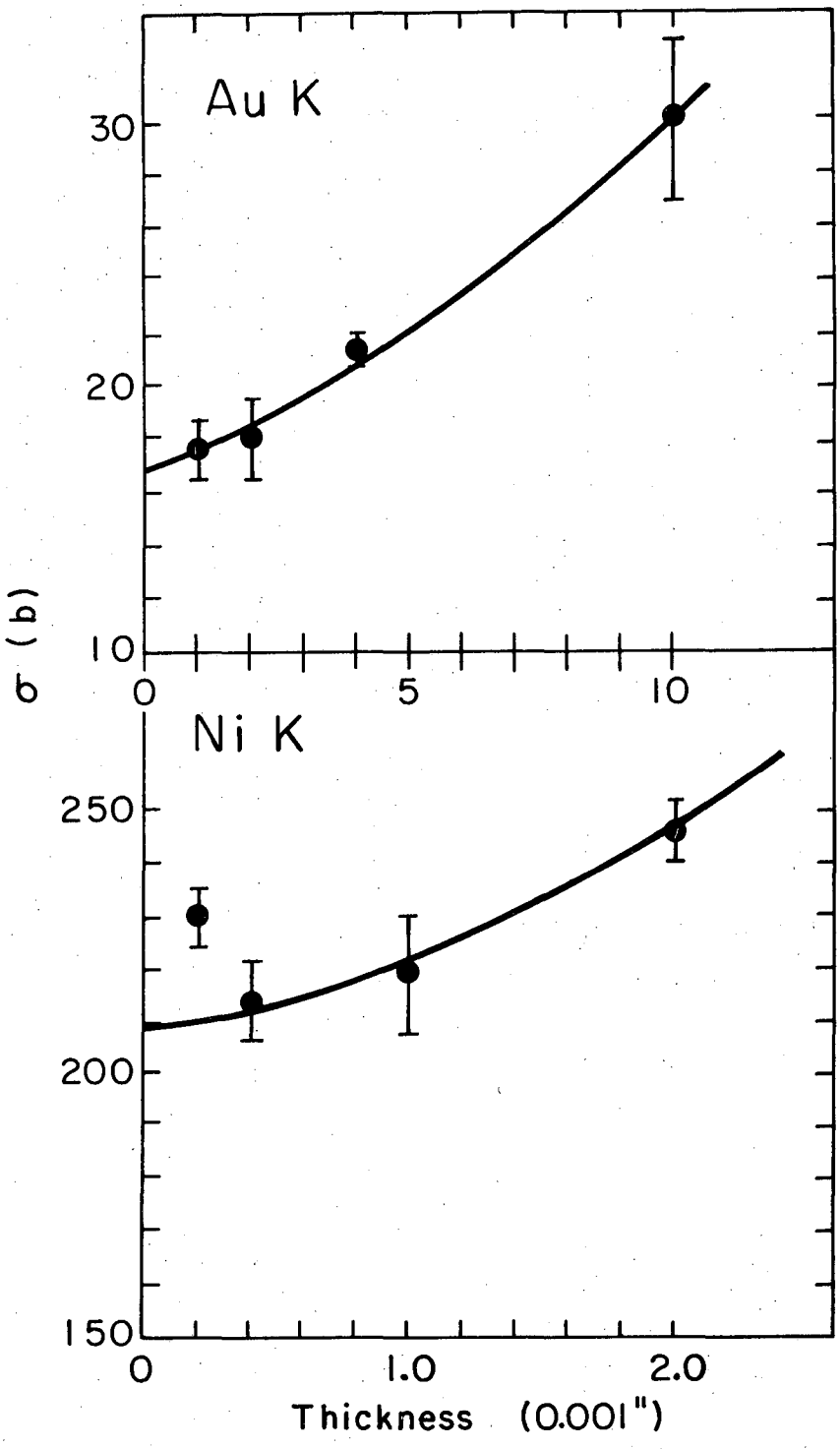

Fig. 14. Experimental cross section versus target thickness. Error bars represent relative error only. Curve approximates the quadratic thickness dependence.

TABLE 2.1 Finite target thickness correction as percentage of total cross section for 4.88 GeV protons on various targets

Element	Z_2	Thickness ($gr/cm^2 \times 10^3$)	Correction (%)
Ni	28	22.6	2.2
Zr	40	33	4.0
Mo	42	51.80	5.6
Ag	47	133.35	11.8
Tb	65	105.03	10.7
Ta	73	84.00	6.7
Pt	78	13.6	0.7
Au	79	49	2.8
Pb	82	57.9	2.7
U	92	48.43	1.9

The second assumption (2b) is justified for very high energy secondary electrons, while the first assumption (2a) is reasonable for low energy secondary electrons. However, low energy secondary electrons can contribute to K x-ray production in low atomic number target elements, whereas the high energy secondary electrons can be responsible for K x-ray production in any atomic number target element. In addition, the bremsstrahlung radiation is negligible in the former case but significant in the latter. Thus we are left with the second assumption (2b), as being rather more realistic.

Applying all of the above to our calculation, we found that the correction due to secondary production of K x-rays in the target was of the order of 10%. The uncertainty involved in this correction was of the same magnitude (± 10%). For most of the targets used in our experiments the secondary K x-ray production or finite target thickness correction was the same in magnitude as the uncertainties of other corrections though significantly larger than the real target thickness uncertainty itself. The values of this correction, for the 4.88 Gev protons on various targets, are given in Table 2.1 for illustrative purposes.

2.7 Detector Efficiency

During the entire run the positions of the Ag foil, target, and the two detectors remained unchanged. This was essential in that only one calibration (of efficiency) for each detector would be necessary. The detector efficiency determination was made by placing at the position of the target a series of calibrated radioactive sources,

one at a time. The standard radioactive sources manufactured by the Radiochemical Center, Amersham, England, included ^{248}Am, ^{133}Ba, ^{57}Co, ^{22}Na, ^{60}Co, and ^{88}Y. The γ rays produced from the radioactive decay of these nuclei give an energy range from 60 Kev to 1.836 MeV. For each peak of the spectrum of the radioactive sources the net number of counts in that peak was found by subtracting the background from the total number of counts, as described in Chapter 2.4. This number, then, was divided by the number of decays of the radioactive source which would yield the gamma ray under consideration over the time of measurement. The obtained number was then the efficiency of the detector at the particular energy of the gamma ray and for the given geometrical configuration of the target-detector system. By plotting all these numbers as efficiency versus photon-energy, an efficiency curve for a given detector and geometrical configuration was obtained. A typical efficiency curve for a planar Ge(Li) detector is given in Fig. 15. Since the efficiencies of the various photon absorption processes increase with atomic number, it is advantageous to use germanium instead of silicon detectors. This is true for very high energy x-rays and obviously gamma rays. However, for lower energy x-rays below 50 kev silicon detectors are more useful.[42] At these low photon energies for sufficiently large volume of semiconductor material of either Ge or Si, the absorption of the photon will be more or less complete. In terms of efficiency then, there will be no difference between a Ge(Li) or a Si(Li) detector. However, the "energy gap" or "forbidden zone" is 1.1 eV for silicon but only 0.7 eV for germanium, so that the fluctuation of the leakage current through the detector and

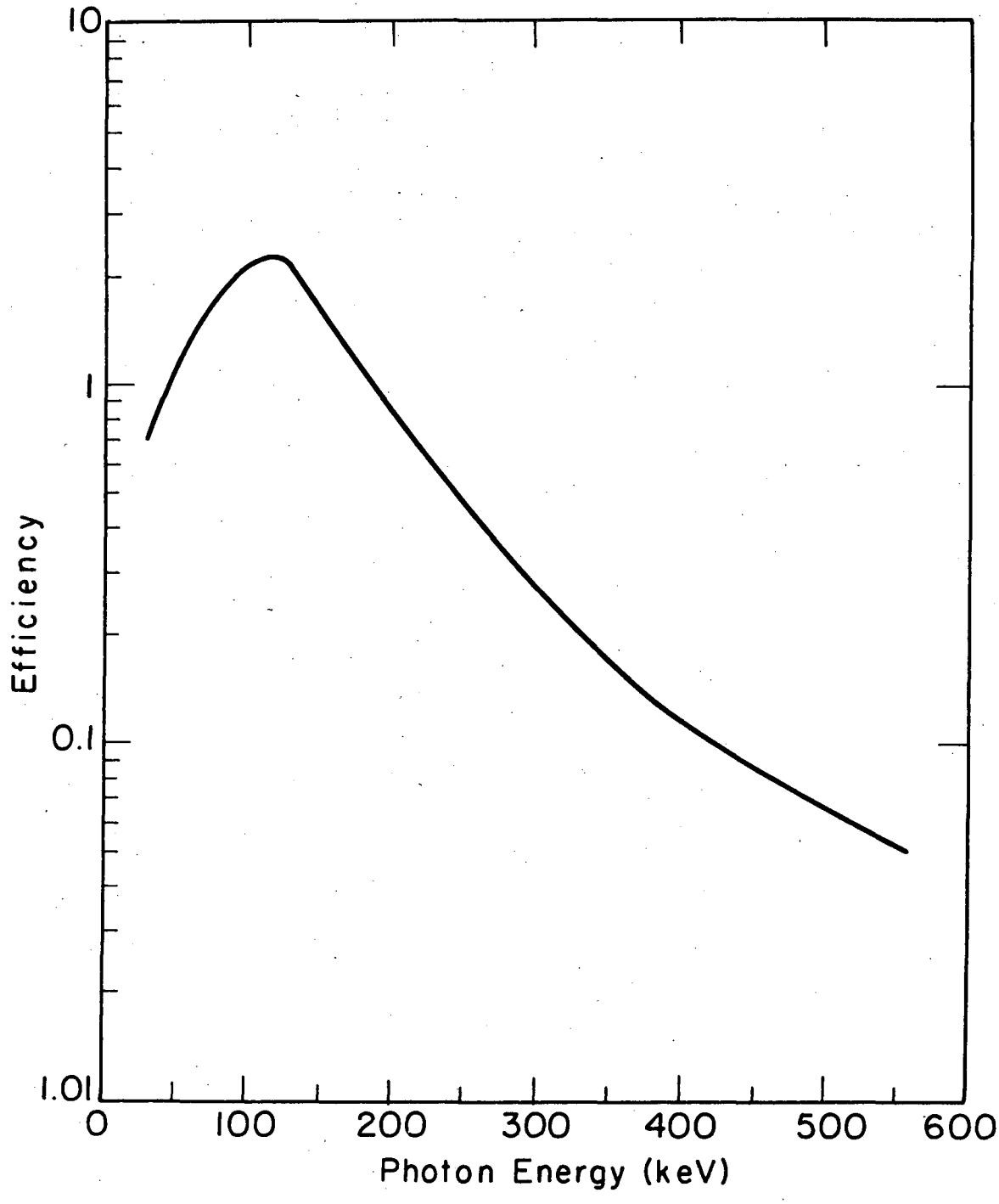

XBL 7711-6401

Fig. 15. Ge(Li) planar detector efficiency--arbitrary scale--versus photon energy. The efficiency curve takes also into account the geometrical configuration of the target-detector system.

the noise of the preamplifier can be much higher for germanium than silicon detectors. On the other hand the statistical fluctuation in the primary process of electron-hole production is higher for the silicon detector since the energy ε needed to form one electron-hole pair is 3.23 eV for silicon but 2.34 eV for germanium. Given that the resolution is determined by the line's full width at half maximum (FWHM) ΔE, one has for the line resolution to a good approximation [43]

$$\Delta E = 2.3\left[E\varepsilon + \overline{(\text{Noise})^2}\right]^{1/2} \tag{2.12}$$

where in Eq. (2.11) E is the photon energy in eV. For low E then it may happen that ΔE is smaller for a silicon detector than a germanium one. This is because from the previous development $E\varepsilon$ is always bigger for silicon detectors for a given photon energy but Noise^2 is smaller for silicon detectors too. It turns out that for photon energies lower than 50 keV ΔE can be smaller for silicon detectors. Thus Si(Li) detectors are preferable over Ge(Li) detectors as having better resolution.[42] It should be noted, in passing, that the diffusion of lithium ions into the germanium or silicon semiconductors has as result a much larger depletion layer than that of any other p-n junction semiconductor. Hence Ge(Li) or Si(Li) detectors have improved efficiency and resolution as well compared with other types of semiconductor detectors.

Returning now to the discussion of our experiment from the efficiency calibration curves for each of the detectors used at the actual geometrical configuration, we can deduce the value of the

quantity $\frac{\Delta\Omega}{4\pi}\,\epsilon_{d_{K_i}}$ of Eq. (2.2) corresponding to the energy of the K_i x-ray line. Since in our experimental measurement we have used the Ag monitor foil, a detector efficiency calibration was also made for all detectors used, by placing the sources this time at the Ag foil position. This was essential in forming the ratio of Eq. (2.5) given that, due to the different geometrical configuration of the Ag foil-detector system from that of the target-detector one, the geometrical factor $\frac{\Delta\Omega}{4\pi}$ was different in each case.

Finally, for K_i x-ray lines whose energy was lower than 60 kev an extrapolation of the efficiency versus energy curve had to be done in order to include all the necessary values of the x-ray energies.

2.8 Absorption Correction

The final quantity which needs to be calculated before one can derive the value of the K vacancy production cross section from Eq. (2.2) is that of the absorption reduction factor C_{K_i} for the K_i x-ray line. The absorption correction consists of two parts. One is the absorption of x-rays going through matter such as air, Be absorbers, plastic windows e.t.c., which exist between the target and the detector. The other correction is the self-absorption of the x-ray within the target itself. We consider the two absorption corrections separately, in deriving the total absorption reduction factor C_{K_i} .

It is well known that attenuation of electromagnetic radiation as it passes through matter occurs as an intensity diminution and not as an energy change, following the exponential law

$$I(x) = I_o\, e^{-\mu x} \tag{2.13}$$

where in Eq. (2.13) I_o is the initial intensity of the electromagnetic beam, I(x) its intensity after traversing a thickness x of a homogeneous material of total linear attenuation coefficient μ. Thus, for a number n of different materials j each of thickness t_j and total linear attenuation coefficient μ_j respectively, the total attenuation of a beam of electromagnetic radiation going through all of them is given by

$$I(\sum_{j=1}^{n} t_j)/I_o = \prod_{j=1}^{n} e^{-\mu_j t_j} \tag{2.14}$$

where in Eq. (2.14) $\sum_{j=1}^{n} t_j = t_1 + t_2 + \ldots + t_n$, and Π stands for the product of n terms each of the form $e^{-\mu_j t_j}$. It must be borne in mind that the total linear attenuation coefficient μ_j depends on the energy of the quanta of electromagnetic radiation going through the material j.

Next we examine the attenuation of electromagnetic radiation produced in a material of thickness t and at the same time absorbed in it as it traverses it. Let us assume that the production of electromagnetic radiation in the material under consideration (target) by an external cause (heavy ion beam) is uniform throughout its mass and equal to I_o quanta per square centimeter per unit length of the material. If at a depth x of the material there are I(x) quanta per square centimeter and if the linear attenuation coefficient of the patericular radiation produced in that material is μ, one has over a length dx:

$$dI(x) = I_o' \, dx - \mu \, I(x) \, dx \tag{2.15}$$

Integration of (2.15) over a total length t and with boundary condition I(X) = 0 yields for I(x) the equation

$$I(x) = I_o' \, \frac{1-e^{-\mu x}}{\mu} \tag{2.16}$$

If now there were no attenuation, I_o' t quanta per square centimeter should exist at the x=t end of the material (assumed to be an orthogonal slab). Thus the attenuation of the electromagnetic radiation in this case is:

$$\frac{I(t)}{I_o'} = \frac{1 - e^{-\mu t}}{\mu} \tag{2.17}$$

It is now apparent that the total attenuation of the K_i x-ray will be given by an appropriate combination of Eq. (2.14) and (2.17). Thus, the absorption reduction factor C_{K_i} of the K_i x-rays is going to be the inverse of the total attenuation of the K_i x-rays. Hence, we have

$$C_{K_i} = \left[\left(\prod_j e^{-\mu_j(i) t_j} \right) \frac{1 - e^{-\mu_2(i) t_2}}{\mu_2 t_2} \right]^{-1} \tag{2.18}$$

where in Eq. (2.18) the symbol $\mu(i)$ indicates that the attenuation coefficient μ is for the K_i x-rays, μ_2, t_2 refer to the target material and thickness respectively, and μ_j, t_j to the same quantities for air, absorbers, etc. The values for the t_j's reflect the path of the K_i x-rays through the respective j materials. The value of the

target thickness t_o is of importance. Since the target due to its rotation formed a 45 degree angle with the normals on the face of each detector, a different value of effective t_2 has to be calculated for the detectors than that of Eq. (2.10). Here we have for the effective thickness of the target t_2

$$t_2 = \frac{t_2'}{\cos 45^\circ} \tag{2.19}$$

The values of the total linear attenuation coefficient energies are available in detailed tables.[44] Thus, the quantity C_{K_i} in Eq. (2.7) is given by Eq. (2.18) in conjunction with Eq. (2.19).

2.9 Experimental Results

Having already discussed the various quantities that appear in Eq. (2.2), which equation is used for the determination of the K vacancy production cross-section, we are ready to present the experimental values for that cross section. A few words are in order, however, concerning the values of the fluorescent yield ω_K of Eq. (2.2) for the various target elements. Although there is an uncertainty in both theoretical calculations and experimental measurements as to the true value of the fluorescent yield, this uncertainty is least in the case of the K-shell.[45] Thus, a judicious selection of the values of ω_K for our calculations was made among the various sources of relevant information.[1][36][45]

a. 4.88 Gev protons

Targets ranging from Ni (Z_2 = 28) to U (Z_2 = 92) were irradiated with a 4.88 Gev proton beam provided by the Lawrence Berkeley Laboratory Bevatron/Bevalac facility.[26] It has been already described how the cross section σ_K^{vac} was calculated from Eq. (2.2) by appropriately measuring the rest of the quantities involved in that equation. The uncertainties in the various steps of the procedure, which eventually determined the uncertainty of the cross-section, are as follows:

i. Protons per ion chamber reading Pic : ± 4%. This includes counting statistics, ^{11}C cross section, positron counter efficiency and graphite target thickness.

ii. Detector efficiency: ± 8% Si(Li), ± 14% Ge(Li).

iii. Average number of deadtime corrected with Ag K_α x-ray counts per ion chamber reading $\langle X \rangle$: ± 7% Si(Li), ± 13% Ge(Li).

iv. Target angle, thickness, absorption coefficient: ± 2%

v. Counting statistics: ± 2%

vi. Cross section of the reaction $^{12}C(p,X)^{11}C$: ± 0.6 mb

All uncertainties above are expressed in terms of one standard deviation. The following Table 2.2 gives the values of the measured K vacancy production cross-sections σ_K^{vac} along with their uncertainties also expressed in terms of one standard deviation $\Delta\sigma_K^{vac}$, where

$$\Delta\sigma_K^{vac} = \left\{ \overline{\left[\sigma_K^{vac} - \sigma_K^{vac} \right]^2} \right\}^{1/2} \qquad (2.20)$$

TABLE 2.2 K-Vacancy cross section from 4.88 GeV protons

Element	Z_2	σ_K^{vac} (barns)	$\Delta\sigma_K^{vac}$ (barns)
Ni	28	210	25
Zr	40	102	12
Mo	42	94	12
Ag	47	58	10
Tb	65	31	7
Ta	73	22	4
Pt	78	18	4
Au	75	17	3
Pb	82	15	3
U	92	11	3

b. 250 MeV/amu carbon ions

Targets ranging from Ti (Z_2 = 22) to U(Z_2 = 92) were irradiated with a 250 MeV per nucleon or 3 GeV total energy carbon ion beam.[46] The ^{12}C beam was, similarly to the proton beam, provided by the Bevatron/Bevalac facility of the Lawrence Berkeley Laboratory. The experimental procedure was identical to that of the 4.88 GeV protons and has been already described in detail. The uncertainties in the various steps of the procedure here are given below in terms of plus or minus one standard deviation.

i. Carbon ions per ion chamber reading P_{ic}: ± 6%. This again includes counting statistics, ^{11}C cross section, positron counter efficiency, and graphite target thickness.

ii. Detector efficiency: ± 8% Si(Li), ± 14% Ge(Li).

iii. Average number of deadtime corrected with Ag Kα x-ray counts per ion chamber reading $\langle X \rangle$:± 9% Si(Li), ± 15% Ge(Li)

iv. Target angle, thickness, absorption coefficient: ± 2%

v. Counting statistics: ± 2.5%

vi. Cross section of the reaction $^{12}C(^{12}C,X)^{11}C$: ± 2.1 mb.

The values of the measured K-vacancy production cross sections σ_K^{vac} with their uncertainties $\Delta\sigma_K^{vac}$ with their uncertainties $\Delta\sigma_K^{vac}$ are given in Table 2.3. Here again $\Delta\sigma_K^{vac}$ is defined by Eq. (2.20).

TABLE 2.3 K-Vacancy cross section from 3 GeV carbon ions

Element	Z_2	σ_K^{vac} (barns)	$\Delta\sigma_K^{vac}$ (barns)
Ti	22	1.87×10^4	5.2×10^3
Ni	28	1×10^4	2.8×10^3
Mo	42	3.22×10^3	470
Ag	47	2.15×10^3	400
Tb	65	6.72×10^2	120
Ta	73	4.04×10^2	77
Au	79	3×10^2	58
Pb	82	2.24×10^2	51
U	92	1.45×10^2	25

III. COMPARISON OF EXPERIMENT WITH THEORY AND CONCLUSIONS

3.1 Introduction

In this chapter, we are going to compare our theoretical predictions for the K-vacancy production cross section, as developed in Ch. 1, with the experimental results which were presented in Ch. 2. Although only two sets of experimental data exist at relativistic heavy ion energies they could provide useful guidance for additional experiments as well as insight for refinement of the theoretical calculations.

It has been pointed out that at lower projectile energies the K-vacancy cross section can fit a universal curve[4] in all theories used for the calculation of that cross section. This universal curve is independent of the nature of the projectile and target elements as well as the energy of the projectile and essentially depends only on the ratio of projectile and K-shell electron velocities. It would be very important to find out how this universal curve is modified at relativistic projectile energies.

In addition, it would be very instructive to compare our relativistic heavy ion theory with its counterpart for relativistic electrons.[29] Similarities and/or differences in the derivation of the two theories might lead to further improvement of the theoretical calculations.

Finally, depending on the conclusions of the comparison of theory with experiment certain speculative statements could be made concerning the significance of our results and observations.

3.2 Comparison of the 4.88 GeV proton data with theory.

First, we calculate the values of the longitudinal and transverse components of the K-vacancy cross section. To do so, we make use of Eq. (1.36) for the longitudinal cross section σ_K^{ℓ} and of Eq. (1.60) for the transverse cross section σ_K^{t}. The values for the function f_K, in the expression of the longitudinal cross sections, are obtained from the already existing tables[19] for f_K versus η_K^{ℓ} and θ_K. Similarly, the numerical values of the function g_K versus η_K^{t} and β^2, in the expression for the transverse component, are obtained from the tables of Appendix A which have been calculated as part of the present work. The total K-vacancy production cross section, in terms of the longitudinal and transverse terms, is given by Eq. (1.28). On the basis of the results of Ch. 1, we can easily construct Table 3.1. The target elements which appear in Table 3.1 are, for obvious reasons, the same as those irradiated by the 4.88 GeV proton beam. The next step, in our development, is to compare the last column of Table 3.1 giving the total theoretical K vacancy cross section $\sigma_K^{th.}$ with the experimental values of the same cross section $\sigma_K^{exp.}$ which are given in Table 2.2. Thus, we form the ratio $\sigma_K^{exp}/\sigma_K^{th.}$ for all the irradiated target elements. The results appear in Table 3.2. In the same Table 3.2 the standard deviation of the ratio $\sigma_K^{exp.}/\sigma_K^{th.}$ is also given. This standard deviation is solely determined on the basis of the standard deviations of the measured cross sections $\sigma_K^{exp.}$ given in Table 2.2. The error involved in the calculation of $\sigma_K^{th.}$ is rather negligible when compared with that of the experimental measurement of $\sigma_K^{exp.}$. Hence, Table 3.2 is readily obtained. The results of Table 3.2 are also plotted in Fig. 16.

TABLE 3.1 Theoretical values of σ_K^{ℓ}, σ_K^{t}, and σ_K for 4.88 GeV protons ($\beta = 0.9868$).

Element	Z_2	σ_K^{ℓ} (barns)	σ_K^{t} (barns)	σ_K (barns)
Ni	28	146.70	71.589	218.28
Zr	40	65.68	54.43	120.11
Mo	42	55.00	50.37	105.37
Ag	47	41.99	45.39	87.38
Tb	65	17.15	18.45	36.70
Ta	73	12.85	12.36	25.21
Pt	78	10.43	8.48	18.91
Au	79	9.67	7.64	17.31
Pb	82	8.49	6.84	15.33
U	92	5.99	2.58	8.57

TABLE 3.2 Ratio of $\sigma_K^{exp.}/\sigma_K^{th.}$ and its standard deviation $\Delta\sigma_K^{exp.}/\sigma_K^{th.}$ for 4.88 GeV protons.

Element	Z_2	$\frac{\sigma_K^{exp.}}{\sigma_K^{th.}}$	$\frac{\Delta\sigma_K^{exp.}}{\sigma_K^{th.}}$
Ni	28	0.962	0.115
Zr	40	0.831	0.058
Mo	42	0.892	0.113
Ag	47	0.663	0.114
Tb	65	0.870	0.196
Ta	73	0.982	0.156
Pt	78	0.951	0.211
Au	79	0.982	0.173
Pb	82	0.978	0.195
U	92	1.283	0.350

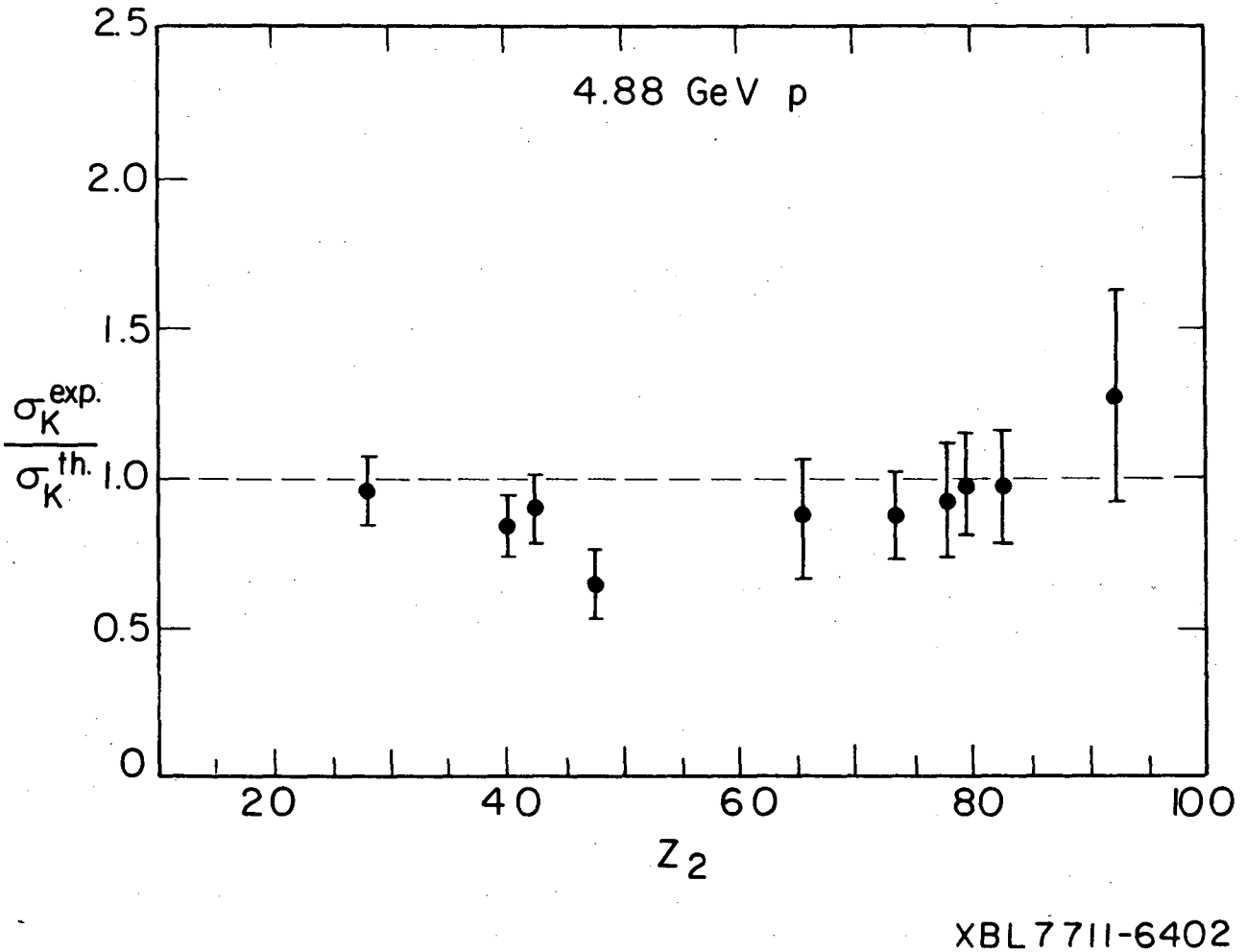

Fig. 16. Ratios of experimental to theoretical K vacancy cross section for 4.88 GeV protons. Error bars reflect one standard deviation of the experimental cross sections.

Our first observation from either Table 3.2 or Fig. 16 is that the theoretical K-vacancy production cross-section is consistently larger than the corresponding experimental cross-section. The only exception is uranium. In any case, the ideal value of the ratio $\sigma_K^{exp.}/\sigma_K^{th.}$ of one is within the experimental error bars of the calculated values of this ratio. The only two exceptions are Zr and Ag. There is no apparent explanation for this behavior. In the case of Ag, it appears as though its experimental value is too low which may indicate a possible error in our experimental measurement. On the other hand, the theoretical value for the total cross section of U is much smaller than the experimental one, although the former is within the error limits of the latter. The theoretical value of the transverse component σ_K^t for U is apparently too low. The latter can be seen from Table 3.1. As far as the general trend of lower experimental values for σ_K than the ones predicted by the theory is concerned the following remark may be of significance. In the calculation of the total K-vacancy cross section, and for that matter any other shell vacancy, Eq. (1.28) was used. It is possible, however, that both longitudinal and transverse interactions may not be excited simultaneously by the incoming projectile.

The Coulomb interaction induces no parity change with respect to reflection on any plane that contains $\hbar\bar{q}$ because its interaction operator is even under this reflection. On the other hand, the virtual photon interaction induces a parity change with respect to reflection on the plane through $\hbar\bar{q}$ perpendicular to the $(\bar{p},\bar{p}')$ plane, thereby transmitting one unity of odd parity. Consequently, any atomic system which is invariant under space rotations and reflections, i.e. isotropic, is excited from the same initial state to final-states of differing parity

by the longitudinal and the transverse component of the interaction. In our case the final states are always in the continuum. Then, the aforementioned effect is not expected to produce any dramatic results as it could in the case of excitation to discrete final states. However it may have a contribution to diminishing the maximum possible cross section given by the sum of the longitudinal and transverse components.

3.3 Comparison of the 3 GeV carbon data with theory

Using Eqs. (1.36), (1.60), and (1.28) once more, the values of σ_K^{ℓ}, σ_K^{t}, and σ_K may be calculated for the 250 MeV/N carbon ions in a similar fashion to that of the 4.88 GeV protons. The results are given in Table 3.3. For comparison purposes, the target nuclei irradiated in the experiment have also been selected in the numerical calculations. Comparison of the last column of Table 3.3 to the results of Table 2.3 indicates that theoretical values for the K-vacancy cross section are for all targets larger than the corresponding experimentally measured values of the same cross section. It is also seen that the discrepancy between theory and experiment becomes bigger as the atomic number Z_2 of the target element increases. Another observation, which can be made from the same Table 3.3, is the relative contribution of the longitudinal σ_K^{ℓ} and transverse σ_K^{t} cross sections to the total σ_K cross section. It is seen that at this energy (250 MeV/amu) the contribution of the transverse component to the total cross section is not important, the degree of significance being diminished with heavier target atoms.

Returning to our first observation, we note that the discrepancy between theory and experiment is not due to any relativistic effect,

TABLE 3.3 Theoretical values of σ_K^{ℓ}, σ_K^{t}, and σ_K in 250 MeV/amu carbon ions ($Z_2 = 6, \beta = 0.6152$).

Element	Z_2	σ_K^{ℓ} (barns)	σ_K^{t} (barns)	σ_K (barns)
Ti	22	21792.	313	22105
Ni	28	11400	191	11591
Mo	42	3840	38	3878
Ag	47	2876	18	2894
Tb	65	1021	2	1023
Ta	73	658	1.5	659.5
Au	79	494	1.4	495.4
Pb	82	404	1.2	405.2
U	92	205	0.07	295.07

because then the experimental value of cross section ought to be larger than its theoretical value. Exactly the opposite is the case here, namely the theoretical value of the cross section is larger than its experimental value for all targets. A number of effects, which might explain the discrepancy, were considered. These were polarization,[49] binding,[50] and charge exchange[52][54] effects.

The polarization effects take into account:

(1) The deflection of the projectile in the field of the target nucleus.

(2) The perturbation of the target atomic states by the projectile.

Both effects are due to the finite charge of the incoming projectile. Although both effects are very important for slowly moving projectiles they become less and less significant as the energy of the incoming projectile becomes relativistic. Qualitatively, the momentum loss of a relativistic projectile to an atomic electron of a target atom is a very small fraction of its total momentum so that the interaction is not going to lead to any deflection of the projectile. Furthermore, the heavy ion projectile - target atomic electron interaction time t is of the order

$$t \sim \frac{b}{\gamma c} \tag{3.1}$$

where in Eq. (3.1) b is the impact parameter and γ is that of the projectile. Equation (3.1) implies that the faster the projectile the shorter the interaction time between projectile and target. Hence, due to adiabiticity the faster the projectile moves the smaller

the deformation of the atomic orbits of the electrons of the target. We have calculated the contribution of the polarization effect which increases the theoretical value (PW A) of the cross sections.[46] It is found that it adds 2%, 4%, and 12%, respectively, for Ni, Ag, and Pb at our projectile energy. Obviously this correction moves the value of the cross section in the opposite direction to that indicated by the experimental results.

The second correction, which was considered here, was that of the binding effect. In the PWBA calculation atomic electrons are assumed to be free. However, for K shell electrons and high-Z_2 elements the corresponding binding energy is of the order of 100 keV. Consequently the velocity of those atomic electrons is of the order of 0.5 c (c light-speed). It is again apparent that this effect becomes smaller as the velocity of the projectile becomes larger since the projectile sees the atomic electrons as free if its velocity is much larger than that of the electrons. The effect of this correction is to decrease the theoretical cross section and is, hence, in the correct direction with respect to the experimental values of the cross section. The binding effect may introduce a negative correction of order $(Z_1/Z_2)^3$ to the cross section and may thus be regarded as having origins in a subtractive second term of the expansion in series - in the PWBA only the first term of order $(Z_1/Z_2)^2$ is retained.[51] It was estimated that the two effects, polarization and binding, will approximately cancel out each other leaving the theoretical value of the cross section (PWBA) practically unchanged.

The third effect, which has a positive contribution to the theoretical value of the cross section σ_K, is that of charge-exchange. This effect accounts for the capture of one or more electrons by the completely ionized incoming projectile. The electron capture by the heavy ion can be a non-radiative process if the energy of the projectile is low. At projectile energies higher than 150 MeV/N is a radiative capture may also become significant.[52] The radiative capture is essentially the inverse reaction of the photoelectric effect.[53] It has been found that the charge-exchange effect for ^{12}C projectiles at 250 MeV/amu is of the order of 5×10^{-7} to 5×10^{-8} for the various target elements used in our experiment.[54] This means that out of 10^8 (carbon ions) completely stripped of their 6 electrons 50 to 5 ions, respectively, will pick up an electron on the average depending on the target element they are going through. Hence, this correction seems to be unimportant.

It was suggested[55] that for relativistic heavy ions the cross section σ_K should approach the integrated McKinley-Feshbach cross section σ_{MF} for the scattering of relativistic electrons on nuclei. The McKinley-Feshbach cross section σ_{MF} is essentially the well known Mott electron scattering formula expanded in powers of Z_1e^2 to the third order.[56][57] What this expansion does is essentially to take into account the $\left(\frac{Z_1}{Z_2}\right)^3$ effect mentioned earlier in connection with the binding effect.[51]

The difference is that the McKinley-Feshbach expression is relativisticly correct whereas the expression used to calculate the binding effect was classical.[50] The following correction factor R

was defined by

$$R = \frac{\int_{E_K}^{T_m} \frac{d\sigma_{MF}}{dT}\, dT}{\int_{E_K}^{T_m} \frac{d\sigma_K}{dT}\, dT} \tag{3.2}$$

where in Eq. (3.2) E_K is the K-shell binding energy, T_m is the maximum kinetic energy transferred to the atomic electron from the heavy ion projectile, and σ_K is the longitudinal PWBA K-shell vacancy cross section. The quantity T_m is given by[56]

$$T_m = 2mc^2\beta^2\gamma^2 \tag{3.3}$$

with β,γ those of the projectile. Evaluating Eq. (3.2) we found that again such a correction to the PWBA cross section could not account for the discrepancy between experiment and theory.[46]

Finally a fitting of the theoretical and experimental values of σ_K was attempted by replacing the Z_1^2 factor in the theoretical cross section by $[Z_1^{eff.}]^2$. The latter factor was given by

$$Z_1^{eff} = Z_1 - \alpha Z_2 \tag{3.4}$$

where α is an unknown quantity to be determined from the fitting of theory with experiment. Thus by setting

$$r = \left(1 - \alpha \frac{Z_2}{Z_1}\right)^2 = \frac{\sigma_K^{exp.}}{\sigma_K^{th.}} \tag{3.5}$$

TABLE 3.4 Modification of the ratio $\sigma_K^{exp}/\sigma_K^{th}$ by introducing the correction factor r.

Element	Z_2	$\sigma_K^{th.}$	$\sigma_K^{th.}/r$	$\sigma^{exp.}$	$\frac{\sigma_K^{exp.}}{\sigma_K^{th.}}$	$r\frac{\sigma_K^{exp.}}{\sigma_K^{th.}}$
Ti	22	22105	19341	18700	0.846	0.967
Ni	28	11591	9763	1000	0.863	1.024
Mo	42	3878	2980	3220	0.830	1.080
Ag	47	2894	2150	2150	0.743	1.000
Tb	65	1023	670	672	0.657	1.003
Ta	73	659.5	407	405	0.614	0.995
Au	79	495.4	293	300	0.606	1.027
Pb	82	405.2	233.5	225	0.555	0.964
U	92	295.07	157.	145	0.468	0.924

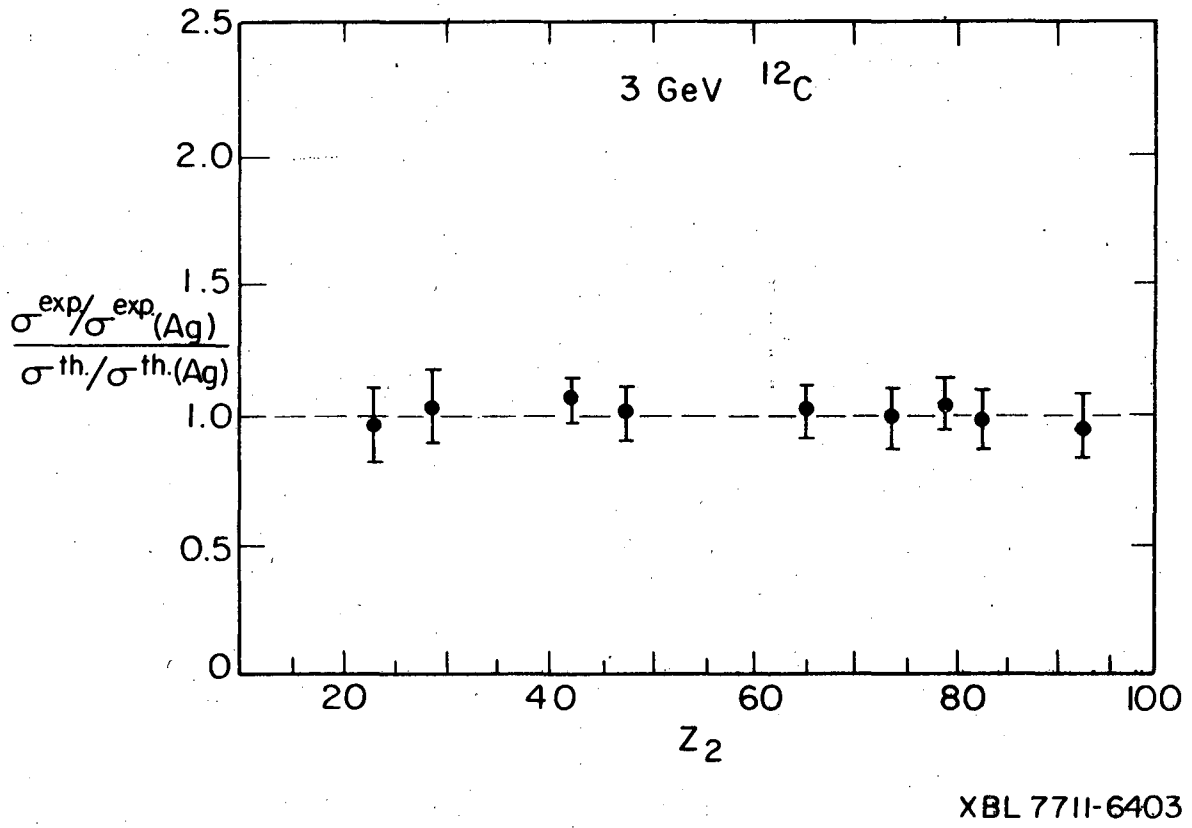

Fig. 17. Ratios of experimental to theoretical K vacancy cross section for 3 GeV ^{12}C ions. The ratios are normalized with respect to the corresponding Ag ratio. The theoretical value of each cross section has been divided by the respective factor r. Error bars reflect one standard deviation.

the quantity α was determined for each target. The value obtained for α was the following:

$$\alpha = (1.762 \pm 0.268) \times 10^{-2} \tag{3.6}$$

Incorporating the correction factor of Eq. (3.5) with its value determined by Eq. (3.6) into the theoretical cross section $\sigma_K^{th.}$, we obtain the results of Table 3.4.

The ratio $[\sigma_K^{exp.}/\sigma_K(Ag)^{exp.}]/[\sigma_K^{th.}/\sigma_K(Ag)^{th.}]$ is also plotted versus target atomic number in Fig. 17. The reason for plotting the ratio of experimental and theoretical cross sections divided by their respective Ag cross sections is to minimize the value of the error of each target element. Apparently we obtain remarkably good agreement between theory and experiment by introducing the correction of Eq. (3.5). It implies an effective projectile charge reduction by an amount proportional to the target atomic number. There is no obvious physical explanation of this effect, though it could mean that the faster moving deeply bound electrons of higher Z_2 elements can respond to screen the K electrons. We were led to this correction by the observation of increasing discrepancy between theory and experiment with increasing target atomic number Z_2. In any case further experimental measurements with different projectiles and at various relativistic energies are necessary before anything concrete can be concluded.

3.4 Extension of the Universal Curve Fit of the K-shell Vacancy Cross Section to Relativistic Energies.

For the energy range up to 150 MeV per nucleon incident heavy ion all three theories, PWBA, BEA, and SCA, for the calculation of the

K-shell vacancy cross section predict that the cross section under consideration should fit a universal curve.[4] All three theories predict also that the K-shell vacancy cross section should be a function of the K-shell binding energy E_K, the atomic numbers of the projectile Z_1 and target Z_2, and the ratio of projectile velocity to K-shell electron velocity η_K/θ_K. We can easily see that this is the case in the PWBA calculation. Clearly for projectile energies lower than 150 MeV per nucleon only the longitudinal component of the cross section is of importance. We thus have from Eqs. (1.36), (1.37), and (1.38):

$$\frac{E_K^2 \sigma_K^{\ell}}{Z_1^2} = \theta_K^2 \left(\frac{Z_K^4 \sigma_K^{\ell}}{Z_1^2} \right) R_\infty^2 \tag{3.7}$$

If we plot the quantity of Eq. (3.7) versus η_K/θ_K which is proportional to $(v/v_K)^2$, we obtain a universal curve whose shape is similar to that of Fig. 2[4] and which is also shown in Fig. 18. The same applies to the BEA calculation with a corresponding universal curve almost identical to that of the PWBA calculation.[4]

As the projectile energy becomes relativistic, one has to include the transverse component of the K-vacancy in a universal curve fit of the cross section. To do so we start from Eq. (1.60). We have:

$$\frac{E_K^2 \sigma_K^{t}}{Z_1^2} = 1.889 \times 10^2 \ \beta^2 \ E_K^2 \ g_K(\eta_K, \beta^2) \tag{3.8}$$

In addition we have

$$\frac{\eta_K}{\theta_K} = \frac{1}{2} \ \frac{mc^2}{E_K} \beta^2 \tag{3.9}$$

so that Eq. (3.8) becomes

$$\frac{E_K^2 \sigma_K^t}{Z_1^2} = 1.889 \times 10^2 \frac{\beta^6 m^2 c^4}{4} \frac{g_K}{\left(\frac{\eta_K}{\theta_K}\right)^2} \tag{3.10}$$

or

$$\frac{E_K^2 \sigma_K^t}{Z_1^2} = 1.235 \times 10^{-17} \beta^6 \frac{g_K}{\left(\frac{\eta_K}{\theta_K}\right)^2} \text{ (keV}^2\text{-cm}^2\text{)} \tag{3.11}$$

Thus in order to obtain the universal curve valid at relativistic projectile energies one has to superimpose the curve of Eq. (3.11) to that of Eq. (3.7). It should be noted that there is a β dependence on the curve of Eq. (3.11). This can be seen in Fig. 18 where the new universal curve for the PWBA calculation is plotted for two different values of the β of the incident heavy ion. For convenience, the same results appear in Table 3.5 along with the corresponding BEA calculation which is only good for non-relativistic projectile energies. In Fig. 18 the experimental points corresponding to the 4.88 GeV proton data have been included. The agreement between theory and experiment is again along the same lines as described in Section 3.2 and also depicted in Fig. 16. Obviously, more experimental data are needed to corroborate the degree of agreement of our theoretical calculations to experimental results. Finally, the usefulness of the universal curve is that it allows for an easy comparison between theory and experimental data for any projectile of any energy on any

TABLE 3.5 Universal K-vacancy production curve for non-relativistic PWBA and BEA and relativistic PWBA theories.

$E_K^2 \sigma_K / Z_1^2$ (keV^2 - $cm^2 \times 10^{19}$)

n_K/θ_K	PWBA non-relativistic(G_k) σ_K^{ℓ}	BEA non-relativistic σ_K	PWBA relativistic(β=0.9) $\sigma_K^{\ell} + \sigma_K^{t}$	PWBA relativistic(β=0.999) $\sigma_K^{\ell} + \sigma_K^{t}$
0.5	0.60	0.80	0.60	0.60
0.8	0.75	0.90	0.75	0.95
1.0	0.90	1.00	0.90	1.23
2.0	0.70	0.80	0.75	1.10
3.0	0.50	0.50	0.58	1.65
4.0	0.42	0.40	0.50	1.71
5.0	0.35	0.32	0.46	1.45
10.0	0.22	0.18	0.23	0.75

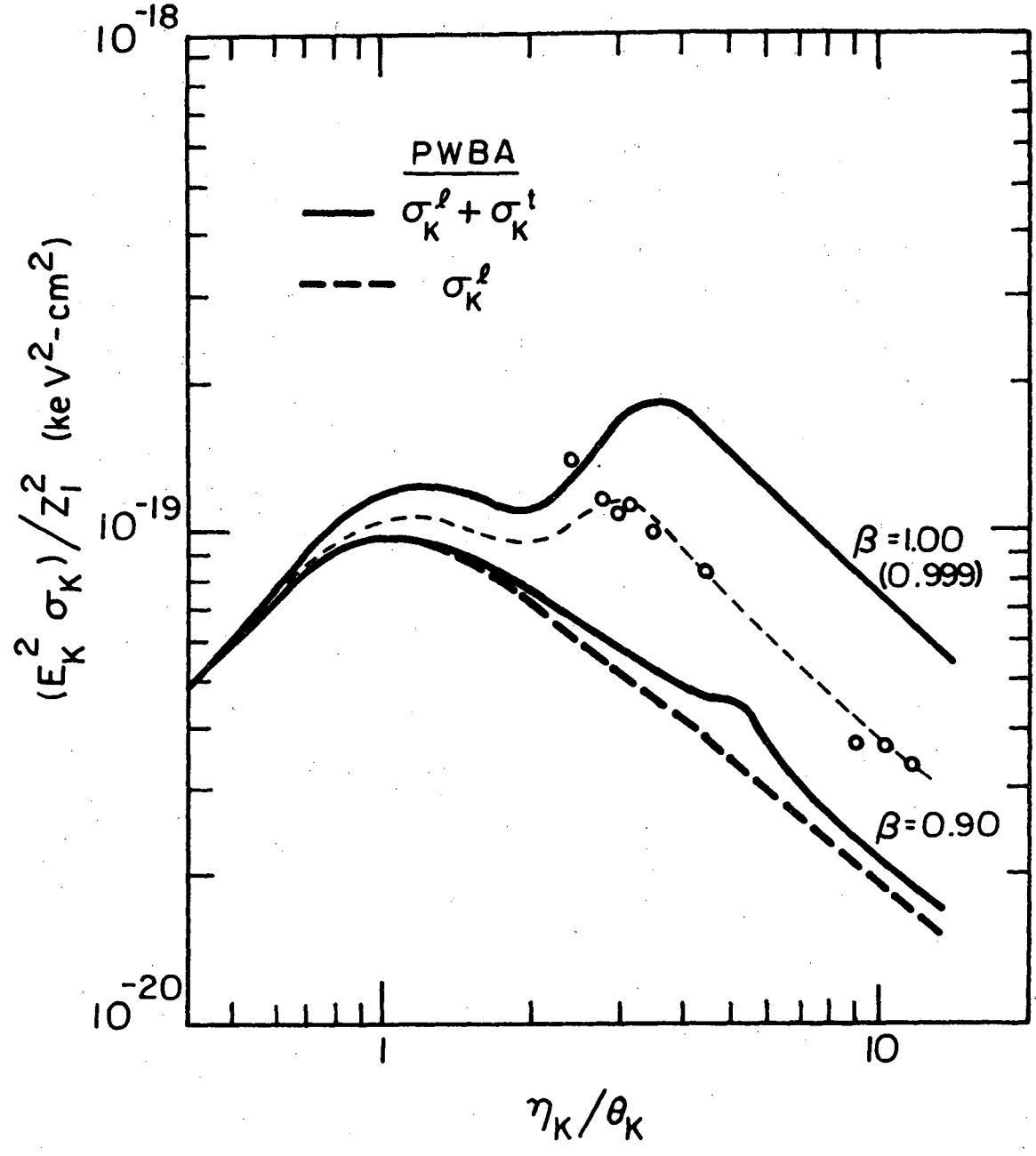

Fig. 18. PWBA universal curve modified by the relativistic correction. The open circles are the experimental points for the 4.88 GeV protons.

target. However, at the relativistic limit of the PWBA calculation the corresponding universal curve has as parameter the β factor of the projectile. This is so because σ_K^{ℓ} is a function of η_K and θ_K while σ_K^{t} is a function of η_K, θ_K, and β^2. Consequently, the above statement concerning the usefulness of the universal curve representation of the K-vacancy cross section is not entirely right. In the relativistic domain, one needs instead of one universal curve a family of universal curves having as parameter the quantity β of the projectile. Figure 18 provides 2 or 3 members of this family of universal curves.

3.5 Comparison of Relativistic Heavy Ions and Relativistic Electrons K-Ionization Theories

It has been mentioned already that a theory exists for the K-vacancy production cross section by relativistic electrons.[29] It would be instructive to compare the derivation of the relativistic electron theory with that for the relativistic heavy ion developed in this work.

In the theory of K-vacancy production by relativistic electrons the trajectories of the electrons are considered. Depending on their impact parameter, the collisions of the incoming electrons with the atomic nuclei are divided into close and distant collisions. If the impact parameter is larger than certain value b_c, one considers the interaction of incoming electron-target nucleus as a virtual photon interaction. This virtual photon interaction is described by the well known Weizsäcker-Williams approximation.[47] On the other hand, if the impact parameter is smaller than the value b_c the interaction is simply of Coulombic nature and is described by the equally well known

Møller scattering formula.[58] The crucial problem in the calculation is the determination of the value b_c, the total cross section of the process being the sum of the two terms, distant and close. In that calculation the critical impact parameter b_c, between close and distant collisions, is determined by comparing the collision time t of the incoming electron and the atomic nucleus, given by

$$t \simeq \frac{b}{\gamma v} \tag{3.12}$$

with the period T of the motion of the K-shell electrons, given by

$$T = \frac{2\pi\, a_o}{Z_2} \tag{3.13}$$

In Eqs. (3.12) and (3.13) b is the impact parameter of the incoming electrons with velocity v, α_o is the Bohr radius, Z_2 the target nucleus atomic number, and v_K is the velocity of K-shell electrons. Depending on whether t is > or < than T one has a distant or a close collision, respectively. The equation t = T determines the critical impact parameter b_c. It is obvious that such abrupt transition from one type of interaction to another is rather unphysical, although it is the only way by which such a formalism of the problem can be handled.

In the relativistic heavy-ion ionization of the K-shell an entirely different formalism was used. Assuming that the incoming heavy ions are represented by plane waves, the impact parameter problem is altogether eliminated. Furthermore, the interaction Hamiltonian includes both the instantaneous Coulomb interaction and the virtual photon interaction. Roughly speaking, one could establish a one to one correspondence between the two terms in the total cross section

of each theory. Thus, the close collision term in the relativistic electron cross section corresponds to the longitudinal term of the relativistic heavy ion cross section. Moreover, the distant collision term of the relativistic electron theory corresponds to the transverse term of our relativistic heavy ion theory. It is apparent that our treatment of the incoming projectile as a wave represents a more physical picture than that of the treatment of the incoming projectile as having a trajectory and hence an impact parameter. In this respect our approach to the problem is superior to any other considering trajectories instead of waves. This is not to conceal the fact that other approximations introduced subsequently in the derivation of the PWBA calculation may make our theory to deviate from physical reality as much as any other or even more. In any case, the point to be made from our discussion is that a theory attempting to correctly describe the atomic ionization by projectiles of any kind ought to treat them as waves rather than particles.

3.6 Conclusions and Recommendations

From the presentation thus far certain facts have been brought forward. First, from the few experimental data and the theoretical calculation of the K-vacancy production cross section it can be safely concluded that the K-shell section, after initially falling with energy past match of projectile speed and Bohr orbital speed, starts rising as the energy of the heavy ion projectiles becomes more and more relativistic. However, more experimental data are needed at very relativistic energies. Thus, measurements with protons of energies ranging from a few GeV to several tens of GeV are essential. Second, for heavier projectiles

than protons there is a significant discrepancy between theory and experiment. This is due mainly to the Z_1^2 dependence of the K-vacancy cross section. Thus, measurements of the cross section are necessary with heavy ions, such as ^4He, ^{12}C, ^{20}Ne, ^{40}Ar, at energies between 250 MeV/amu and 1 or 2 GeV/amu which is anyway the current upper limit of acceleration. From such measurements not only will valuable information be gained about the atomic number of the projectile dependence on the K-vacancy production but also information concerning the contribution of the longitudinal and transverse components to the total cross section. Third, from the information obtained by experiment one could refine or else further develop the current theories of K-vacancy production so that better understanding of the processes involved may become possible.

It is of interest to speculate on the significance in terms of applications of the rising value of the cross section at higher energies. It is well known that electron, proton, and x-ray beams have been used as a tool for trace element analysis by inducing characteristic x-ray emission on various elements.[18][59] The limitation in the sensitivity of either method comes from the background produced during the irradiation of the sample under examination. The main causes of background are: i. bremsstrahlung from secondary electrons,[60] ii. bremsstrahlung from the projectile in the case of electrons or heavy ions.[61] iii. Compton scattering of γ-rays from nuclear excited states.[62] Out of the three causes of the continuous background the first one is the most important. Thus, electron beams are in this respect the least qualified among the three possibilities - electrons,

heavy ions, photons. It is also well known that the photoexcitation cross sections are much higher than those by heavy ions.[44] On the other hand, the background problem is less severe in the case of heavy ions than that of photons. Thus, it is believed that x-ray beams and proton beams of a few MeV have the same trace detection sensitivity limits, which are of the order of about 1 ppm.[63][64] There are, however, a few problems associated with this kind of trace element analysis. First, one is restricted to use samples of thickness of a few mg/cm^2 because of range limitations. Second, protons and heavy ions can selectively excite small portions of the sample at a time while photons excite much larger portions of the sample. This is due to the focusing properties of each of the two kinds of beams. Third, protons of a few MeV have extremely small cross sections for the K x-rays of heavy elements so that one has to resort to L x-rays, a process by itself limiting the sensitivity of the method.

It is conceivable that one could use relativistic heavy ions in the trace element analysis of heavier elements contained in massive samples. The cross section for the K x-ray production of heavy elements by heavy ions is higher at relativistic projectile energies. This is clearly an advantage over low energy protons or heavy ions. The disadvantage associated with relativistic projectiles is that of the higher background when compared with low energy projectiles. Another advantage of relativistic heavy ions over non-relativistic ones, in the trace analysis, is that the former have a much larger range in matter. Thus, relativistic heavy ions have a considerable flexibility over the size of a sample containing trace elements while non-relativistic

heavy ions are very much restricted in this respect. Finally, it is important to remember the general advantage of heavy particles when compared with photons. By using the former rather than the latter, we can determine not only the presence of a trace element in a sample but also its location within the matrix, as the sample is otherwise called. It is therefore possible that one could use relativistic heavy ions in the detection and location of trace elements with high atomic number in massive samples by simply scanning those samples with heavy ion beams. The subject of trace element analysis by photon (XRF), protons (PIXE), and high energy heavy ions (HEHIX) has become very popular indeed most recently. Photon (XRF) analyses of environmental air and water pollution monitoring samples and of biological specimens including blood, hair, and tissue has been reported the last few years.[59],[63] More recently proton (PIXE) analysis has been used or has been proposed to be used in such diverse fields as biology, medicine, bioenvironmental and environmental studies, nutrition, agriculture, and archeology. Thus, ashed human tissues from different organs and a variety of diseases have been analyzed by PIXE in an effort to correlate human disease and tissue content of trace elements.[65] The protein quality of leguminous plants has been also investigated by PIXE analysis.[66] By the same method the elemental variations in the blood of gamma-irradiated mice have been measured,[67] measurements of the trace elements of drinking water have been made,[68] analyses in viticulture and oenology have been carried out,[69] ancient pottery analysis has been reported,[70] and analysis of meteoritic samples has also been done.[71] Finally,

high energy heavy ion induced x-ray emission (HEHIX) has been considered and found successful in the trace element analysis of biological samples.[72] The term high energy heavy ions refers to energies of up to 2 MeV/amu for projectiles as heavy as Xe(Z_1 = 54). It is worth noting that in all mentioned cases of trace element analysis the investigators had or were able to produce samples of the order of mg/cm^2 in thickness or else they had to examine the surface of a sample. Furthermore, the trace elements that were measured quantitatively ranged predominantly in atomic number from nineteen to about sixty.

An obvious possible application of relativistic heavy ions as tool for trace element analysis in the area of biomedical sciences is, for instance, the case where one wants to know the location and degree of deposition of trace heavy elements in the human body. Another possible application in the area of materials science is the case where one is interested to know the extent and location of impurities within the bulk of a non-destructible piece of matter. These and other applications are open to investigation and exploration in the future.

In conclusion, a lot of work is still needed in the area of high energy heavy ion inner shell vacancy production. The rewards of such work in terms of better understanding nature as well as possible technological applications are worthy, the author believes, of its undertaking.

APPENDIX A Tables for the K-Shell Transverse Cross Section.

The transverse component of the K-vacancy production cross section is given by

$$\sigma_K^t = 1.889 \times 10^2 \, Z_1^2 \, \beta^2 \, g_K \qquad \text{(barns)} \tag{A.1}$$

In Eq. (A.1) Z_1 is the atomic number of the projectile, $\beta = \frac{v}{C}$ with the v the velocity of the projectile, and g_K in its exact form is given by the following expression:

$$g_K(\eta_K^t \, , \, \theta_K \, , \, \beta^2) =$$

$$= \int_{y=\theta_K}^{\infty} \int_{x=o}^{1} dx \; \frac{(1-x) \exp\left[\frac{2}{\sqrt{y}} \arctan \frac{2\sqrt{y}}{y-1-Q}\right]}{(1-\beta^2 x^2)^2 (1+y)\left(1 - \exp\left(-\frac{2\pi}{\sqrt{y}}\right)\right)\left[(Q+1+y)^2 - 2yQ\right]}^2$$

(A.2)

In Eq. (A.2) we have:

$$Q = \frac{(1+y)^2}{4x \, \eta_K^t} \tag{A.3}$$

$$\theta_K = \frac{E_K}{Z_2^2 \, R_\infty} \tag{A.4}$$

$$\eta_K^t = \frac{1}{2} \frac{mc^2}{Z_2^2 \, R_\infty} \beta^2 \tag{A.5}$$

with Z_2 the atomic number of the target element, E_K its K-shell binding energy, and R_∞ the infinite mass Rydberg constant equal to 13.61 eV.

The double integral of Eq. (A.2) cannot be calculated analytically so that one has to evaluate it numerically. However, since it depends on three parameters (η_K^t, β^2, θ_K) it would be rather impossible to construct extensive tables of the numerical values of the function g_K. It was therefore assumed that

$$\theta_K = 1 \tag{A.6}$$

Equation (A.6) is the first approximation one can make in calculating the function g_K of Eq. (A.2). This is so in view of the fact that θ_K approaches one as Z_2 increases. With the approximation of Eq. (A.6), one obtains then for g_K

$$g_K(\eta_K{}^t, \theta_K, \beta^2) \xrightarrow{\theta_K = 1} g_K(\eta_K{}^t, \beta^2) \tag{A.7}$$

The function $g_K(\eta_K{}^t, \beta^2)$ is then given by Eq. (1.57), and can be easily tabulated versus $\eta_K{}^t$ and β^2. This has been done by numerically integrating the integrants of Eq. (1.57). The results appear in the following tables and provide a convenient way of calculation of the numerical value of the transverse cross section σ_K^t of Eq. (A.1). The error in the numerical evaluation of g_K is of the order of 1%. In the following tables the actual value for $\beta = 1.00$ is 0.999.

β	η_K	1.0	1.5	2.0	2.5	3.0
1.00		2.554-03	3.192-03	3.533-03	4.292-02	8.640-02
0.99		1.605-03	2.059-03	2.312-03	2.094-02	4.616-02
0.98		1.217-03	1.589-03	1.803-03	1.331-02	3.106-02
0.97		1.004-03	1.320-03	1.521-03	9.674-03	2.345-02
0.96		8.650-04	1.157-03	1.332-03	7.541-03	1.879-02
0.95		7.640-04	1.032-03	1.193-03	6.140-03	1.562-02
0.94		6.866-04	9.346-04	1.086-03	5.152-03	1.331-02
0.93		6.250-04	8.567-04	1.000-03	4.421-03	1.157-02
0.92		5.743-04	7.925-04	9.289-04	3.859-03	1.020-02
0.91		5.320-04	7.383-04	8.685-04	3.416-03	9.094-03
0.90		4.960-04	6.920-04	8.166-04	3.060-03	8.189-03
0.89		4.647-04	6.517-04	7.715-04	2.765-03	7.436-03
0.88		4.375-04	6.164-04	7.318-04	2.520-03	6.798-03
0.87		4.134-04	5.851-04	6.965-04	2.313-03	6.253-03
0.86		3.921-04	5.572-04	6.649-04	2.136-03	5.782-03
0.85		3.730-04	5.321-04	6.365-04	1.983-03	5.372-03
0.84		3.558-04	5.094-04	6.108-04	1.849-03	5.012-03
0.83		3.402-04	4.888-04	5.874-04	1.733-03	4.694-03
0.82		3.250-04	4.699-04	5.659-04	1.629-03	4.412-03
0.81		3.130-04	4.527-04	5.461-04	1.537-03	4.159-03
0.80		3.011-04	4.367-04	5.280-04	1.455-03	3.931-03
0.75		2.538-04	3.731-04	4.548-04	1.149-03	3.076-03
0.70		2.205-04	3.276-04	4.022-04	9.525-04	2.520-03
0.65		1.959-04	2.936-04	3.626-04	8.172-04	2.136-03
0.60		1.771-04	2.675-04	3.320-04	7.196-04	1.859-03
0.55		1.624-04	2.469-04	3.077-04	6.466-04	1.652-03
0.50		1.507-04	2.305-04	2.883-04	5.907-04	1.493-03
0.45		1.413-04	2.172-04	2.725-04	5.471-04	1.371-03
0.40		1.338-04	2.064-04	2.597-04	5.127-04	1.274-03

β	η_K	3.5	4.0	4.5	5.0	5.5
1.00		1.190-01	1.717-01	2.053-01	2.312-01	2.461-01
0.99		6.804-02	9.802-02	1.191-01	1.384-01	1.514-01
0.98		4.790-02	6.914-02	8.570-02	1.010-01	1.126-01
0.97		3.732-02	5.404-02	6.809-02	8.103-02	9.141-02
0.96		3.060-02	4.450-02	5.682-02	6.309-02	7.754-02
0.95		2.591-02	3.783-02	4.886-02	5.388-02	6.756-02
0.94		2.244-02	3.289-02	4.288-02	5.193-02	5.996-02
0.93		1.974-02	2.906-02	3.820-02	4.647-02	5.394-02
0.92		1.760-02	2.601-02	3.443-02	4.204-02	4.904-02
0.91		1.585-02	2.351-02	3.132-02	3.339-02	4.496-02
0.90		1.440-02	2.143-02	2.871-02	3.531-02	4.151-02
0.89		1.317-02	1.967-02	2.649-02	3.267-02	3.855-02
0.88		1.212-02	1.816-02	2.458-02	3.040-02	3.598-02
0.87		1.122-02	1.686-02	2.291-02	2.341-02	3.372-02
0.86		1.043-02	1.572-02	2.144-02	2.666-02	3.173-02
0.85		9.745-03	1.472-02	2.015-02	2.511-02	2.996-02
0.84		9.133-03	1.383-02	1.899-02	2.373-02	2.837-02
0.83		8.589-03	1.304-02	1.796-02	2.248-02	2.694-02
0.82		8.102-03	1.233-02	1.703-02	2.136-02	2.545-02
0.81		7.664-03	1.168-02	1.619-02	2.030-02	2.447-02
0.80		7.268-03	1.110-02	1.542-02	1.941-02	2.340-02
0.75		5.758-03	8.875-03	1.245-02	1.580-02	1.919-02
0.70		4.757-03	7.382-03	1.044-02	1.333-02	1.629-02
0.65		4.054-03	6.326-03	9.010-93	1.155-02	1.719-02
0.60		3.541-03	5.548-03	7.944-03	1.022-02	1.261-02
0.55		3.155-03	4.960-03	7.131-03	9.214-03	1.139-02
0.50		2.858-03	4.505-03	6.499-03	8.421-03	1.044-02
0.45		2.626-03	4.148-03	6.001-03	7.794-03	9.692-03
0.40		2.442-03	3.865-03	5.605-03	7.294-03	9.088-03

β	η_K	6.0	6.5	7.0	7.5	8.0
1.00		2.564-01	3.331-01	3.585-01	3.793-01	3.919-01
0.99		1.607-01	1.958-01	2.155-01	2.334-01	2.446-01
0.98		1.211-01	1.427-01	1.584-01	1.738-01	1.840-01
0.97		9.931-02	1.149-01	1.280-01	1.415-01	1.508-01
0.96		8.489-02	9.725-02	1.084-01	1.205-01	1.289-01
0.95		7.445-02	8.475-02	9.453-02	1.054-01	1.132-01
0.94		6.644-02	7.533-02	8.403-02	9.394-02	1.011-01
0.93		6.006-02	6.792-02	7.576-02	8.486-02	9.161-02
0.92		5.484-02	6.191-02	6.906-02	7.747-02	8.379-02
0.91		5.047-02	5.693-02	6.351-02	7.133-02	7.726-02
0.90		4.675-02	5.272-02	5.881-02	6.612-02	7.172-02
0.89		4.355-02	4.910-02	5.479-02	5.479-02	6.695-02
0.88		4.076-02	4.596-02	5.130-02	5.777-02	6.279-02
0.87		3.831-02	4.321-02	4.824-02	5.436-02	5.914-02
0.86		3.614-02	4.077-02	4.553-02	5.134-02	5.590-02
0.85		3.420-02	3.860-02	4.312-02	4.866-02	5.301-02
0.84		3.240-02	3.666-02	4.096-02	4.624-02	5.042-02
0.83		3.088-02	3.490-02	3.901-02	4.407-02	4.807-02
0.82		2.940-02	3.330-02	3.725-02	4.209-02	4.594-02
0.81		2.815-02	3.186-02	3.560-02	4.030-02	4.400-02
0.80		2.696-02	3.053-02	3.417-02	3.865-02	4.223-02
0.75		2.228-02	2.530-02	2.838-02	3.217-02	3.521-02
0.70		1.901-02	2.167-02	2.435-02	2.765-02	3.031-02
0.65		1.664-02	1.901-02	2.140-02	2.435-02	2.672-02
0.60		1.484-02	1.700-02	1.917-02	2.185-02	2.400-02
0.55		1.346-02	1.544-02	1.744-02	1.990-02	2.188-02
0.50		1.237-02	1.422-02	1.608-02	1.837-02	2.021-02
0.45		1.150-02	1.324-02	1.499-02	1.715-02	1.887-02
0.40		1.080-02	1.246-02	1.412-02	1.616-02	1.780-02

β	η_K	8.5	9.0	9.5	10.0	10.5
1.00		4.007-01	4.087-01	4.156-01	4.199-01	4.255-01
0.99		2.527-01	2.602-01	2.667-01	2.707-01	2.760-01
0.98		1.915-01	1.984-01	2.045-01	2.083-01	2.135-01
0.97		1.577-01	1.643-01	1.701-01	1.737-01	1.786-01
0.96		1.354-01	1.416-01	1.471-01	1.506-01	1.553-01
0.95		1.193-01	1.251-01	1.304-01	1.337-01	1.382-01
0.94		1.069-01	1.124-01	1.175-01	1.206-01	1.250-01
0.93		9.702-02	1.023-01	1.071-01	1.101-01	1.143-01
0.92		8.893-02	9.400-02	9.863-02	1.015-01	1.056-01
0.91		8.215-02	8.700-02	9.145-02	9.426-02	9.818-02
0.90		7.638-02	8.103-02	8.532-02	8.803-02	9.182-02
0.89		7.140-02	7.587-02	8.001-02	8.263-02	8.630-02
0.88		6.706-02	7.136-02	7.536-02	7.789-02	8.145-02
0.87		6.323-02	6.738-02	7.125-02	7.370-02	7.716-02
0.86		5.984-02	6.384-02	6.759-02	6.997-02	7.333-02
0.85		5.680-02	6.067-02	6.531-02	6.661-02	6.988-02
0.84		5.407-02	5.782-02	6.135-02	6.359-02	6.677-02
0.83		5.160-02	5.523-02	5.866-02	6.084-02	6.394-02
0.82		4.936-02	5.288-02	5.622-02	5.333-02	6.136-02
0.81		4.731-02	5.073-02	5.398-02	5.604-02	5.899-02
0.80		4.543-02	4.876-02	5.193-02	5.393-02	5.682-02
0.75		3.800-02	4.093-02	4.375-02	4.553-02	4.812-02
0.70		3.279-02	3.542-02	3.797-02	3.958-02	7.193-02
0.65		2.897-02	3.136-02	3.369-02	3.516-02	3.733-02
0.60		2.606-02	2.826-02	3.043-02	3.179-02	3.380-02
0.55		2.379-02	2.584-02	2.787-02	2.914-02	3.103-02
0.50		2.200-02	2.393-02	2.585-02	2.704-02	2.883-02
0.45		2.057-02	2.239-02	2.422-02	2.535-02	2.700-02
0.40		1.941-02	2.115-02	2.290-02	2.399-02	2.561-02

β	η_K	11.0	11.5	12.0	12.5	13.0
1.00		4.282-01	4.736-01	4.937-01	5.043-01	5.154-01
0.99		2.785-01	2.966-01	3.104-01	3.189-01	3.282-01
0.98		2.158-01	2.263-01	2.363-01	2.434-01	2.513-01
0.97		1.809-01	1.883-01	1.962-01	2.022-01	2.091-01
0.96		1.575-01	1.634-01	1.700-01	1.752-01	1.813-01
0.95		1.404-01	1.454-01	1.510-01	1.557-01	1.612-01
0.94		1.271-01	1.315-01	1.364-01	1.407-01	1.457-01
0.93		1.164-01	1.204-01	1.248-01	1.288-01	1.333-01
0.92		1.075-01	1.112-01	1.153-01	1.189-01	1.231-01
0.91		1.001-01	1.035-01	1.072-01	1.107-01	1.146-01
0.90		9.370-02	9.693-02	1.004-01	1.036-01	1.073-01
0.89		8.814-02	9.120-02	9.449-02	9.754-02	1.010-01
0.88		8.325-02	8.617-02	8.928-02	9.219-02	9.548-02
0.87		7.891-02	8.171-02	8.468-02	8.745-02	9.058-02
0.86		7.504-02	7.773-02	8.056-02	8.322092	8.621-02
0.85		7.156-02	7.415-02	7.687-02	7.942-02	8.228-02
0.84		6.841-02	7.092-02	7.353-02	7.599-02	7.874-02
0.83		6.555-02	6.798-02	7.050-02	7.287-02	7.552-02
0.82		6.294-02	6.529-02	6.773-02	7.003-02	7.258-02
0.81		6.054-02	6.283-02	6.520-02	6.742-02	6.989-02
0.80		5.834-02	6.057-02	6.286-02	6.502-02	6.741-02
0.75		4.952-02	5.150-02	5.352-02	5.541-02	5.750-02
0.70		4.323-02	4.503-02	4.686-02	4.856-02	5.043-02
0.65		3.854-02	4.020-02	4.189-02	4.344-02	4.515-02
0.60		3.494-02	3.649-02	3.806-02	3.950-02	4.109-02
0.55		3.212-02	3.357-02	3.505-02	3.640-02	3.789-02
0.50		2.987-02	3.124-02	3.265-02	3.393-02	3.534-02
0.45		2.805-02	2.937-02	3.071-02	3.193-02	3.327-02
0.40		2.658-02	2.784-02	2.914-02	3.030-02	3.160-02

β	η_K 13.5	14.0	14.5	15.0	15.5
1.00	5.244-01	5.285-01	5.346-01	5.403-01	5.428-01
0.99	3.361-01	3.399-01	3.455-01	3.507-01	3.530-01
0.98	2.582-01	2.617-01	2.668-01	2.716-01	2.738-01
0.97	2.153-01	2.185-01	2.233-01	2.277-01	2.297-01
0.96	1.869-01	1.899-01	1.944-01	1.984-01	2.004 01
0.95	1.662-01	1.691-01	1.733-01	1.771-01	1.789-01
0.94	1.504-01	1.531-01	1.571-01	1.606-01	1.623-01
0.93	1.376-01	1.403-01	1.440-01	1.473-01	1.490-01
0.92	1.272-01	1.297-01	1.332-01	1.364-01	1.380-01
0.91	1.184-01	1.208-01	1.242-01	1.271-01	1.287-01
0.90	1.108-01	1.132-01	1.164-01	1.192-01	1.207-01
0.89	1.043-01	1.066-01	1.097-01	1.124001	1.138-01
0.88	9.865-02	1.008-01	1.038-01	1.063-01	1.077-01
0.87	9.359-02	9.571-02	9.862-02	1.010-01	1.023-01
0.86	8.908-02	9.114-02	9.395-02	9.627-02	9.757-02
0.85	8.503-02	8.703-02	8.976-02	9.198-02	9.325-02
0.84	8.138-02	8.332-02	8.596-02	8.811-02	8.933-02
0.83	7.805-02	7.995-02	8.251-02	8.458-02	8.577-02
0.82	7.502-02	7.687-02	7.936-02	8.136-02	8.252-02
0.81	7.224-02	7.405-02	7.648-02	7.841-02	7.954-02
0.80	6.968-02	7.145-02	7.382-02	7.569-02	7.679-02
0.75	5.944-02	6.106-02	6.316-02	6.479-02	6.577-02
0.70	5.214-02	5.363-02	5.554-02	5.699-02	5.788-02
0.65	4.669-02	4.808-02	4.985-02	5.116-02	5.198-02
0.60	4.249-02	4.380-02	4.545-02	4.666-02	4.742-02
0.55	3.919-02	4.043-02	4.199-02	4.311-02	4.383-02
0.50	3.655-02	3.774-02	3.921-02	4.027-02	4.095-02
0.45	3.442-02	3.556-02	3.697-02	3.798-02	3.863-02
0.40	3.269-02	3.379-02	3.515-02	3.611-02	3.670-02

β	η_K	16.0	16.5	17.0	17.5	18.0
1.00		5.478-01	5.499-01	5.537-01	5.552-01	5.594-01
0.99		3.578-01	3.597-01	3.633-01	3.648-01	3.688-01
0.98		2.783-01	2.801-01	2.835-01	2.850-01	2.888-01
0.97		2.340-01	2.358-01	2.390-01	2.404-01	2.441-01
0.96		2.045-01	2.062-01	2.093-01	2.106-01	2.141-01
0.95		1.829-01	1.845-01	1.874-01	1.887-01	1.921-01
0.94		1.661-01	1.676-01	1.705-01	1.717-01	1.750-01
0.93		1.526-01	1.541-01	1.568-01	1.580-01	1.612-01
0.92		1.415-01	1.429-01	1.455-01	1.466-01	1.498-01
0.91		1.320-01	1.334-01	1.360-01	1.370-01	1.401-01
0.90		1.240-01	1.253-01	1.278-01	1.288-01	1.318-01
0.89		1.169-01	1.183-01	1.206-01	1.216-01	1.245-01
0.88		1.108-01	1.120-01	1.143-01	1.153-01	1.181-01
0.87		1.053-01	1.065-01	1.088-01	1.097-01	1.125-01
0.86		1.004-01	1.016-01	1.038-01	1.047-01	1.074-01
0.85		9.605-02	9.723-02	9.933-02	1.002-01	1.028-01
0.84		9.206-02	9.321-02	9.526-02	9.613-02	9.869-02
0.83		8.843-02	8.945-02	9.155-02	9.240-02	9.491-02
0.82		8.512-02	8.622-02	8.816-02	8.899-02	9.145-02
0.81		8.207-02	8.315-02	8.505-02	8.586-02	8.827-02
0.80		7.927-02	8.033-02	8.218-02	8.297-02	8.533-02
0.75		6.801-02	6.898-02	7.065-02	7.137-02	7.352-02
0.70		5.994-02	6.084-02	6.236-02	6.302-02	6.502-02
0.65		5.389-02	5.473-02	5.614-02	5.676-02	5.862-02
0.60		4.921-02	5.001-02	5.133-02	5.191-02	5.367-02
0.55		4.552-02	4.628-02	4.753-02	4.808-02	4.975-02
0.50		4.256-02	4.330-02	4.448-02	4.501-02	5.660-02
0.45		4.017-02	4.088-02	4.201-02	4.252-02	4.405-02
0.40		3.822-02	3.891-02	4.000-02	4.049=02	4.197-02

β	η_K 18.5	19.0	19.5	20.0	25.0
1.00	5.607-01	5.617-01	5.637-01	5.653-01	5.783-01
0.99	3.701-01	3.710-01	3.729-01	3.745-01	3.841-01
0.98	2.900-01	2.909-01	2.927-01	2.942-01	3.065-01
0.97	2.752-01	2.461-01	2.478-01	2.493-01	2.613-01
0.96	2.152-01	2.161-01	2.177-01	2.192-01	2.309-01
0.95	1.931-01	1.940-01	1.956-01	1.970-01	2.084-01
0.94	1.760-01	1.769-01	1.783-01	1.797-01	1.909-01
0.93	1.622-01	1.630-01	1.644-01	1.658-01	1.767-01
0.92	1.507-01	1.515-01	1.529-01	1.542-01	1.649-01
0.91	1.410-01	1.418-01	1.431-01	1.444-01	1.549-01
0.90	1.326-01	1.334-01	1.347-01	1.359-01	1.462-01
0.89	1.253-01	1.261-01	1.273-01	1.286-01	1.387-01
0.88	1.189-01	1.197-01	1.209-01	1.221-01	1.320-01
0.87	1.132-01	1.140-01	1.151-01	1.163-01	1.260-01
0.86	1.081-01	1.089-01	1.100-01	1.111-01	1.207-01
0.85	1.035-01	1.043-01	1.053-01	1.065-01	1.159-01
0.84	9.941-02	1.001-01	1.011-01	1.022-01	1.115-01
0.83	9.561-02	9.635-02	9.733-02	9.842-02	1.075-01
0.82	9.213-02	9.286-02	9.381-02	9.488-02	1.038-01
0.81	8.893-02	8.965092	8,058-02	9.163-02	1.004-01
0.80	8.598-02	8.670-02	8.760-02	8.863-02	9.732-02
0.75	7.411-02	7.478-02	7.557-02	7.65-02	8.465-02
0.70	6.555-02	6.619-02	6.689-02	6.780-02	7.544-02
0.65	5.911-02	5.972-02	6.036-02	6.122-02	6.846-02
0.60	5.412-02	5.471-02	5.529-02	5.611-02	6.302-02
0.55	5.018-02	5.074-02	5.128-02	5.207-02	5.870-02
0.50	4.701-02	4.756-02	4.806-02	4.882-02	5.521-02
0.45	4.444-02	4.497-02	4.544-02	4.618-02	5.237-02
0.40	4.234-02	4.286-02	4.331-02	4.403-02	5.00-02

β	η_K	30.0	35.0	40.0	45.0	50.0
1.00		5.863-01	5.916-01	5.952-01	5.985-01	5.994-01
0.99		3.949-01	4.002-01	4.037-01	4.069-01	4.078-01
0.98		3.142-01	3.193-01	3.228-01	3.260-01	3.269-01
0.97		2.688-01	2.739-01	2.774-01	2.805-01	2.832-01
0.96		2.382-01	2.432-01	2.467-01	2.498-01	2.506-01
0.95		2.156-01	2.206-01	2.240-01	2.271-01	2.279-01
0.94		1.980-01	2.029-01	2.063-01	2.093-01	2.101-01
0.93		1.837-01	1.885-01	1.919-01	1.949-01	1.957-01
0.92		1.718-01	1.766-01	1.799-01	1.829-01	1.837-01
0.91		1.616-01	1.664-01	1.696-01	1.726-01	1.734-01
0.90		1.529-01	1.576-01	1.608-01	1.638-01	1.646-01
0.89		1.452-01	1.499-01	1.531-01	1.560-01	1.568-01
0.88		1.385-01	1.430-01	1.462-01	1.492-01	1.499-01
0.87		1.324-01	1.370-01	1.401-01	1.430-01	1.438-01
0.86		1.270-01	1.315-01	1.346-01	1.375-01	1.383-01
0.85		1.221-01	1.265-01	1.296-01	1.325-01	1.333-01
0.84		1.176-01	1.220-01	1.251-01	1.279-01	1.287-01
0.83		1.135-01	1.179-01	1.209-01	1.238-01	1.245-01
0.82		1.098-01	1.141-01	1.171-01	1.199-01	1.207-01
0.81		1.063-01	1.106-01	1.136-01	1.164-01	1.171-01
0.80		1.031-01	1.074-01	1.103-01	1.131-01	1.139-01
0.75		9.020-02	9.424-02	9.712-02	9.983-02	1.005-01
0.70		8.073-02	8.461-02	8.740-02	9.004-02	9.072-02
0.65		7.353-02	7.728-02	7.998-02	8.256-02	8.323-02
0.60		6.790-02	7.153-02	7.416-02	7.669-02	7.734-02
0.55		6.341-02	6.693-02	6.951-02	7.198-02	7.262-02
0.50		5.977-02	6.321-02	6.573-02	6.816-02	6.879-02
0.45		5.681-02	6.017-02	6.264-02	6.504-02	6.566-02
0.40		5.439-02	5.758-02	6.011-02	6.247-02	6.308-02

β	η_K	55.0	60.0	65.0	70.0	75.0
1.00		6.013-01	6.026-01	6.048-01	6.054-01	6.059-01
0.99		4.097-01	4.110-01	4.132-01	4.138-01	4.143-01
0.98		3.288-01	3.301-01	3.323-01	3.328-01	3.333-01
0.97		2.832-01	2.845-01	2.867-01	2.872-01	2.877-01
0.96		2.525-01	2.538-01	2.559-01	2.565-01	2.570-01
0.95		2.298-01	2.310-01	2.332-01	2.337-01	2.342-01
0.94		2.120-01	2.132-01	2.154-01	2.159-01	2.164-01
0.93		1.197-01	1.988-01	2.009-01	2.014-01	2.020-01
0.92		1.855-01	1.867-01	1.889-01	1.894-01	1.899-01
0.91		1.752-01	1.765-01	1.786-01	1.791-01	1.796-01
0.90		1.664-01	1.676-01	1.697-01	1.702-01	1.707-01
0.89		1.586-01	1.598-01	1.619-01	1.624-01	1.629-01
0.88		1.517-01	1.529-01	1.550-01	1.555-01	1.560-01
0.87		1.456-01	1.468-01	1.488-01	1.493-01	1.498-01
0.86		1.400-01	1.412-01	1.433-01	1.438-01	1.443-01
0.85		1.350-01	1.362-01	1.382-01	1.387-01	1.392-01
0.84		1.304-01	1.316-01	1.336-01	1.341-01	1.346-01
0.83		1.262-01	1.274-01	1.294-01	1.299-01	1.304-01
0.82		1.224-01	1.236-01	1.256-01	1.251-01	1.255-01
0.81		1.188-01	1.200-01	1.220-01	1.225-01	1.230-01
0.80		1.156-01	1.167-01	1.187-01	1.192-01	1.197-01
0.75		1.021-01	1.033-01	1.052-01	1.057-01	1.062-01
0.70		9.233-02	9.346-02	9.535-02	9.582-02	9.630-02
0.65		8.479-02	8.590-02	8.777-02	8.822-02	8.870-02
0.60		7.887-02	7.997-02	8.179-02	8.224-02	8.271-02
0.55		7.413-02	7.520-02	7.700-02	7.744-02	7.791-02
0.50		7.027-02	7.134-02	7.311-02	7.354-02	7.401-02
0.45		6.711-02	6.817-02	6.992-02	7.034-02	7.0-1-02
0.40		6.452-02	6.556-02	6.729-02	6.771-02	6.818-02

β	η_K	80.0	85.0	90.0	95.0	100.0
1.00		6.075-01	6.076-01	6.078-01	6.083-01	6.083-01
0.99		4.159-01	4.159-01	4.161-01	4.166-01	4.166-01
0.98		3.349-01	3.349-01	3.342-01	3.356-01	3.347-01
0.97		2.893-01	2.893-01	2.896-01	2.901-01	2.901-01
0.96		2.585-01	2.586-01	2.588-01	2.593-01	2.593-01
0.95		2.358-01	2.358-01	2.361-01	2.365-01	2.365-01
0.94		2.180-01	2.180-01	2.182-01	2.187-01	2.187-01
0.93		2.035-01	2.035-01	2.038-01	2.042-01	2.042-01
0.92		1.914-01	1.914-01	1.917-01	1.921-01	1.922-01
0.91		1.811-01	1.811-01	1.814-01	1.818-01	1.819-01
0.90		1.722-01	1.722-01	1.725-01	1.729-01	1.730-01
0.89		1.644-01	1.644-01	1.647-01	1.651-01	1.652-01
0.88		1.575-01	1.575-01	1.578-01	1.582-01	1.582-01
0.87		1.513-01	1.513-01	1.516-01	1.520-01	1.521-01
0.86		1.458-01	1.458-01	1.460-01	1.465-01	1.465-01
0.85		1.407-01	1.407-01	1.410-01	1.414-01	1.414-01
0.84		1.361-01	1.361-01	1.364-01	1.368-01	1.368-01
0.83		1.319-01	1.319-01	1.322-01	1.326-01	1.326-01
0.82		1.280-01	1.280-01	1.283-01	1.287-01	1.287-01
0.81		1.244-01	1.245-01	1.247-01	1.251-01	1.252-01
0.80		1.211-01	1.212-01	1.214-01	1.218-01	1.219-01
0.75		1.075-01	1.076-01	1.079-01	1.083-01	1.083-01
0.70		9.770-02	9.771-02	9.796-02	9.837-02	9.839-02
0.65		9.007-02	9.009-02	9.034-02	9.074-02	9.076-02
0.60		8.407-02	8.409-02	8.433-02	8.473-02	8.475-02
0.55		7.925-02	7.927-02	7.951-02	7.990-02	7.992-02
0.50		7.533-02	7.535-02	7.559-02	7.597-02	7.599-02
0.45		7.211-02	7.213-02	7.237-02	7.275-02	7.277-02
0.40		6.947-02	6.949-02	6.973-02	7.010-02	7.012-02

β	η_K	∞
1.00		6.166-01
0.99		4.249-01
0.98		3.439-01
0.97		2.983-01
0.96		2.676-01
0.95		2.448-01
0.94		2.269-01
0.93		2.124-01
0.92		2.003-01
0.91		1.900-01
0.90		1.811-01
0.89		1.733-01
0.88		1.664-01
0.87		1.602-01
0.86		1.546-01
0.85		1.495-01
0.84		1.449-01
0.83		1.407-01
0.82		1.368-01
0.81		1.332-01
0.80		1.299-01
0.75		1.163-01
0.70		1.063-01
0.65		9.862-02
0.60		9.256-02
0.55		8.770-02
0.50		8.373-02
0.45		8.048-02
0.40		7.780-02

APPENDIX B Relativistic Derivation of Limits of Integration.

At the end of section 1.4 the limits of integration of Eq. (1.25) over q were derived using a non-relativistic formalism. It is shown here that the same limits, q_{min} and q_{max} given by Eqs. (1.30) and (1.32), can be derived in a relativistic formalism.

i. For the minimum momentum q_{min} transferred to the electron:

$$\hbar^2 q_{min}^2 = \left|\bar{p}\right| - \left|\bar{p}'\right|^2 = \left[\left[\frac{E^2 - M^2c^4}{c^2}\right]^{1/2} - \left[\frac{(E-w)^2 - M^2c^4}{c^2}\right]^{1/2}\right]^2 \quad \text{(B.1)}$$

In Eq. (B.1) E is the total energy of the projectile and w is the energy transferred from the projectile to the electron. We assume again that $w << E$. Then one obtains from Eq. (B.1):

$$\hbar^2 q_{min}^2 = \left[\left[\frac{E^2 - M^2c^4}{c^2}\right]^{1/2} = \left[\frac{E^2 - M^2c^4}{c^2} - \frac{2Ew - w^2}{c^2}\right]^{1/2}\right]^2$$

$$\simeq \left[\left[\frac{E^2 - M^2c^4}{c^2}\right]^{1/2} - \left[\frac{E^2 - M^2c^4}{c^2} - \frac{2Ew}{c^2}\right]^{1/2}\right]^2$$

$$= \left[\frac{E^2 - M^2c^4}{c^2}\right]\left[1 - \left[1 - \frac{2Ew}{E^2 - M^2c^4}\right]^{1/2}\right]^2$$

$$\simeq \frac{E^2 - M^2c^4}{c^2}\left[1 - \left[1 - \frac{1}{2}\frac{2Ew}{E^2 - M^2c^4}\right]\right]^2$$

$$= \frac{E^2}{c^2(E^2 - M^2c^4)} \; w^2 = \frac{\gamma^2 M^2 c^4}{c^2 \beta^2 c^2} w^2 = \frac{\gamma^2 M^2 c^4}{c^4 \gamma^2 M^2 v^2} w^2 = \frac{w^2}{v^2}$$

so that

$$q_{min}^2 = \frac{w^2}{\hbar^2 v^2} \tag{B.2}$$

which is identical to Eq. (1.30).

ii. For the maximum momentum q_{max} transferred to the electron:

$$\hbar^2 q_{max}^2 = \left[|\bar{p}| + |\bar{p}'| \right]^2 = \left[\left[\frac{E^2 - M^2c^4}{c^2} \right]^{1/2} + \left[\frac{(E-w)^2 - M^2c^4}{c^2} \right]^{1/2} \right]^2$$

$$\simeq \left[\frac{E^2 - M^2c^4}{c^2} \right] \left[2 + \left[1 - \frac{2Ew}{E^2 - M^2c^4} \right]^{1/2} \right]^2$$

$$\simeq 2 \left[\frac{E^2 - M^2c^4}{c^2} \right] = 2p \tag{B.3}$$

where in Eq. (B.3) p is the magnitude of the momentum of the incident projectile. Without appreciable error we may set for relativistic projectile energies

$$q_{max} \simeq \infty \tag{B.4}$$

The result of Eq. (B.3) is identical to that of Eq. (1.32).

REFERENCES

1. W. Bambynek, B. Craseman, R. W. Fink, H. U. Freund, H. Mark, C. D. Swift, R. E. Price, and V. P. Rao, Rev. Mod. Phys. 44, 716 (1972).
2. J. D. Garcia, Phys. Rev. A 1, 280 (1970).
3. J. H. McGuire and P. Richard, Phys. Rev. A 8, 1374 (1973).
4. J. D. Garcia, R. J. Fortner, and T. M. Kavanagh, Rev. Mod. Phys. 45, 111 (1973).
5. E. Merzbacher and H. Lewis, Handbuch der Physik 34, ed. S. Flügge, (Springer Verlag, Berlin, 1958) p. 166.
6. D. H. Madison and E. Merzbacher, "Theory of Charged Particle Excitation," in Atomic Inner-shell Processes, ed. B. Crasemay (Academic Press, New York, 1975).
7. J. Bang and J. M. Hansteen, Kgl.Danske Videnskab. Selskab. Mat. - Fys. Medd. 31, #13 (1959).
8. B. H. Choi and E. Merzbacher, Phys. Rev. 177, 233 (1969).
9. R. Anholt, thesis, U. C. Berkeley (1975), unpublished report LBL-4312.
10. E. J. Williams, Rev. Mod. Phys. 17, 217 (1945).
11. W. Henneberg, Z. Physik 86, 592 (1933).
12. J. D. Jackson, Classical Electrodynamics (John Wiley, New York, 1962) p. 181.
13. H. Feshbach and P. Morse, Methods of Theoretical Physics (McGraw-Hill, New York, 1953) p. 52.
14. J. J. Sakurai, Advanced Quantum Mechanics (Addison-Wesley, Reading, Mass., 1973) pp. 20-74.

15. U. Fano, Ann. Rev. Nucl. Sci. 13, 1 (1963).

16. M. C. Walske, thesis, Cornell U. (1951).

17. J. C. Slater, Phys. Rev. 36, 57 (1930).

18. F. Folkmann, C. Gaarde, T. Huus, and K. Kemp, Nuc. Inst. Meth. 116, 487 (1974).

19. G. S. Khandelwal, B. H. Choi, and E. Merzbacher, Atomic Data 1, 103 (1969).

20. J. Fischer, Ann. Phys. (Leipzig) 8, 821 (1931).

21. N. F. Mott and H. S. W. Massey, The Theory of Atomic Collisions, 3rd edition (Clarendon Press, Oxford, 1965).

22. D. Jamnik and Č. Zupančič, Kgl. Danske Videnskab Selskab. Mat - Fys. Medd. 31, #2 (1957).

23. H. A. Bethe, Handbuch der Physik 24/1 (Springer Verlag, Berlin, 1933) p. 273.

24. M. C. Walske, Phys. Rev. 101, 940 (1956).

25. H. J. Bhabha, Proc. Roy. Soc. 164, 257 (1938).

26. R. Anholt, S. Nagamiya, J. O. Rasmussen, H. Bowman, J. G. Ioannou, and E. Rauscher, Phys. Rev. A 14, 2103 (1976).

27. O. N. Jarvis and C. Whitehead, Phys. Rev. A 5, 1198 (1972).

28. L. M. Middleman, R. L. Ford, and R. Hofstadter, Phys. Rev. A 2, 1429 (1970).

29. H. Kolbenstvedt, J. App. Phys. 38, 4785 (1967).

30. C. Møller, Ann. Phys. 14, 531 (1930).

31. A. H. Compton and S. K. Allison, X-rays in Theory and Experiment, 15th printing (D. Vay Nostrand, Princeton, N. J., 1967), pp. 583-671.

32. F. S. Goulding, Nucl. Instr. Meth. 43, #1, 1 (1966).

33. Hewlett-Packard, Multichannel Analyzer 5400 Series, Analog to Digital Converter 5416 A/B, Digital Processor 5422A, Power Supply/Interface 5410A (Santa Clara, Calif., 1970).

34. Northern Scientific/Inc., NS-610 1024 Channel Analyzer and NS-400 Data Processor (Madison, Wis., 1966).

35. J. O. Rudeloff, L. B. Robinson, J. D. Meng, unpublished report UCRL-18883 (1969).

36. C. M. Lederer, J. M. Hollander, and I. Perlman, Table of Isotopes, 6th edition (John Wiler, New York, 1967).

37. P. Marmier and E. Sheldon, Physics of Nuclei and Particles I (Academic Press, New York, 1969) p. 144.

38. J. B. Cumming, Ann. Rev. Nucl. Sci. 13, 260 (1963).

39. P. J. Lindstrom, D. E. Greiner, H. H. Heckman, B. Cork, and E. S. Bieser, unpublished report LBL-3650 (1975).

40. A. R. Smith and R. H. Thomas, unpublished report LBL-3861 (1975).

41. O. N. Jarvis, C. Whitehead, and M. Shah, unpublished AERE report No. R 6612 (1970).

42. A. J. Tavendale, Ann. Rev. Nucl. Sci. 17, 73 (1967).

43. P. Marmier and E. Sheldon, Physics of Nuclei and Particles I (Academic Press, New York, 1969) pp. 698-730.

44. W. H. McMaster, N. Kerr Del Grande, J. H. Mallet, and J. H. Hubbell, Compilation of X-ray Cross Sections, unpublished report UCRL-50174 (1969).

45. I. Bergström and C. Nordling, "The Auger Effect," in Alpha-, Beta-, and Gamma-ray Spectroscopy, ed. by K. Siegbahn (North-Holland, Amsterdam, 1965) pp. 1523-1543.

46. R. Anholt, J. G. Ioannou, H. Bowman, E. Rauscher, S. Nagamiya, and J. O. Rasmussen, Phys. Let. 59A, 429 (1977).

47. J. D. Jackson, Classical Electrodynamics (John Wiley, New York, 1962) p. 524.

48. R. B. Leighton, Principles of Modern Physics (McGraw-Hill, New York, 1959), pp. 270-273.

49. G. Basbas, W. Brandt, and R. Laubert, Phys. Let. 34A, 277 (1971).

50. G. Basbas, W. Brandt, and R. Laubert, Phys. Rev. A 7, 983 (1973).

51. H. H. Anderson, H. Simonsen, and H. Sørensen, Nucl. Phys. A 125, 171 (1969).

52. G. Raisbeck and F. Yiou, Phys. Rev. A 4, 1858 (1971).

53. J. B. Hasted, Physics of Atomic Collisions (Butterworths, London, 1964), pp. 612-658.

54. H. Crawford, private communication.

55. J. O. Rasmussen, private communication.

56. J. D. Jackson and R. L. McCarthy, Phys. Rev. B 6, 4131 (1972).

57. W. A. McKinley and H. Feshbach, Phys. Rev. 74, 1759 (1948).

58. J. M. Jauch and F. Rohrlich, The Theory of Photons and Electrons (Addison-Wesley, Cambridge, Mass., 1954), p. 256.

59. F. S. Goulding and J. M. Jaklevic, Ann. Rev. Mucl. Sci. 23, 45 (1973).

60. W. Heitler, The Quantum Theory of Radiation (Claredon Press, Oxford, 1954), p. 242.

61. Ibid, p. 375.

62. Ibid, p. 211.

63. F. S. Goulding and J. M. Jaklevic, Nucl. Inst. Meth. 142, 323 (1977).

64. J. M. Jaklevic, private communication.

65. H. A. van Rinsvelt, R. D. Lear and W. R. Adams, Nucl. Inst. Meth. 142, 171 (1977).

66. P. Rupnik, P. Kump, M. Budnar, and I. Kreft, Nucl. Inst. Meth. 142, 205 (1977).

67. R. C. Bearse, C. E. Burns, D. A. Close, and J. J. Malanify, Nucl. Inst. Meth. 142, 143 (1977).

68. P. Sioshansi, A. S. Lodhi, and H. Payrovan, Nucl. Inst. Meth. 142, 285 (1977).

69. J. L. Campbell, B. H. Orr, and A. C. Noble, Nucl. Inst. Meth. 142, 289 (1977).

70. J. Baijot-Stroobants and F. Bodart, Nucl. Inst. Meth. 142, 293 (1977).

71. H. W. Kugel and G. F. Herzog, Nucl. Inst. Meth. 142, 301 (1977).

72. J. B. Cress, R. Zeisler, and E. A. Schweikert, Nucl. Inst. Meth. 142, 111 (1977).

TECHNICAL INFORMATION DEPARTMENT
LAWRENCE BERKELEY LABORATORY
UNIVERSITY OF CALIFORNIA
BERKELEY, CALIFORNIA 94720